IMPROVING THE EFFICIENCY OF DYE-SENSITIZED SOLAR CELLS WITH ULTRASONIC

SPRAY-COATED TiO$_2$ ELECTRODE THAT WAS MODIFIED BY MnO$_2$, CoO, OR SnO$_2$

Mr. Supasun Thanadvanichkul

จุฬาลงกรณ์มหาวิทยาลัย

CHULALONGKORN UNIVERSITY

A Thesis Submitted in Partial Fulfillment of the Requirements

for the Degree of Master of Engineering in Chemical Engineering

Department of Chemical Engineering

Faculty of Engineering

Chulalongkorn University

Academic Year 2018

การปรับปรุงประสิทธิภาพเซลล์แสงอาทิตย์ชนิดสีย้อมไวแสงที่มีอิเล็กโตรดเป็น TiO$_2$ แบบพ่น
เคลือบอัลต้าโซนิก ซึ่งถูกดัดแปลงด้วย MnO$_2$, CoO หรือ SnO$_2$

นายศุภสัณห์ ถนัดวาณิชย์กุล

วิทยานิพนธ์นี้เป็นส่วนหนึ่งของการศึกษาตามหลักสูตรปริญญาวิศวกรรมศาสตรมหาบัณฑิต
สาขาวิชาวิศวกรรมเคมี ภาควิชาวิศวกรรมเคมี
คณะวิศวกรรมศาสตร์ จุฬาลงกรณ์มหาวิทยาลัย
ปีการศึกษา 2561

Thesis Title   IMPROVING THE EFFICIENCY OF DYE-SENSITIZED
                         SOLAR CELLS WITH ULTRASONIC SPRAY-COATED TiO$_2$
                         ELECTRODE THAT WAS MODIFIED BY MnO$_2$, CoO, OR
                         SnO$_2$
By   Mr. Supasun Thanadvanichkul
Field of Study   Chemical Engineering
Thesis Advisor   Akawat Sirisuk, Ph.D.

        Accepted by the Faculty of Engineering, Chulalongkorn University in Partial
Fulfillment of the Requirement for the Master of Engineering

        .... Dean of the Faculty of Engineering
        (Professor SUPOT TEACHAVORASINSKUN, D.Eng.)

THESIS COMMITTEE
        .... Chairman
        (Associate Professor TAWATCHAI CHARINPANITKUL,
        Ph.D.)
        .... Thesis Advisor
        (Akawat Sirisuk, Ph.D.)
        .... Examiner
        (Associate Professor KASIDIT NOOTONG, Ph.D.)
        .... External Examiner
        (Assistant Professor Monrudee Phongaksorn, Ph.D.)

ศุภสัณห์ ถนัดวาณิชย์กุล : การปรับปรุงประสิทธิภาพเซลล์แสงอาทิตย์ชนิดสีย้อมไวแสงที่มี
อิเล็กโตรดเป็น TiO$_2$ แบบพ่นเคลือบอัลตร้าโซนิก ซึ่งถูกดัดแปลงด้วย MnO$_2$, CoO หรือ SnO$_2$. (
IMPROVING THE EFFICIENCY OF DYE-SENSITIZED SOLAR CELLS WITH
ULTRASONIC SPRAY-COATED TiO$_2$ ELECTRODE THAT WAS MODIFIED BY
MnO$_2$, CoO, OR SnO$_2$) อ.ที่ปรึกษาหลัก : อ. ดร.อัครวัต ศิริสุข

งานวิจัยนี้ได้มีการพิจารณาปรับปรุงไทเทเนียมไดออกไซด์อิเล็กโตรดด้วยการเติมโลหะออกไซด์
แมงกานีสไดออกไซด์ โคบอลต์ออกไซด์ หรือ ทินไดออกไซด์ สำหรับใช้ในเซลล์แสงอาทิตย์ชนิดสีย้อมไวแสง
ซึ่งถูกสังเคราะห์ด้วยวิธี โซล-เจล จากนั้นนำไปพ่นเคลือบเป็นฟิล์มบางลงบนกระจกโปร่งแสงนำไฟฟ้าด้วย
เครื่องพ่นเคลือบอัลตร้าโซนิค จำนวน 500 รอบ แล้วนำไปเผาที่อุณหภูมิ 400 องศาเซลเซียสเป็นเวลาสอง
ชั่วโมง โดยปริมาณการเติมโลหะออกไซด์แมงกานีสไดออกไซด์ โคบอลต์ออกไซด์ และทินไดออกไซด์ อยู่
ในช่วงร้อยละ 0, 0.1, 0.5, 1.0 และ 3.0 โดยน้ำหนัก สำหรับประสิทธิภาพของเซลล์แสงอาทิตย์สีย้อมไวแสงที่
เตรียมขึ้นจะถูกทดสอบด้วยเครื่องทดสอบระบบโซลาร์ที่ความเข้มแสง 15 มิลลิวัตต์ต่อตารางเซนติเมตร โดยสี
ย้อมไวแสงที่ใช้ คือ สีย้อมรูทีเนียม N719 และสารละลายอิเล็กโทรไลต์ที่ใช้ คือสารละลายที่ประกอบด้วย ลิ
เธียมไอโอไดด์ (LiI) ไอโอดีน (I$_2$) และ 4-เทิร์ท-บิวทิลไพริดีน (4-TBP) ในอัตราส่วนโมลลาร์ 0.1 ต่อ 0.01 ต่อ
0.1 ซึ่งประสิทธิภาพเซลล์แสงอาทิตย์ชนิดสีย้อมไวแสงที่ใช้อิเล็กโตรดเป็นไทเทเนียมไดออกไซด์ มี
ประสิทธิภาพของเซลล์อยู่ที่ 3.12±0.32% โดยอิเล็กโตรดที่มีการเติมโลหะออกไซด์แมงกานีสไดออกไซด์
โคบอลต์ออกไซด์ และทินไดออกไซด์ ที่เหมาะสมคือร้อยละ 0.5, 0.1 และ 0.5 ตามลำดับ ซึ่งทำให้
ประสิทธิภาพของเซลล์เพิ่มเป็น 4.83±0.36%, 3.23±0.40% และ 6.68±0.43% ตามลำดับ ซึ่งเป็นผลจากการ
เพิ่มขึ้นของปริมาณสีย้อมไวแสงรูทีเนียมที่ถูกดูดซับบนขั้วอิเล็กโทรด ทำให้ค่ากระแสลัดวงจร (J$_{SC}$) และค่า
แรงดันไฟฟ้าขณะเปิดวงจร (V$_{OC}$) เพิ่มขึ้น ส่งผลให้ประสิทธิภาพการแปลงพลังงานของเซลล์แสงอาทิตย์
เพิ่มขึ้นสำหรับอิเล็กโตรดแบบชั้นเดียว และอิเล็กโตรดแบบสองชั้น โดยมีชั้นล่างเป็นไทเทเนียมไดออกไซด์
ร่วมกับชั้นบนเป็นทินไดออกไซด์ที่ร้อยละ 0.5 โดยน้ำหนัก พบว่ามีประสิทธิภาพการแปลงพลังงานของเซลล์
เพิ่มขึ้นจาก 6.68±0.43% เป็น 8.72±0.31% เมื่อเปรียบเทียบกับอิเล็กโตรดแบบชั้นเดียว เนื่องจากเกิดการ
กระเจิงแสงได้ดีภายในเซลล์จากขนาดผลึกที่แตกต่างกันกับไทเทเนียมไดออกไซด์

สาขาวิชา	วิศวกรรมเคมี	ลายมือชื่อนิสิต	
ปีการศึกษา	2561	ลายมือชื่อ อ.ที่ปรึกษาหลัก	

6070329721 : MAJOR CHEMICAL ENGINEERING

KEYWORD: Dye-sensitized solar cells; Ultrasonic spray-coating; Titanium dioxide; Manganese dioxide; Cobalt oxide; Tin dioxide

Supasun Thanadvanichkul : IMPROVING THE EFFICIENCY OF DYE-SENSITIZED SOLAR CELLS WITH ULTRASONIC SPRAY-COATED TiO_2 ELECTRODE THAT WAS MODIFIED BY MnO_2, CoO, OR SnO_2. Advisor: Akawat Sirisuk, Ph.D.

This research investigated the modification of TiO_2 electrode by adding the second metal oxide, namely, manganese dioxide (MnO_2), cobalt oxide (CoO), or tin dioxide (SnO_2) use in for dye-sensitized solar cell (DSSCs). TiO_2 and modified TiO_2 sols were synthesized via sol-gel methods. The sols were sprayed 500 times onto the fluorine-doped tin oxide glass substrates as a thin film using an ultrasonic spray coater. Finally, the thin film electrode was calcined at 400ºC for two hours. The amount of MnO_2, CoO, or SnO_2 was varied at 0, 0.1, 0.5, 1.0, and 3.0%wt. The photovoltaic efficiency of DSSCs was measured using an IV-tester under a light irradiance of 15 mW/cm^2. The dye sensitizer used was ruthenium-based N719 dye and the electrolyte solution composed of lithium iodide (LiI), iodine (I_2), and 4-tert-butylpyridine (4-TBP) in acetonitrile with a molar ratio of LiI:I_2:4-TBP of 0.1:0.01:0.1. The efficiency of DSSCs with pure TiO_2 electrode was 3.12±0.32% with optimum loading of MnO_2, CoO, and SnO_2 with 0.5, 0.1, and 0.5%wt, respectively, the efficiency of DSSC rose to 4.83±0.36%, 3.23±0.40%, and 6.68±0.43%, respectively. This was pattly attributed to the large amount of ruthenium dye molecule adsorbed on the electrode. In addition, both short circuit current density (J_{SC}) and open circuit voltage (V_{OC}) were improved, resulting in greater efficiency of DSSCs with the single-layered electrode. Next, the thin films double-layered electrode with pure TiO_2 as the under layer and 0.5%wt. SnO_2/TiO_2 as the over layer was employed. The cell efficiency rose from 6.68±0.43% to 8.72±0.31%, compared with the single-layered electrode with 0.5%wt. SnO_2 because of enhanced light scattering inside the DSSC from the mismatched crystallite size of TiO_2.

Field of Study: Chemical Engineering   Student's Signature ....

Academic Year: 2018   Advisor's Signature ....

ACKNOWLEDGEMENTS

TABLE OF CONTENTS

LIST OF TABLES

Page

LIST OF FIGURES

CHAPTER 1

INTRODUCTION

1.1 Rationale

Electric power is considered an important fundamental factor for national development. Electricity can be converted into other forms of energy such as heat, light, mechanical energy, etc. Therefore, there is a need to use a large amount of electricity due to population growth. Thus, the amount of electricity consumption keeps increasing in the country. The Electricity Generating Authority of Thailand reported that the consumption of electricity in the year BE 2561 exceeded 180,000 million kW per hour [1].

Electrical energy requires energy from other sources for production, such as fossil fuels, hydropower, wind power, solar energy, etc. According to the forecast, the current level of natural gas reserve is at 6.41 trillion cubic feet of natural gas. This amount of natural gas is estimated to last for approximately 8.6 years. However, due to the increasing growth rate of the country's population, development of renewable energy in various forms needs to be accelerated. This leads to reduction in fuel imports and stronger energy security in Thailand [2].

Renewable energy is generated from renewable energy sources such as sunlight, geothermal heat, etc. Solar energy is a clean natural energy source that does not cause pollution and never runs out. It can be used to generate electricity directly through solar cells [2, 3].

Solar cells can directly convert solar energy into electrical energy. It is based on the photovoltaic effect. The solar cell was first discovered in 1839 by French scientist named Antoine César Becquerel [4]. It was found that electricity generated when the light hit the electrodes of the electrolyte. In 1941, Russell Ohl [5] was developed a P-N type of semiconductor silicon solar cell of single crystal silicon semiconductors at Bell Laboratories. Later in the year 1954, Chapin et al. [6] at Bell Laboratories, improved the efficiency of the solar cell. At present, the P-N type of silicon solar cell is employed to generate electricity. However, the production requires advanced technology and silicon of high purity. As a result, this type of solar cell is quite expensive for a household use.

In 1991, Brian O'Regan and Michael Grätzel [7] at UC Berkeley first reported the high photoelectric conversion efficiency of dye-sensitized cells. That is comparable to that of amorphous Si-based solar cells [8, 9].

Dye-sensitized solar cells (DSSCs) are a part of third generation solar cells. They have gained interest amongst researchers as well as industries due to their low fabrication cost, stability, simple manufacturing process, eco-friendliness, ease of assembly, optical properties, and relatively high photovoltaic efficiency. So it is a promising potential replacement for silicon-based solar cells. The dye-sensitized solar cell is based on a semiconductor formed between photoelectrodes and an electrolyte. Although the efficiency of the dye-sensitized solar cell is currently low, research and development is currently underway to increase the efficiency, durability, and life of DSSC. For example, the development of an inexpensive electrode, development of metal oxide particles that transmit electrons well and a large surface area, and soon. In addition, DSSC still has the potential to produce a much higher efficiency to contribute greatly to renewable electricity generation in the future [10, 11].

Dye-sensitized solar cells generally comprise semiconductor thin-film photoanode such as TiO_2, ZnO, etc. It is coated on fluorine-doped tin oxide (FTO) glass and a counter electrode (platinum or graphite) deposited on FTO glass. In addition, a dye-sensitizer (e.g., ruthenium-based dye N719, N3, etc.) is adsorbed on the photoanode and an electrolyte (I_3^-/I^- redox couples) injected between dye-sensitizer. When the light hits the solar cell, dye molecules adsorbed on the surface will absorb light. After that, the electrons in the ground state will be stimulated to go up to an excited state and the electrons will move through conductive glass out of the cell, generating electricity. Then the electrons will return the counter electrode and born to be the redox reaction with the electrolyte, where the electrolyte can restore the dye to return to the ground state by electron donation [1, 12, 13].

The most popular semiconductor metal oxide is TiO_2 because of its low cost, non-toxicity, high thermal and chemical stabilities, favorable charge carrier properties, and high transparency in the solar spectrum. At present, researchers attempts to

increase the conversion efficiency of DSSC by modification of TiO_2 that leads to a change in its optical and electrical properties. Such modifications include by adding another metal oxide such as ZnO, SnO_2, MnO_2 or other into TiO_2. This modification can increase surface area and prevent the electron recombination with a passivation layer of another high band gap material. In addition, fabricating a DSSC with a double-layered structure can increase light distribution within the cell, resulting in high photovoltaic efficiency. Moreover, there have been other approaches to increase the efficiency conversion by developing a new dye-sensitizer or new electrolyte and resolving the leakage problems of electrolyte after injection into the solar cell [14, 15].

In this research, we were incorporated manganese dioxide (MnO_2), cobalt oxide (CoO), or tin dioxide (SnO_2) to TiO_2 photoanode electrode layers in order to increase the photovoltaic conversion efficiency of dye-sensitized solar cell. These second metal oxide doped on TiO_2 were chosen because they were reported to increase the electron density or induce faster electron transport. The double-layered electrode structure was also employed to increase light absorption by a light scattering inside the cell, leading to a higher photovoltaic efficiency.

1.2 Objectives

I. To enhance the photovoltaic efficiency of dye-sensitized solar cells equipped with titanium dioxide (TiO_2) electrode that was modified by manganese dioxide (MnO_2), cobalt oxide (CoO), or tin dioxide (SnO_2).

II. To improve the photovoltaic efficiency of dye-sensitized solar cells by using a double-layered electrode structure consisting of an over- and under-layer film electrode.

1.3 Research scopes

1.3.1 Part I: Fabrication of the dye-sensitized solar cell with a single-layered electrode

- Titanium dioxide (TiO_2) and the second metal oxide (manganese dioxide (MnO_2), cobalt oxide (CoO), tin dioxide (SnO_2)) were prepared by sol-gel methods.

- The amount of MnO_2, CoO, and SnO_2 that were added to TiO_2 ranged from 0, 0.1, 0.5, 1.0 and 3.0%wt.

- TiO_2 and modified TiO_2 electrode was prepared by using an ultrasonic spray coater.

- The ruthenium-based dye used was N719 dye, the counter electrode was prepared by coating an platinum and the electrolyte solution composed of lithium iodide (LiI), iodine (I_2), and 4-tert-butylpyridine (4-TBP) in acetonitrile (molar ratio LiI:I2:4-TBP = 0.1:0.01:0.1).

- Fabricate components of dye-sensitized solar cells into complete dye-sensitized solar cells.

- Modified TiO_2 electrodes and their surrogates characterized by several techniques

- N_2 physisorption
- X-ray diffractometry (XRD)
- UV-Visible spectroscopy (UV-Vis)
- Inductively coupled plasma-atomic emission spectroscopy (ICP-AES)

- The electrochemical properties of dye-sensitized solar cells were measured by IV-tester.

1.3.2 Part II: **Fabrication of a dye-sensitized solar cell with a double-layered thin film electrode**

One layer of the electrode was chosen from the electrode that produced the highest photovoltage efficiency of dye-sensitized solar cells from Part I.

CHAPTER 2
THEORY

Dye-sensitized solar cells (DSSCs)

Dye-sensitized solar cells (DSSCs) are an efficient type of thin-film photovoltaic cell and efficient low-cost alternatives for conventional solar cells. Modern dye-sensitized solar cells, or Grätzel cells, are based on a concept invented in 1988 by Brian O'Regan and Michael Grätzel [1]. DSSCs are easy to manufacture with traditional roll-printing techniques. They are semi-transparent and semi-flexible, thereby allowing a range of uses that are not applicable to rigid photovoltaic systems. DSSC consists of a photoanode coated with TiO_2 film on conductive glass and a counter electrode of conductive glass coated with platinum. In addition, it contains ruthenium dye coated on thin-film photoanode and an electrolyte of certain organic solvent containing a redox couple.

2.1 Components of DSSCs

2.1.1 Titanium dioxide or Titania (TiO_2); Semiconductor electrode

Titanium dioxide (TiO_2) is mostly used as white pigments because of its outstanding properties, such as brightness, high whiteness, strong hiding power, and non-toxicity. It is also well known for its biological nontoxicity, low cost, and excellent chemical stability. It has been used extensively as a photocatalyst since 1971 [16, 17]. Defects in porous TiO_2 can act as an electron trap and so can boundaries of the granules that are exposed between the nanoparticles. Therefore, the use of the nanoparticles network structure instead of TiO_2 is expected to result in fast electron transfer and high efficiency [16].

In DSSC, consisting of a wide band gap TiO_2 semiconductor, dyes molecule used to absorb light radiation and excited photo-electrons, this is transferred to TiO_2 [18]. The electron was fast to transfer between dyes and TiO_2 can be done in principle, then reducing the loss of photon energy used as heat through the electron-phonon relaxation pathway. In many types of semiconductor metal oxides, titanium dioxide (TiO_2) is expected to play a role in PV equipment due to its high chemical and optical

stability, nontoxicity corrosion resistance and low cost [19]. TiO_2 is a semiconductor material with a band gap of 3.2 eV, corresponding to a wavelength of 390 nm and having three polymorphisms including tetragonal anatase, tetragonal rutile, and orthorhombic brookite. In, Rutile structure is the most thermodynamically stable phase, while the other two are metastable. However, the anatase structure is more preferred than other polymorphs for solar cell applications because it has a higher possibility of bringing energy from the edge and lower aggregation rate of the electron-hole pair [20]. The band structure of rutile and anatase polymorphs of TiO_2 with the respectively relaxed crystal structures is shown in Figure 2.1
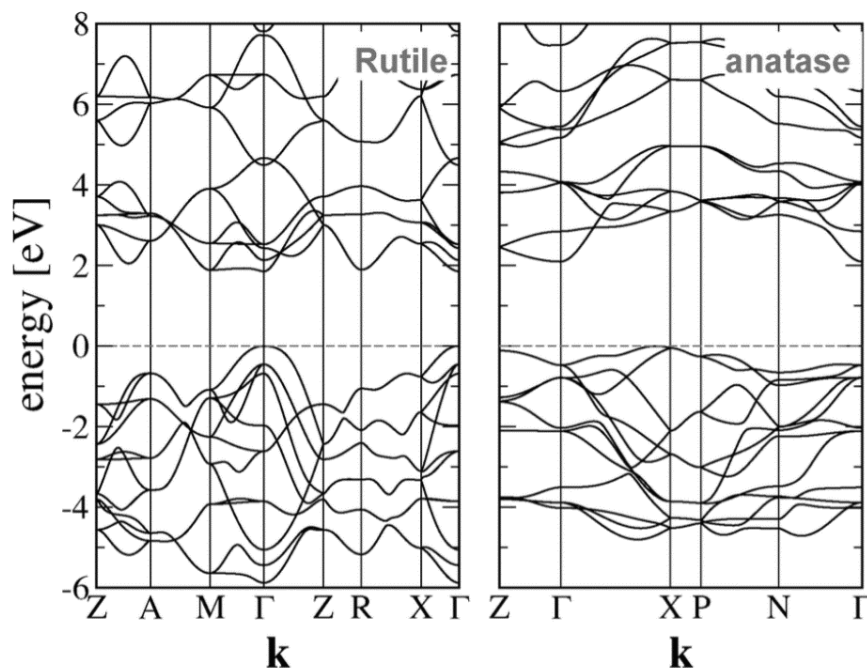
Figure 2.1 Band structure of rutile and anatase [21]

Various methods have been developed to synthesize TiO_2 nanoparticles or TiO_2 films. The most important method for producing titanium dioxide is hydrolysis and sintering of Titanyl sulfate ($TiOSO_4$) and oxidation of titanium tetrachloride ($TiCl_4$). Other synthetic methods are titanium hydroxide from precipitation, titanium from pyrolysis citrate substrate, and titanium tetrachloride ($TiCl_4$) from hydrolysis. However, Geffcken

and Berger in 1939 were first reported the Sol-Gel method to synthesize single oxide coatings of received a lot of attention to synthesize TiO_2 since then [17, 22].

The Sol-Gel route is considered a good method for the synthesis of highly detailed metal oxides and is widely used in the preparation of titanium dioxide particles. most titanium dioxide is used as a pigment, adsorbent, and catalyst [23]. It shows that with the Sol-Gel process, the chemical, physical and electrochemical properties of TiO_2 can be adjusted to improve efficiency. It is a simple and easy way to synthesize nanoparticles at room temperature under atmospheric pressure and this technique does not require complex installation. Since this method is a solution process, it has advantages over other preparation techniques in terms of purity, consistency, and flexibility in introducing contaminants in large concentrations, controlling the number of substances, process control, and composition. On the Sol-Gel process, the growth of TiO_2 colloids in the micrometer range can be effectively controlled by hydrolysis and condensation of titanium alkoxide in the water medium [24].

A sol-gel process [25, 26] occurs in the solution phase of the organometallic precursor was led to hydrolysis, polycondensation, drying, and thermal decomposition. Hydrolysis of the precursors of the metal or non-metal alkoxides takes place with water or alcohols, according to the following scheme:

Hydrolysis:

$$Ti(OR)_4 + 4H_2O \longrightarrow Ti(OH)_4 + 4ROH \qquad (2.1)$$

Where R = alkyl group

Alcohol condensation:

$$Ti(OR)_4 + Ti(OR)_3 (OH) \longrightarrow Ti_2O(OR)_6 + ROH \qquad (2.2)$$

Where R = alkyl group

In addition to water and alcohol, acid or base also helps in the degradation of the substrate. After condensation of the solution with the solvent gel is removed.

The reaction stops with the inclusion of two water molecules:

$$Ti(OR)_4 + 2H_2O \longrightarrow TiO_2 + ROH \qquad (2.3)$$

2.1.2 Counter electrode

A counter electrode (CE) is one of the most important components in DSSCs. The main work of the counter electrode is that

I   It acts as a catalyst by reducing the redox species

II   For collecting the hole from the hole-transporting materials in a solid-state DSSCs.

It has a significant influence on the photovoltaic performance, long-term stability, and cost of the devices. Further, it is helpful that boosting the short-circuit current density (J_{SC}), open circuit voltage (V_{OC}) and fills factor (FF) for increasing the efficiency of DSSCs [27].

Platinum (Pt) is the most preferred material for a counter electrode in DSSCs, due to its electrocatalytic activity towards I_3^- reduction. In 1991, O'Regan and Grätzel [7] were first to the used counter electrode in his DSSCs. The best counter electrode developed for a DSSC is platinum coated by sputtering on the conductive glass. It has a thickness of around 0.2-2 micron. These counter electrode films were shown a high electrical conductivity, catalytic activity towards I_3^- and high reflecting properties. So far, platinum has been the preferred material for the counter electrode, since it is a good catalyst for the triiodide reduction. In general, the preparation of solar cells has a low cost. Therefore, the sputtering technique or by thermal vapor deposition preparation is more popular. Because This technique has transparency on the FTO glass and low cost. These alternative methods require a small quantity of low platinum (10-100 µg/cm^2). This can help reduce production costs and prepare on small plate solar cells. This is increasing the efficiency of photovoltaic conversion of solar cells. However, their

chlorine platinum acid thermal decomposition or by electrochemical reduction of other sputtering technique is not received attention due expensive and not transparent platinum-based sputtered layer [28, 29].

2.1.3 Dye-sensitized

A dye-sensitized component that is the source of this type of solar cell. This is adsorbed on the surface of metal oxide particles and serves to absorb solar energy. Then is causing electrons to be stimulated Then pass electrons to the metal oxide particles. Therefore, the good properties of photosensitive dyes should be to absorb more light in the stability of the wavelength and adhesion on the surface of metal oxide particles [1, 30].

Ruthenium is classified as carboxylates polypyridyl complexes. They were received great interest in the use of dye-sensitized due to their spectroscopic, appropriate redox and excited-state properties. In particular ruthenium (II) complexes with carboxylic pyridine derivatives are metal with a high redox potential to suitable for stimulation and transmission electrons to nanoparticles of semiconductor metal oxide to improve the photovoltage efficiency of a dye-sensitized solar cell. In 1991, O'Regan and Grätzel [7] in Nature were the first usability reported of Ru complexes with trinuclear Ru (II) complex to improved light absorption properties and achieved as a 7.1% conversion efficiency. However, the structure of the ruthenium dye was complicated because contained three ruthenium metal centers (Figure 2.2) [31].
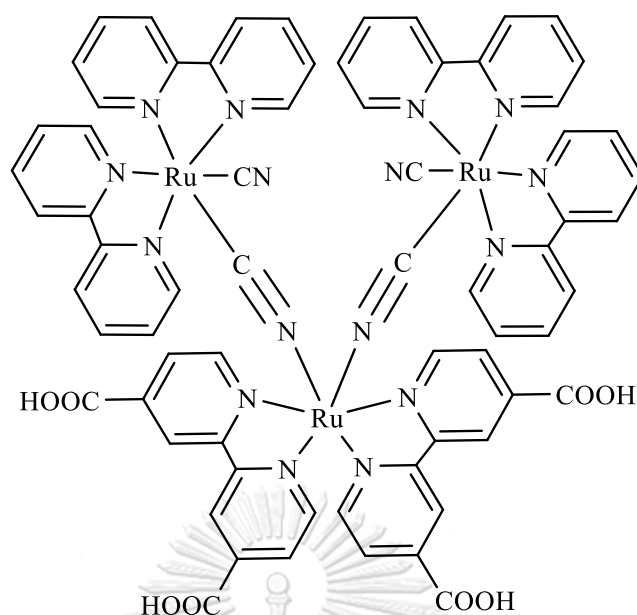
Figure 2.2 A trinuclear Ru (II) complex reported in 1991 by O'Regan and Grätzel [7]

However, there are interesting reports about the use of Ru complexes with another type of carboxylates pyridine ligands such as N719, N3, Black dye, Z-907, etc. (Figure 2.3). They are more option because it has the ability to absorb on the surface of the oxide metal, less structural complexity and close efficacy to the solar cell P-N type of semiconductors solar cell. In 1993 Nazeeruddin et al. [32] were reported a conversion efficiency of DSSC was 10.3% with using cis-Bis(isothiocyanato) bis(2,2'-bipyridyl-4,4'-dicarboxylato ruthenium(II) dye (N3 dye) as dye-sensitize. It was compared to fewer ruthenium centers and is easier than ruthenium dyes reported in 1991. But, in 2005 Nazeeruddin et al. [33] were reported a new dye called di-tetrabutylammonium cis-bis(isothiocyanato)bis(2,2'-bipyridyl-4,4'-dicarboxylato)ruthenium(II) dye (N719 dye) It was similar to N3 but results in highly conversion efficiency for 11.2% [34, 35].
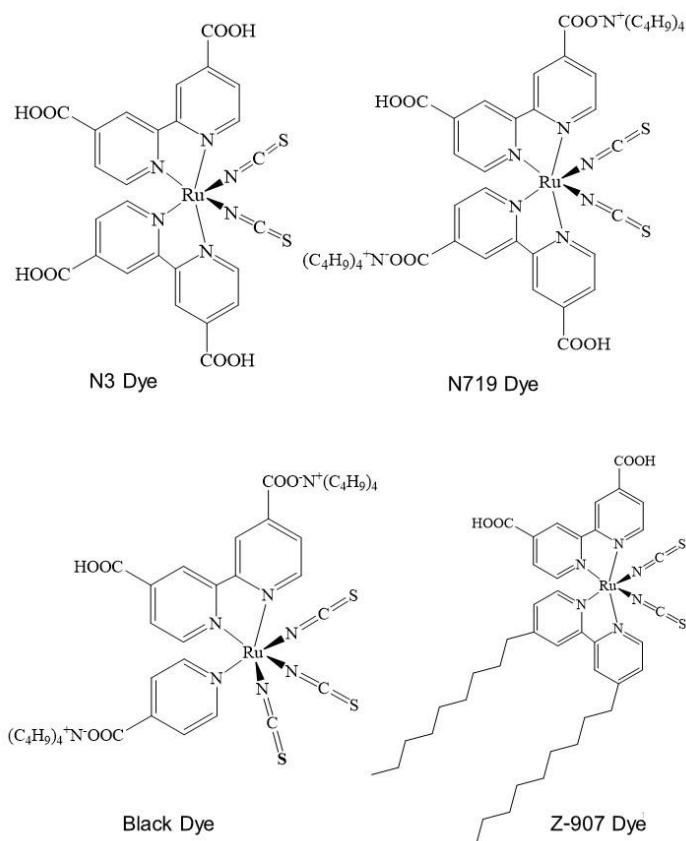
Figure 2.3 Structure of N3, N719, black dye, and Z-907 dye-sensitizers [35]

In addition, there are also reports of the use of other dye-sensitized in DSSCs research. In 2001, Nazeeruddin et al. [36] have designed the N749 dye, also called black dye in by Ru center molecule was three thiocyanato ligands and one terpyridine ligand with three anchoring carboxylic acid groups. This reported a conversion efficiency of DSSCs was 10.4% under solar to photovoltage efficiency in full sunlight (AM 1.5G). In 2003, Grätzel and co-workers [37] have designed a heteroleptic amphiphilic Ru (II) complex also called Z-907 dye. There is consists of long hydrophobic alkyl chains. This reported a conversion efficiency of DSSCs was 6.1%. The device using Z-907 dye-sensitizer is shown stable thermal stress and light. However, the absorption coefficient of black dye and Z-709 dye are lower than N719 dyes [35, 38].

2.1.4 Electrolyte

The electrolyte is a material that provides ionic conductivity between the anode and the cathode electrode in redox electrical between the electrode pairs. Electrolytes are widespread and indispensable in most electrical chemical equipment. The role of electrolytes in supercapacitors, capacitors, fuel cells, electrolytic or batteries [39].

Electrolytes are one of the most important components in DSSCs. It is responsible for transporting of internal electric charge between the electrodes and dye-sensitizer continuously staining. The first of the electrolyte system is a simple system that is easy to prepare. The component was an electrolyte and liquid, has a dual component, redox reaction of triiodide/iodide (I_3^-/I^- redox couples) dissolved in organic solvents such as acetone nitrile, propionitrile, acetonitrile, proplycarbonate, etc. [40]. The most general use is the I_3^-/I^- redox couples because electrons are slow recombination rate [41]. The regeneration of dye is reduced at the counter electrode of I_3^- by the reaction:

$$I^- + 2e^- \longrightarrow 3I_3^- \qquad (2.4)$$

An electrolyte is a great influence on the efficiency of light conversion into electricity and the long-term stability of the device. The performance of the DSSC device is determined by the short current density (J_{SC}), the open circuit voltage (V_{OC}) and the fill factor (FF). These three parameters are significantly affected by electrolytes in DSSC and collaboration of electrolyte and electrolyte connector, for example, J_{SC} may be affected by the transport of double redox in the electrolyte. The fill factor can be affected by the diffusion of the capacitor in the electrolyte and the charge transfer resistance on the electrolyte on the interface of the electrode. In addition, the redox potential of the electrolyte may significantly affect the open circuit voltage [39, 42].

There are many aspects needed for electrolytes used in DSSC.

    I.   The electrolyte must be able to pass through the capacitor between the photoelectrode and the counter electrode.

II. The electrolyte must have rapid transport of the capacitor and create good interfacial contact with semiconductor and electrode layers.

III. Electrolytes must be stable for chemicals, heat, light, electrochemical and infiltration stability. In addition, must not cause deterioration of dye-sensitized.

IV. The electrolyte should not be significantly absorbed in the range of visible light.

At present, this type of electrolyte can give the total efficiency of cells higher than 10% due to the efficiency of faster ion transport but there are disadvantages. The volatile solvent is easy to volatile by causes problems of disappearance or leakage of the solution from the cell body. There makes result in total efficiency, lifetime and the durability of dye-sensitized solar cells was decreases of the light sensitivity. This considers an important problem for cells that use electrolyte systems liquid phases [43].

2.2 Operating principles

Dye-Sensitized Solar (DSSC) or Grätzel cells named after the inventor. Basic operating principle and energy level is shown in Figure 2.4. The following sections describe all the electrochemical processes involved. Nanocrystalline TiO_2 is placed on the photoelectrode to provide a large surface area that is necessary for absorbing photosensitive dyes (Dye molecules) [44, 45].
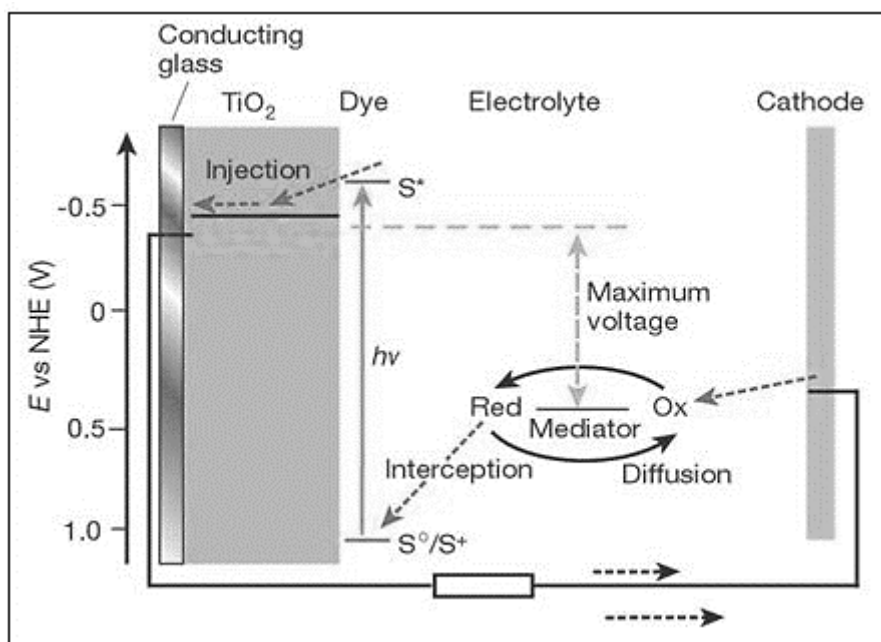
Figure 2.4 Operating principle and energy level diagram of DSSCs [45]

STEP I   Excitation process

Where absorbing photons or sunlight energy, the dye molecules are excited from the highest occupied molecular orbitals or HOMO status (S) to the lowest unoccupied molecular orbital or LOMO status (S^*) . This process is represented by Equation 2.5.

$$S + photons \longrightarrow S^*$$ (2.5)

STEP II   Injection process

The electrons molecular (S^*) across the conductor band of the nanostructured semiconductor of the TiO_2, the dye molecules will become oxidized molecule (S^+). This process is represented by Equation 2.6.

$$S^* + TiO_2 \longrightarrow e^-_{(TiO_2)} + S^+$$ (2.6)
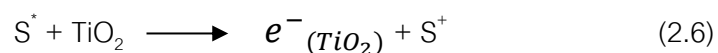
STEP III   Energy generation

The electrons that are injected will be transported between TiO_2 nanoparticles and will then be extracted to a load where the finished work will be sent as electrical energy. This process is represented by Equation 2.7.

$$e^-_{(TiO_2)} + CE \longrightarrow TiO_2 + e^-_{(CE)} + \text{electrical energy} \quad (2.7)$$
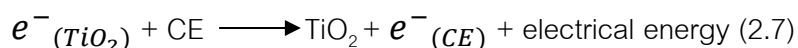
STEP IV   Regeneration of dye

Electrolytes containing, I^- / I_3^- redox ions are used as electron media between TiO_2 photoelectrode and platinum coated on the counter electrode. Therefore, the dye-oxidizing molecules will be reconstructed by receiving electrons from the I- ion redox mediator that get oxidized to triiodide (I_3^-). This process is represented by Equation 2.8.

$$S^+ + \frac{3}{2}I^- \longrightarrow S + \frac{1}{2}I_3^- \quad (2.8)$$
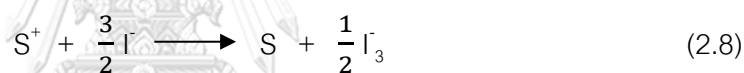
STEP V   Electron recapture reaction

In the regenerate of iodide (I^-), an electron with an external load is reduced and the ion is triiodide (I_3^-) on the counter electrode. This process is represented by Equation 2.9.

$$\frac{1}{2}I_3^- + e^-_{(CE)} \longrightarrow \frac{3}{2}I^- + CE \quad (2.9)$$
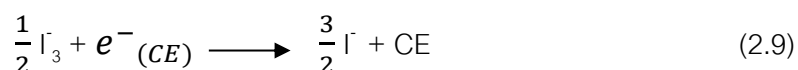
In, 2005 Nazeeruddin et al. [33] reports the movement of electrons in the conductor band of the wide band gap nanostructure semiconductor, the wide band gap that accompanies the diffusion of charge-compensating cations that compensate for the charge in the electrolyte near the nanoparticle surface. Therefore, the production of electrical energy in DSSC does not cause permanent changes or transformation in a chemical.

2.3 Characteristic of the photovoltaic cell

The photovoltage efficiency can be computed by using the I-V curve. There are three significant parameters of DSSC such as short-circuit current (I_{SC}), Open-circuit voltage (V_{OC}) and the fill factor (FF). This is discussed in the following
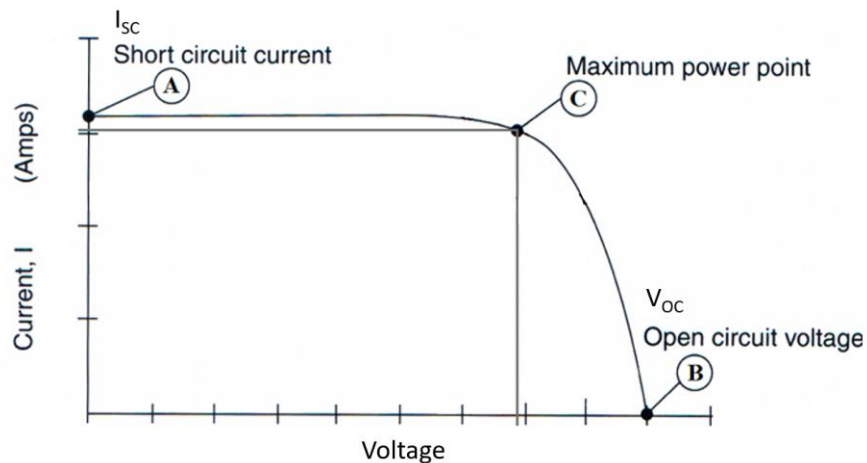
Figure 2.5 IV-curve of photovoltaic cell [46]

In Figure 2.5 is shown an IV-curve of the photovoltaic cell is a relationship between the current flowing through an electronic device and the applied voltage; short-circuit current; ISC (point A), open circuit voltage; VOC (point B) and maximum power point; MPP (point C) [46].

The solar cell's I-V curve is the overlap of the I-V curve of the diode. The solar cell in the dark with the light generated light has the effect of sliding the I-V curve into the fourth quadrant where energy can be extracted From the diode, the cell illumination is added to the normal "dark" current in the diode so that the diode equation follows [47]:

$$\text{I} = I_0 \left[\exp \frac{qV}{nkT} - 1 \right] - I_L \tag{2.10}$$

where I_0 is Dark Saturation Current (A) and I_L is Light Generated Current

The characteristic I-V curve of the solar cell shows the current characteristics and voltage (I-V) of solar cells are module that provides a detailed explanation of the ability and efficiency of solar energy conversion. The electrical I-V characteristics of the solar cell are important in determining the output efficiency of the equipment and solar energy efficiency [48].

2.3.1 Short-circuit current (J_{SC})

The short-circuit current (I_{SC}) is the voltage across the solar cell is zero (i.e., when the solar cell is short-circuited) of the current through the solar cell. Usually, the short-circuit current is shown on the I-V curve below (Figure 2.6).
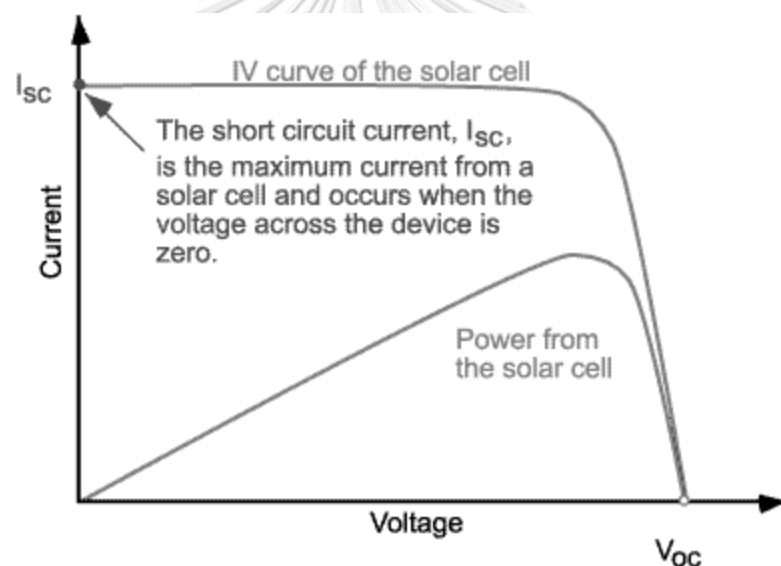
Figure 2.6 The short-circuit current of a solar cell with the I-V curve [49]

The Short circuit current is caused by the collection and creation of light carriers. For the ideal solar cell, the mechanism of moderate resistance to loss, mainly the short-circuit current and the current that produces light is the same. Therefore, short circuit current is the largest current which may be pulled out from the solar cell. The short-circuit current depends on the factors are described below:

    I.   The area of the solar cell.

    II.   The number of photons (i.e., the power of the incident light source).

    III.   The spectrum of the incident light.

    IV.   The optical properties (absorption and reflection) of the solar cell.

    V.   The lifetime collection probability of the solar cell.

When comparing solar cells of the same material, the most important material parameters are length, diffusion and coating surface area. In cells that have completely stimulated surfaces and the creation of short-circuit current equations can be estimated as follows Equation 2.11.

$$J_{SC} = qG\,(L_n \ + \ L_p) \tag{2.11}$$

Where G is the generation rate, L_p, and L_n are the hole and electron diffusion lengths respectively. Although this equation makes many assumptions unrealistic for conditions found in most solar cells, the above equation still indicates that the short-circuit current depends on the rate of formation and the length of the diffusion [49].

2.3.2 Open-circuit voltage (V_{OC})

The open-circuit voltage (V_{OC}) is the highest voltage available from the solar cell and occurs at the zero current. The open-circuit voltage corresponds to the amount of forwarding bias on the solar cell due to the bias of the separation of solar cells and the light generated current. The open circuit voltage is shown on the I-V curve below (Figure 2.7) [50, 51].
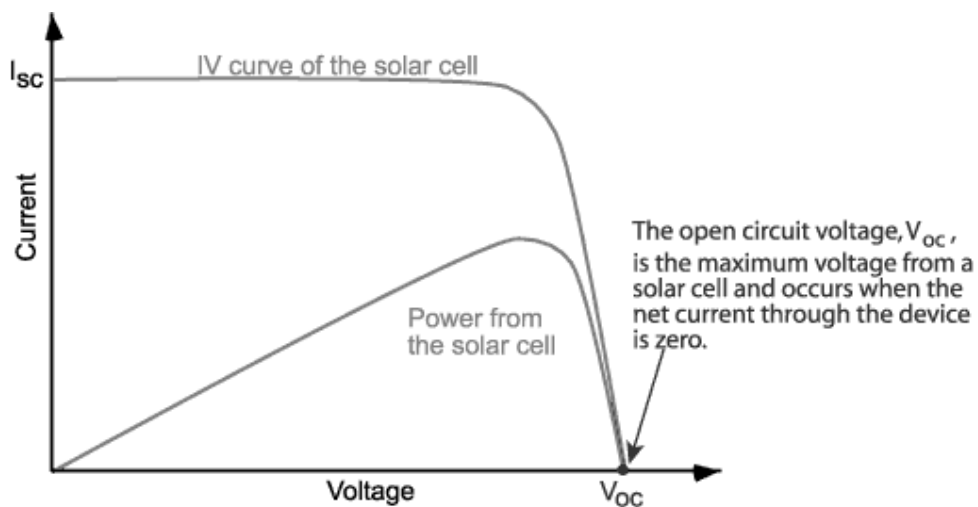
Figure 2.7 The open-circuit voltage of the solar cell with the I-V curve [50]

An equation 2.12 for the open-circuit voltage (V_{OC}) is found by setting the net current equal to zero in the solar cell equation.

$$V_{OC} = \frac{nKT}{q} \ln\left(\frac{I_L}{I_0} + 1\right) \tag{2.12}$$

Where I_0 is Dark Saturation Current (A), I_L is Light Generated Current (A), n is Ideality Factor, and T is Temperature (K).

The above equation shows that V_{OC} depends on the saturated currents of solar cells and the currents generated by light, while I_{SC} usually has a slight change. The main effect is the saturation of electricity because this may differ. Together according to the order of size Saturation electricity I_0 depends on recombination in the solar cell. Open

circuit voltage is a unit to measure the amount of recombination in a device. Silicon solar cells on high-quality single crystal materials have open-circuit voltage as high as 730 mV under one sun condition (AM1.50), while commercial devices for crystalline silicon crystals generally have circuit voltage Open about 600 mV. When the short-circuit current (I_{SC}) is decreased when increasing the band gap, the open-circuit voltage will increase as the gap of the band increases. In the ideal device, the V_{OC} is limited by the new combination of radiation and analysis. Use the principle of fine balance to determine the lowest possible value for J_0. [51].

2.3.3 Fill factor (FF)

The short-circuit current and open-voltage are the highest current and voltage respectively from solar cells. However, at both operational points, energy from solar cells is zero. "Fill factor", known as "FF", is a parameter used in conjunction with V_{OC} and I_{SC} to determine the maximum energy from solar cells. Fill factor is defined as the ratio of maximum energy from solar cells to V_{OC} and I_{SC} products. The Fill factor graphic is a measure of the "square" of the solar cell and is also the area of the largest rectangle that will fit the IV curve [52].
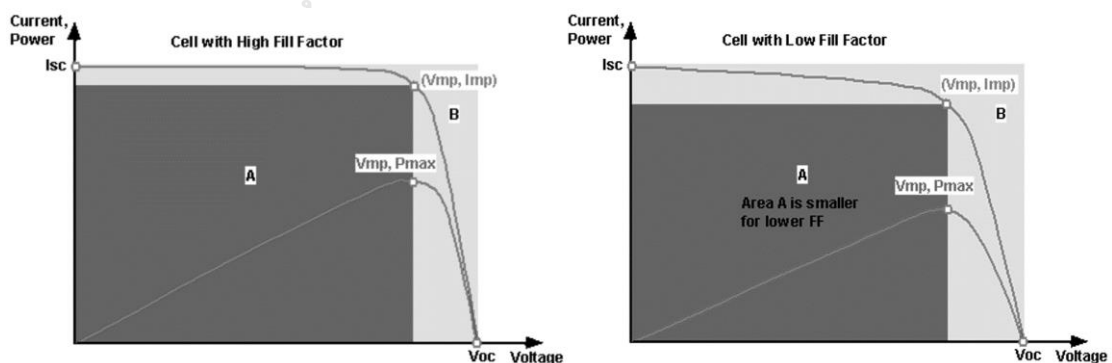
Figure 2.8 The Graph of cell output current (Top line) and power (Bottom line) as a function of voltage [52]

In Figure 2.8 shown is the cell short-circuit current (ISC) and open-circuit voltage (VOC) points, as well as the maximum power point (V_{max}, I_{max}) and difference of the curve changes for a cell with low Fill factor or high Fill factor.

Therefore, the fill factor is most commonly determined by the measurement of the I-V curve and is defined as the maximum power divided by the products of I_{SC} x V_{OC} according to Equation 2.13.

$$FF = \frac{J_{max} \times V_{max}}{J_{SC} \times V_{OC}}$$ (2.13)

Where J_{SC} and V_{OC} are the short-circuit current density (mA/cm^2) and open-circuit voltage (V) respectively, J_{max}, and V_{max} are the short-circuit current density and the open-circuit voltage at maximum power point (P_{max}) of the I-V curve.

2.3.4 Photovoltaic efficiency

The photovoltage efficiency or Incident Photon to Current Conversion Efficiency (IPCE) is the most commonly used parameter to compare solar cell about performance. The efficiency is defined as the ratio of the output of solar cell energy to the input of solar energy. In addition, the efficiency depends on the spectrum and intensity of the temperature of the solar cell and the incident sunlight. Therefore, conditions are effective for measurement must be carefully controlled to compare the performance of one device with another.

The photovoltage efficiency of the solar cell is defined as part of the incident energy that is converted into electricity and using the Equation 2.13.

$$\eta = \frac{V_{OC} J_{SC} FF}{P_{in}} \text{ x } 100\%$$ (2.13)

Where FF is the fill factor, V_{OC} is the open circuit voltage (V), J_{SC} is the short current density (mA/cm^2), and P_{in} is the incident light power (W/cm^2).

CHAPTER 3

LITERATURE REVIEWS

This chapter presents the literature review associated with dye-sensitized solar cells

3.1 Modification of TiO_2 electrode with a mixed metal oxide of DSSC

3.1.1 Modification of TiO_2 electrode with manganese dioxide of DSSCs

Prasetio et al. [53] employed the TiO_2/MnO_2 composite film as working electrode of dye-sensitized solar cell with N719 dye. The TiO_2/MnO_2 composite film electrode was prepared by the doctor blade method. In Figure 3.1 was shown the band gap energy of modified TiO_2 decreased as more MnO_2 was added. At the optimum MnO_2 concentration of 6.0 at.%, the open-circuit voltage increased from 0.4948 to 0.5049 V, the short circuit current density increased from 0.0487 to 0.0707 mA/cm^2 , fill factor increased from 0.2773 to 0.3008 and the photovoltaic efficiencies increased from 0.0067 up to 0.0108 % as compared to the DSSCs with pure TiO_2 photoanode. The presence of TiO_2/MnO_2 composite in DSSCs led to improvements of up to 40% in the conversion efficiency of DSSCs.
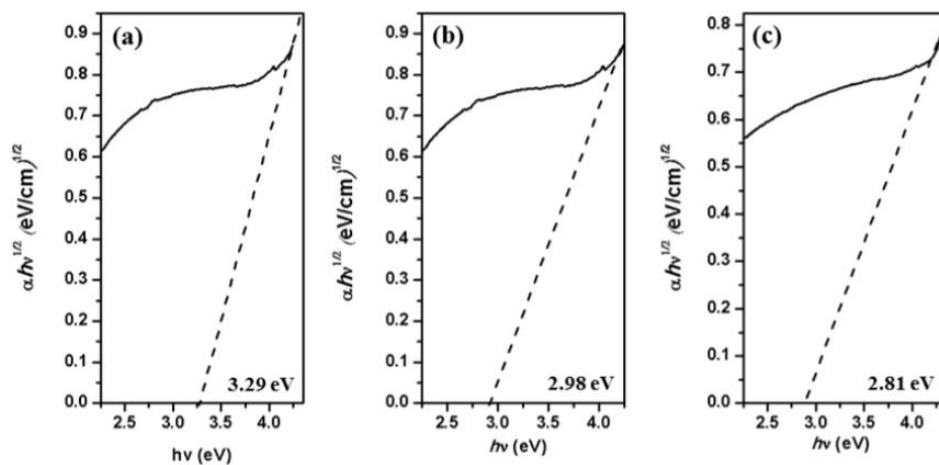
Figure 3.1 Plot $(\alpha h\nu)^{(1/2)}$ vs hν of (a) TiO_2, (b) TiO_2/MnO_2 2% and (c) TiO_2/MnO_2 6% samples [53]

Shalan et al. [54] successfully prepared Mn-doped TiO_2 nanoparticle photoanode by the hydrothermal method. Adding Mn to TiO_2 reduced TiO_2 particle size and increased surface area (see table 3.1). In this study, the photovoltaic efficiency of DSSC under irradiation of 100 mW/cm^2 white light was 1.85%.

Table 3.1 Physical properties of TiO_2 , Mn/TiO_2 and Co/TiO_2. [54]

Sample	S_{BET} (m^2/g)	Crystallite size (nm)
TiO2 (NPs)	99.30	13.0
Mn-TiO2	171.18	7.0
Co-TiO2	78.59	15.2

Yacoubi et al. [55] prepared the Mn/TiO_2 electrode by a sol-gel method. The quantity of manganese added was 6%. As a result, the crystallinity improved, the band gap was smaller and the photovoltaic efficiency for the DSSC increased. For the photoanode by annealed at 400ºC was increase the short circuit current density increased, leading to an increase in photovoltaic efficiency from 2.69 to 3.71 %.

3.1.2 Modification of TiO_2 electrode with cobalt oxide of DSSCs

Ünlü et al. [56] studied the addition of Co to TiO_2. The Co/TiO_2 was synthesized by microwave-assisted hydrothermal method with a molar ratio of Co/TiO_2 at 1:100 and was then coated on FTO-glass using a spin coater. The photovoltaic efficiency of DSSCs with dithizone as a sensitizer was at 1.27 % and with N719 at 4.46 % as compared to the DSSCs with TiO_2 electrode.

Khan et al. [57] deposited Co/TiO$_2$ nanoparticles on the FTO glass using a spray pyrolysis technique. The Co/TiO$_2$ nanocomposite was prepared as multilayer thin films of 1, 2, 3, and 4 layers. In Figure 3.2 XRD results indicated that layers 1 and 2 were of anatase phase and layers 3 and 4 were of brookite phase. In Figure 3.3 UV–Vis results show suggested that the 4th layer film possessed high light absorption in the visible region. The band gap energies of layers 1, 2, 3, and 4 decreased. Finally, the photovoltaic efficiency went up to 5.6% using 3 stacked layers of photoanode.
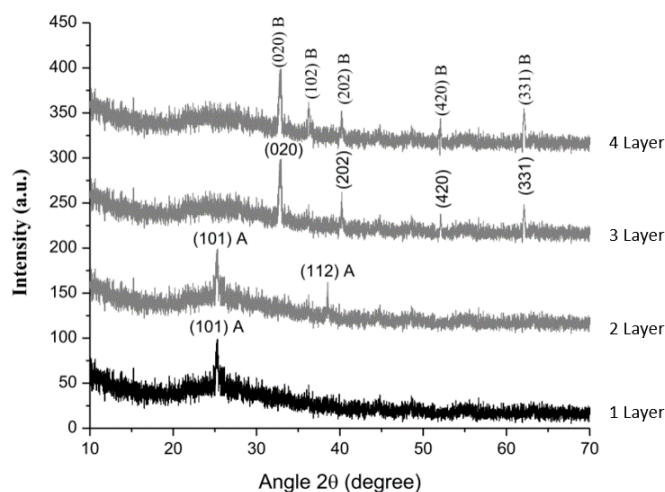
Figure 3.2 XRD pattern of 1, 2, 3 and 4 layers of Co doped TiO2 thin films [57]
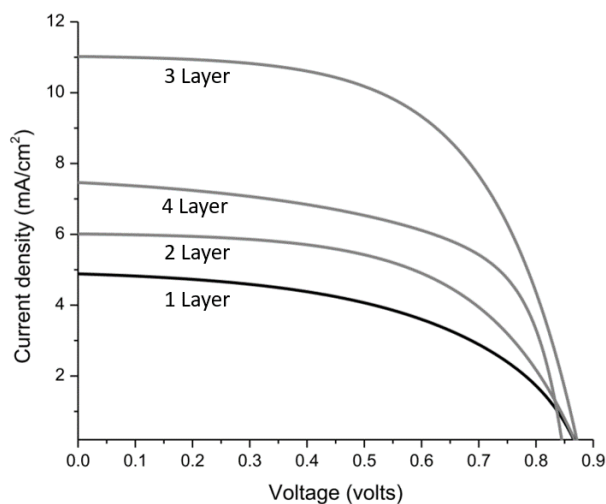
Figure 3.3 *I-V characteristics of cobalt doped TiO$_2$ multilayer photoanode* [57]

3.1.3 Modification of TiO_2 electrode with tin dioxide of DSSCs

Musyaro'ah et al. [58] employed the SnO_2 as semiconductor oxide electrode of DSSCs that was prepared by the modified kopresipitasi method on the float glass substrates. The DSSCs also included electrolyte gel-based polymer PEG with BM 1000, plate carbon as the counter electrode (cathode), and N-749 as a dye sensitizer. In this study I-V tester was measured with xenon lamp with an intensity of 100 mW/cm^2. IV-curve of photovoltaic cell was shown in Figure 3.4 that increases of current density increased and the photovoltaic efficiency increased to 0.041%.
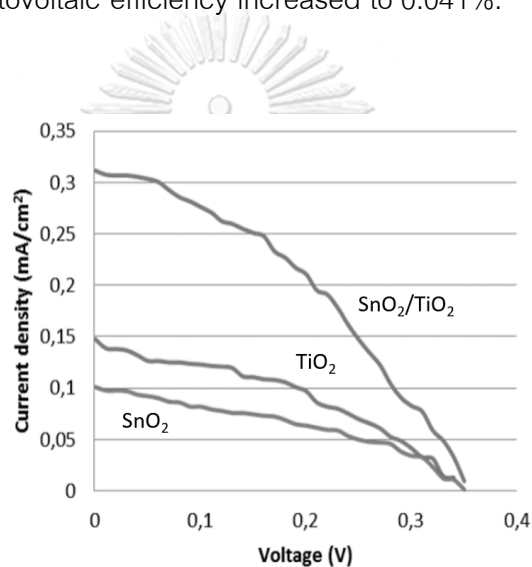
Figure 3.*4* I-V characteristics of DSSCs [58]

Javed et al. [59] successfully modified TiO_2 nanohexagon arrays (TNHAs) with SnO_2 using a one-step facile immersion and the coated onto the FTO glass. The photoanode based on the SnO_2/TNHAs in SnO_2 quantities of 0.25 mol/L K_2SnO_3 precursor exhibited higher short-circuit current, open-circuit voltage and the photovoltaic performance, compared with that based on pure TNHAs (Seen as in Figure 3.5). The photovoltaic efficiency increased up to 6.43%. The presence of SnO_2 in DSSCs led to a 134% improvement in DSSC conversion efficiency.
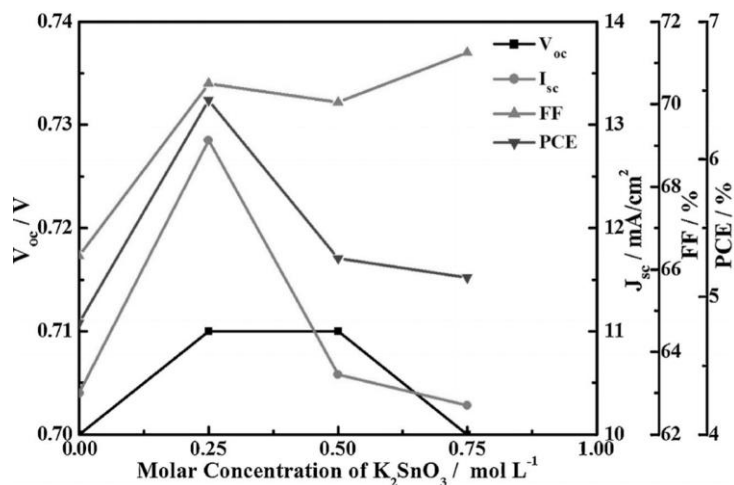
Figure 3.5 Variations of the photovoltaic Properties of the DSSCs based on the
SnO$_2$/TNHAs with various molar concentrations of K$_2$SnO$_3$ [59]

3.2 The multi-layered structure of the TiO$_2$ electrode of DSSCs

Wang et al. [60] employer the bilayer single-crystalline photoanode of TiO$_2$ nanoparticle (HNP) as underlayer and a TiO$_2$ spindle (SP) as overlayer (HNP/SP) was shown in Figure 3.6. HNP has a fast electron transport and large effective surface area. In addition, TiO$_2$ spindles had a direct electron transport pathway and strong light scattering effect. The photoelectric conversion efficiency increased up to 8.65% DSSC with for HNP/SP electrode, which is 25% higher than that of DSSC with HNP/HNP electrode and far superior to that of DSSC with SP/SP electrode.
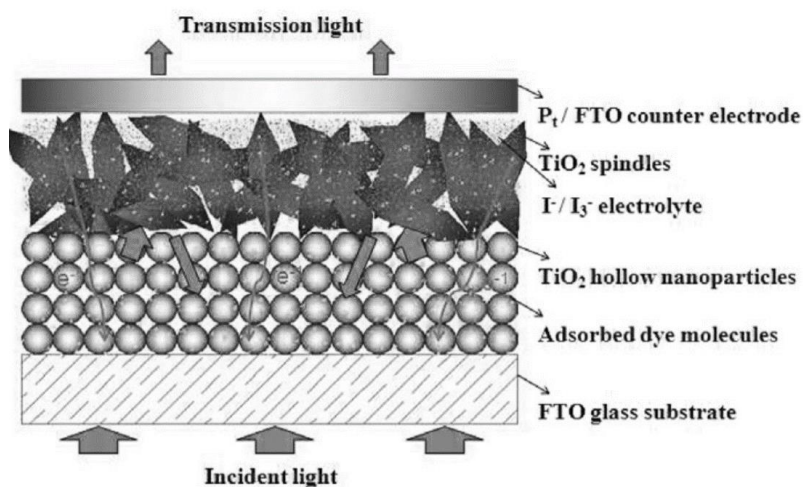
Figure 3.6 Schematics of the DSSC with the bilayer HNP/SP electrode [60]

Zhao et al. [61] employed TiO_2 double light-scattering layers (TiO_2-DLL) of the photoelectrode, consisting of overlayer of TiO_2 hollow spheres (TiO_2-HS) and underlayer of TiO_2 nanosheets (TiO_2-NS) in dye-sensitized solar cells (DSSCs) was shown in Figure 3.7. The IV-test measurement was performed under constant irradiation of 100 mW/cm^2. The TiO_2-DLL film achieved the highest conversion efficiency up to 5.08%, which is 23.3% higher than that of the DSSC with TiO_2-HS film and 8.3% higher than that of the DSSC with TiO_2-NS film. This is attributed to TiO_2-DLL film having a relatively high specific surface area and enhanced light-scattering capability.
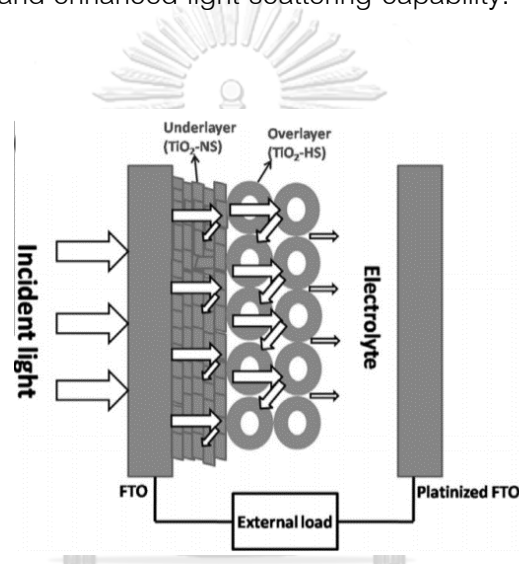
Figure 3.7 Schematic diagram of DSSCs based on TiO_2 double layer film [61]

Wu et al. [62] employed double-layered TiO_2 photoelectrode, consisting of hierarchical TiO_2 flowers (HTFs) as the overlayer and TiO_2 nanoparticles (TNPs) as the underlayer for dye-sensitized solar cells (DSSCs) was shown in Figure 3.8. The double layered photoanode was prepared via a mild and simple one-step hydrothermal reaction of TiO_2 nanoparticles/FTO glass substrate in an alkaline solution. For an underlayer, TNPs was 20 nm in diameter and served as a transparent photoanode for efficient dye adsorption. The overlayer consisting of HTFs was 3–5 mm in diameter that was embedded on TiO_2 nanosheets enhanced light-scattering and fast electron transport. This novel double layered photoanode achieved the highest conversion efficiency up to of 7.4%, which was higher than that of single-layered TNP-based photoanodes.
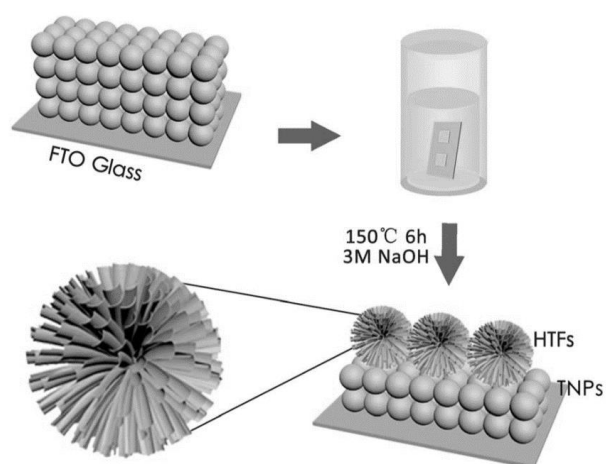
Figure 3.*8* Schematic of the fabrication process of the double layered photoanode via hydrothermal reaction in alkaline solution [62]

CHAPTER 4

EXPERIMENTAL

This chapter refers to all materials, methods of preparation, and characterization of dye-sensitized solar cells. The chapter consists of 6 parts: (I) Materials; (II) Preparation of TiO_2 and modified TiO_2 sols; (III) Preparation of components of dye-sensitized solar cells; (IV) Fabrication of dye-sensitized solar cells; (V) The study of physical characterization; and (V) The electrochemical properties of dye-sensitized solar cells.

4.1 Materials used in the study

Titanium (IV) isopropoxide (Ti[OCH(CH_3)$_2$]$_4$, TTIP), nitric acid (70%, HNO_3), sodium hydroxide (NaOH), lithium iodide (LiI), iodine (I_2), 4-tert- butylpyridine (4-TBP), ammonium sulfate ((NH_4)$_2SO_4$), cobalt nitrate hexahydrate (Co(NO_3)$_2$*6H_2O), and manganese (II) chloride tetrahydrate ($MnCl_2 \cdot 4H_2O$) were purchased from Sigma-Aldrich. Tin (II) acetate (Sn(CH_3CO_2)$_4$) was purchased from Sigma. Ethanol (C_2H_5OH), acetone (C_3H_6O) and acetonitrile (C_2H_3N) were purchased from QREC Chemical. Sulfuric acid (97%, H_2SO_4) was purchased from Merck. Di-tetrabutylammonium cis-bis (isothiocyanato) bis(2,2'-bipyridyl-4,4'-dicarboxylato) ruthenium (II) dye (N719), sealing film (25 μm thick sealing film) and fluorine-doped tin oxide (FTO) conducting glass with a thickness of 2 mm and a resistance of 15 $Ω/cm^2$ were purchased from Solaronix SA (Switzerland). All other chemical reagents in this study were analytical reagent grade and used without further purification.

4.2 Preparation of TiO_2 and modified TiO_2 sols

4.2.1 Preparation of TiO_2 sol

TiO_2 was synthesized via a sol-gel method using titanium (IV) isopropoxide (TTIP) and nitric acid as a precursor and a catalyst, respectively. The molar ratio of TTIP, deionized water and nitric acid was kept constant at 1:12:0.087. First, adding TTIP to a solution of nitric acid in deionized water. After adding TTIP, white precipitate was instantaneously formed. The mixture was mixed for three days under vigorously stirring at room temperature until clear homogeneous sol was obtained. Then the pH of the clear sol was adjusted in the cellulose membrane. Distilled water used in the dialysis process was changed daily until a pH of sol reached 3.5. Finally, TiO_2 sol was kept in a refrigerator until further use.

4.2.2 Preparation of modified TiO_2 sols

In this research, the precursors of manganese, cobalt, and tin were manganese (II) chloride tetrahydrate ($MnCl_2 \cdot 4H_2O$, cobalt nitrate hexahydrate ($Co(NO_3)_2 * 6H_2O$), or tin (II) acetate ($Sn(CH_3CO_2)_4$) respectively. The desired amount of each precursor was shown in Table 4.1 to be dissolved in deionized water. Then its pH was adjusted to 3.5 by using 5 M of nitric acid. The solution was then added to TiO_2 sol under constant stirring according to the desired amount of metal oxide at 0, 0.1, 0.5, 1.0 and 3.0%wt. The mixture was continuously stirred for 30 minutes or until homogeneity was obtained at room temperature. The mixture was re-stirred at room temperature prior to the spray coating process.

Table 4.1 The amount of the second metal oxide precursor needed to add to TiO_2 sol.

Sol	Precursor	%wt.	The volume of TiO_2 sol (ml)	The volume of precursor solution (ml)
MnO_2/TiO_2	0.5 g of $MnCl_2 \cdot 4H2O$ in 50 ml of DI water	0.1	50.00	0.13
		0.5	50.00	0.65
		1.0	50.00	1.30
		3.0	50.00	3.99
CoO/TiO_2	0.5 g of $Co(NO_3)_2 \cdot 6H_2O$ in 50 ml of DI water	0.1	50.00	0.33
		0.5	50.00	1.7
		1.0	50.00	3.32
		3.0	50.00	10.2
SnO_2/TiO_2	0.5 g of $Sn(CH_3CO_2)_4$ in 50 ml of DI water	0.1	50.00	0.14
		0.5	50.00	0.68
		1.0	50.00	1.37
		3.0	50.00	4.19

Note: TiO_2 sol 100 ml = TiO_2 1.80 g

4.3 Preparation of components of dye-sensitized solar cells

4.3.1 Preparation of TiO_2 photoanode and modified TiO_2 electrode

The electrode was prepared on FTO glasses, which was cut to small glass pieces with a dimension of 2.0 × 2.5 cm^2. The glass pieces were cleaned three times by using detergent solution, acetone, and ethanol, respectively, in an ultrasonic bath for 15 minutes in each step. Finally, the glasses were wiped off using a tissue wetted with ethanol. Finally, FTO glasses were kept in an ethanol solution until further used. The FTO glasses were dried with a blow dryer to dry when used.

The glass was covered in aluminum foil, in which a hole with a diameter of 0.5 cm was cut. The schematic diagram of the layout of the electrode was displayed in Figure 4.1 as follows). After that, TiO_2 or modified TiO_2 sol was deposited on the FTO glass using an ultrasonic spray coater. The liquid feed rate to the ultrasonic nozzle for

TiO$_2$ or modified oxide/TiO$_2$ sol was set at 1 mL/min. The power for frequency generator of the ultrasonic nozzle was set at 3.5-3.6 W and level of ultrasonic machine movement speed was level 4 out of 5 speed.
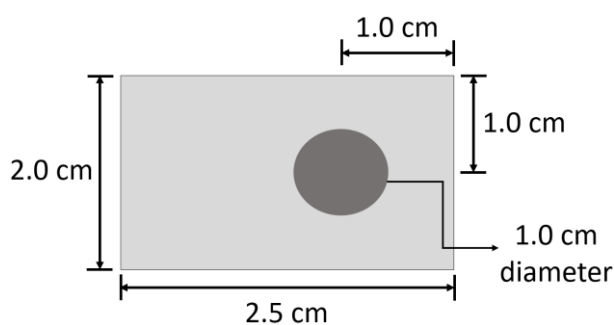
Figure 4.1 The schematic diagram of the layout of photoanode

Five hundred coats of TiO$_2$ or modified /TiO$_2$ was applied. This produced a film thickness of approximately 10 μm. Finally, an electrode was calcined at 400ºC for 2 hours and left at room temperature to be cooled.

To apply the dye, an electrode was gradually heated to 90ºC and was held for 10 minutes to remove water. Then the electrode was immersed in the di-tetrabutylammonium cis-bis (isothiocyanato) bis(2,2'-bipyridyl-4,4'-dicarboxylato) ruthenium (II) dye (N719) solution for 20-24 hours in the dark. Finally, the electrode was washed with ethanol to remove excess dye and was dried with a blow dryer.

4.3.2 Preparation of the platinum film counter electrode

The platinum film counter electrode was prepared on FTO glasses, which was cut to small glass pieces with a dimension of 2.0 × 2.5 cm^2. Then two small holes with a diameter of 1 mm were drilled on FTO glasses for subsequent filling of electrolyte solution after cell assembly was completed. Next, the glass pieces were cleaned three times with the same dimension as described in Section 4.3.1.

To apply a platinum film on FTO glasses. The sputtering area was restricted to 2.0 × 2.0 cm^2 in size by masking the excess area on the glass. Finally, the platinum film was deposited on the FTO glass using ion sputtering machine (JEOL: JFC1100E) at 10 mA of ion current for six minutes. The schematic diagram is displayed in Figure 4.2.
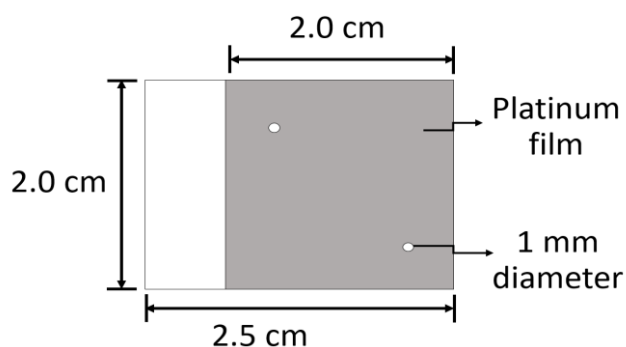
Figure 4.2 The schematic diagram of the platinum film counter electrode

4.3.3 Preparation of ruthenium dye solution

N719 dye - di-tetrabutylammonium cis-bis (isothiocyanato) bis(2,2'-bipyridyl-4,4'-dicarboxylato) ruthenium (II) - powder was weighed and was dissolved in ethanol to produce a 0.3 mM dye solution. The mixture was sonicated in an ultrasonic bath for 30 minutes or until a homogeneous solution was obtained.

4.3.4 Preparation of electrolyte solution

The electrolyte solution was a mixture of 0.05 M iodine (I$_2$), 0.5 M lithium iodide (LiI) and 0.5 M 4-tert-butylpyridine (4-TBP) in acetonitrile. The molar ratio between I$_2$, LiI and 4-TBP were 0.01:0.1:0.1. The electrolyte solution prepared by mixing 0.38 g of iodine (I$_2$), 2 g of lithium iodide (LiI) and 2.20 mL of 4-tert-butylpyridine (4-TBP) in 30 mL of acetonitrile. Finally, the solution was stirred for 30 minutes or until homogeneity was obtained.

4.4 Fabrication of dye-sensitized solar cells

The dye-sensitized solar cells were configured in a typical sandwiched cell by combining the two electrodes. The TiO_2 or modified TiO_2 electrode was placed on the top of the platinum film electrode glass with a 25 µm thick sealing film inserted in the middle. The sealing film was cut into a square with a dimension of 2.0 × 2.0 cm^2 and the middle area of film hollowed out. The drawing of the sealing material was shown in Figure 4.3. Finally, the two electrodes with sealing sheet were clipped together with 2 clips on the opposite end of the glass and the sealing film was melted to seal their electrodes by a heat gun.
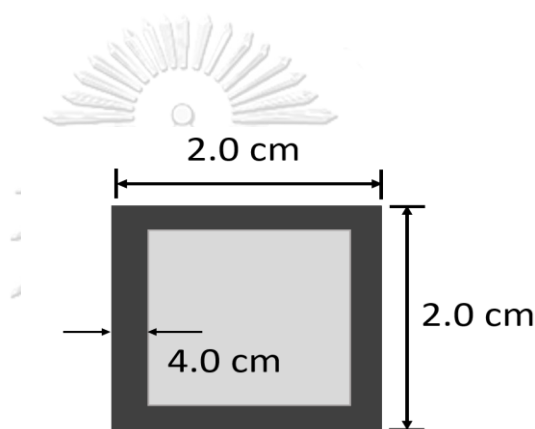
Figure 4.3 The shape of sealing material as a sealant between two electrodes

To add the electrolyte solution, the solution was added dropwise on top of one hole until the solution completely filled and spilled out of the other hole. The schematic diagram of the component of dye-sensitized solar cells was shown in Figure 4.4. After that, both holes were sealed off using a clear adhesive tape to prevent the electrolyte solution from leaking out. Finally, the resulting cell was ready for measurement.
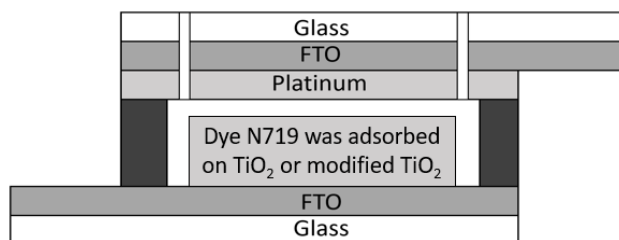
Figure 4.4 The schematic diagram of the component of a DSSCs

4.5 The study of physical characterization

4.5.1 N_2 physisorption

N_2 physisorption was measured using a Micromeritics Chemisorb 2750 to determine the BET specific surface area of TiO_2 and modified TiO_2. The powder using TiO_2 or modified TiO_2 powder was preheated at 200ºC for 1 hour under pure N_2 flow. After that, a carrier gar of 30% N_2/He mixture flowed through the sample. Then the catalyst was cooled under liquid nitrogen, during which 30% N_2/He mixture was adsorbed on the catalyst surface until completion. Finally, the catalyst was left at room temperature and detected the amount of nitrogen desorption was measured to determine specific surface area.

4.5.2 X-ray diffractometry (XRD)

The X-ray diffractometry (XRD) was performed using a SIEMENS D5000 X-ray diffractometer with CuK_α radiation (λ = 1.54439 Å) and Ni filter to determine the crystalline phase and crystallite size of TiO_2 or modified TiO_2. The spectrum was scanned at a rate of 0.04 min^{-1} in the 2θ range of 20 to 80º at room temperature.

To determine the crystallite size of the catalyst was to be calculated by the Debye-Scherrer equation (4.1) [63].

$$D = \frac{K\lambda}{\beta cos\theta} \qquad (4.1)$$

where D is the average size of the crystal, K is a dimensionless shape factor, λ is the x-ray wavelength, β is the x-ray diffraction broadening (radian), and θ is observed peak angle (degree).

4.5.3 UV-Visible spectroscopy (UV-Vis)

UV-Visible spectroscopy (UV-Vis) was performed using a Perkin Elmer Lambda 650 UV-Visible spectrophotometer to determine the amount of dye adsorbed on the photoanode electrode, the band gap energy of catalysts and reflection of electrodes.

4.5.3.1 Determine the amount of dye adsorbed on photoanode electrodes

The absorption peak at 310 nm was obtained by a UV-Visible spectrophotometer to determine the amount of N719 dye on TiO_2 and modified TiO_2 film. The dye on the film was dissolved in a solution of 0.1 M NaOH in deionized water and ethanol with molar ratio 1:1 volume fraction.

4.5.3.2 Determine the band gap energy of catalysts and reflection of electrodes

The light absorption of the catalysts was evaluated by UV-Visible spectrophotometer to determine the absorption spectra of TiO_2 and modified TiO_2 in the wavelength range of 200 to 800 nm with a 1 nm step size.

The UV-Vis spectrum can be used to determine the band gap energy of semiconductor material by plotting the graph between $(\alpha h\nu)^{(1/n)}$ versus photon energy ($h\nu$).

where α is the optical absorption coefficient, $h\nu$ is the photon energy and n is The power factor n is allowed direct (n = 0.5) forbidden direct (n = 1.5), allowed indirect (n = 2), and forbidden indirect (n = 3) transitions. In this research the power factor was using direct type (n = 0.5)

4.5.4 Inductively coupled plasma-atomic emission spectroscopy (ICP-AES)

Inductively coupled plasma-atomic emission spectroscopy (ICP-AES) was performed using a 2100 DV spectrometer to determine the amount of metal deposited on the surface of TiO_2. For analysis, modified TiO_2 powder was digested in a solution of sulfuric acid (97%, H_2SO_4) and ammonium sulfate (($NH_4)_2SO_4$) For 0.05 g of modified TiO_2 powder, one used 7 ml of 97% H_2SO_4 in deionized water 10 ml and 2.7 g of ($NH_4)_2SO_4$, while being constantly stirred until the homogenous solution was obtained. The solution was then diluted up to 50 ml with deionized water. Finally, the concentration of metal in the determined using a calibration curve.

4.6 The electrochemical properties of dye-sensitized solar cells

The electrochemical properties of dye-sensitized solar cells were determined by an IV-tester with impedance spectrometer (Autolab /PGSTAT101). The current-voltage characterization of dye-sensitized solar cells was conducted under a 50W daylight LED lamp with a light irradiance of 15 mW/cm^2 condition. In this experiment, the distance between the dye-sensitized solar cells and the light source was adjusted in order to maintain the same light intensity in the every measurement of electrochemical properties of DSSC. The light intensity of daylight LED lamp was calibrated by a monocrystalline silicon solar cell panel module (size 5W) to determine the required distance between sample solar cell and light source that produced a light intensity of 15 mW/cm^2. [64, 65].

The short current density (J_{SC}), the open circuit voltage (V_{OC}), and the fill factor (FF) were used to calculate the photovoltaic efficiency of a dye-sensitized solar cell (η). An area of our solar cell was 0.196 cm^2.

The efficiency of a dye-sensitized solar cell (η) was calculated using Equation 4.4.

$$\eta = \frac{V_{OC} J_{sc} FF}{P_{in}} \text{ x } 100\% \qquad (4.4)$$

Where FF is the fill factor, V_{OC} is the open circuit voltage (V), J_{SC} is the short current density (mA/cm^2), and P_{in} is the incident light power (W/cm^2).

CHAPTER 5

RESULTS AND DISCUSSION

This chapter presents the performance of DSSCs with the addition of varying amount of mixed metal oxides such as MnO_2, CoO or SnO_2 into TiO_2 electrode and the performance of DSSCs with the double-layered electrode.

5.1 Modification of TiO_2 electrode layer by adding the second metal oxide

5.1.1 Modification of TiO_2 electrode layer by adding MnO_2

TiO_2 sol was prepared by a sol-gel method and was modified by adding the varying amount of MnO_2 into TiO_2 at 0.1, 0.5, 1.0, and 3.0%wt. The MnO_2/TiO_2 sol was coated 500 times on an FTO glass substrate by ultrasonic spray coater and was calcined at 400ºC for two hours. The TiO_2 modified with MnO_2 has been widely studied because they are environmentally friendly, non-toxic, and inexpensive. MnO_2 is the metal oxide semiconductor used as a cathode electrode in dry battery, ultracapacitor, and catalyst [66]. Moreover, MnO_2 has a direct band gap energy of 2.5 eV. So it can decrease the band gap energy of TiO_2 and increase active surface area of TiO_2 [53].

The X-ray diffraction (XRD) patterns of pure TiO_2 and various MnO_2/TiO_2 were shown in Figure 5.1. The XRD peaks were detected at 2θ of 25.4º, 38.0º, 48.1º, 54.4º, 56.5º, 69.3º, and 75.3º, which were assigned to anatase phase TiO_2. The XRD peaks at 27.4º, 36.1º, 41.1º, and 62.7º corresponded to rutile phase of TiO_2, while a small peak at 2θ of 30.8º was assigned to the brookite phase of TiO_2 [67]. These diffraction peaks were according to JCPDS (joint committee on powder diffraction standards) card numbers 21-1272, 21-1276, and 29-1360 confirming the anatase, rutile and brookite phase of TiO_2 phase with tetragonal geometry, respectively.
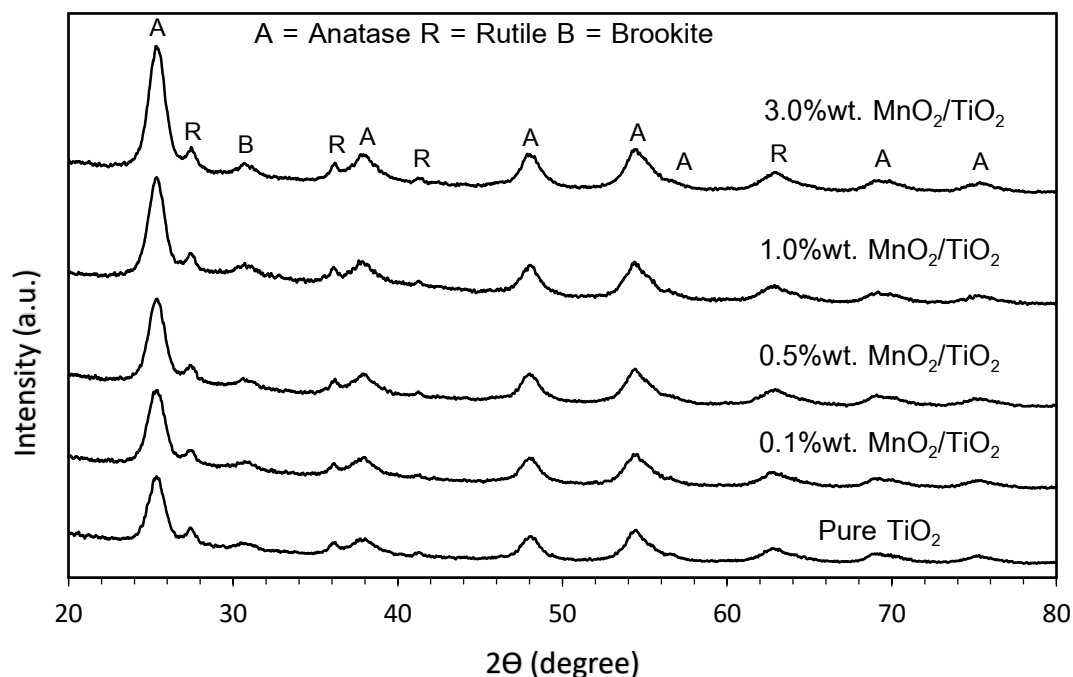
Figure 5.1 XRD patterns of MnO_2/TiO_2 powders at various percentages of MnO_2

The main phase was anatase with some amount of rutile and little amount of brookite in all samples. Moreover, no XRD peak associating with MnO_2 was detected due to the small amount of MnO_2 that was added to the TiO_2 sol. Therefore, we did not observe any peak of MnO_2 in MnO_2/TiO_2.

The crystallite size of TiO_2 phase in pure TiO_2 and various of MnO_2/TiO_2, which was calculated using Debye-Scherer equation, was listed in Table 5.1 and the method of crystallite calculation was presented in Appendix A. The size of anatase in pure TiO_2 was 8.1 nm. When a small amount of MnO_2 at 0.1 to 3%wt. was added to TiO_2, the crystallite size became smaller. This suggested that addition of MnO_2 retarded the growth of TiO_2 crystals.

The phase composition of TiO_2 and MnO_2/TiO_2 were displayed in Table 5.1. All sample consists of primarily anatase phase and some rutile and brookite phases. The calculation of TiO_2 weight fraction was shown in Appendix B. Variation in MnO_2 content had some effect on the phase composition.

The amount of MnO_2 on MnO_2/TiO_2 film was confirmed by using Inductively coupled plasma atomic emission spectroscopy (ICP-AES). The calculation for the amount of metal oxide from ICP was demonstrated in Appendix E. From Table 5.1, the content of MnO_2 in TiO_2 was slightly lower than expected value probably due to a variation in the amount of TiO_2 present in the sol.

The specific surface area was determined using N_2 physisorption analysis and single-point BET analysis. The specific surface area of 0.1 - 0.5%wt. MnO_2/TiO_2 was increased compare with pure TiO_2 because of its smaller crystallite size than TiO_2. However, the surface area of 1.0 - 3.0%wt. MnO_2/TiO_2 was decreased due to the surface area of pure TiO_2 nanoparticles was blocked in pore or their own surface with a large amount of MnO_2.

Table 5.1 Crystallite size, specific surface area, amount of MnO_2 and weight fraction of anatase, rutile and brookite of pure TiO_2 and MnO_2/TiO_2 powders calcined at 400ºC for two hours

Sample	Crystallite size (nm)	Specific surface area (m²/g)	Amount of MnO_2 from ICP (%wt.)	Weight fraction		
				W_A	W_R	W_B
Pure TiO_2	8.1	104.3	-	0.66	0.14	0.20
0.1%wt. MnO_2/TiO_2	7.1	107.9	0.09	0.68	0.10	0.21
0.5%wt. MnO_2/TiO_2	7.1	111.4	0.48	0.71	0.10	0.19
1.0%wt. MnO_2/TiO_2	7.5	102.0	0.91	0.73	0.10	0.17
3.0%wt. MnO_2/TiO_2	7.9	100.4	2.80	0.74	0.09	0.17

W_A: Weight fraction of anatase phase

W_R: Weight fraction of rutile phase

W_B: Weight fraction of brookite phase

The band gap energy of pure TiO_2 and various MnO_2/TiO_2 was calculated and estimated by a Tauc plot (see Figure 5.2). The band gap energy was reported in Table 5.2. The band gap energy of MnO_2/TiO_2 become smaller as MnO_2 content was increased, resulting in greater ability to absorb light in the visible region [53]. In DSSC, doping of metal oxide brought about the formation of new energy level to facilitate electron transport of dye electron [68].

Figure 5.2 UV-visible absorption characteristic between $(\alpha h\nu)^{(1/n)}$ versus photon energy $(h\nu)$ of pure TiO_2 and MnO_2/TiO_2

Table 5.2 Band gap energy of TiO_2 and various MnO_2/TiO_2 that were calcined at 400°C for 2 hours

Sample	Wavelength (nm)	Band gap energy (eV)
Pure TiO_2	394	3.15
0.1%wt. MnO_2/TiO_2	403	3.08
0.5%wt. MnO_2/TiO_2	407	3.04
1.0%wt. MnO_2/TiO_2	421	2.94
3.0%wt. MnO_2/TiO_2	438	2.83

To determine the amount of ruthenium-based N719 dyes adsorbed on MnO_2/TiO_2 film, the N719 dye was dissolved in a mixture of 0.1 M NaOH solution and ethanol solution at a volume ratio of 1:1. The amount of dye solution was measured using a UV-spectrophotometer at a wavelength of 310 nm. The measurement was performed for three electrode samples for each condition of MnO_2/TiO_2. The calculation

of the amount of dye adsorbed was shown in Appendix C. The average amount of dyes measured was listed in Table 5.3. The amount of N719 dye adsorbed on MnO_2/TiO_2 film was greater than that on pure TiO_2 film. An increase in the amount of N719 dye was consistent with the specific surface area (see Table 5.1). The film with 0.5%wt. MnO_2/TiO_2 contained the largest concentration of dry at $3.16 \pm 0.005 \times 10^7$ mol / cm^2.

Table 5.3 Concentration of N719 dye contained in the pure TiO_2 and MnO_2/TiO_2 electrodes were calcined at 400°C for 2 hours

Sample	Concentration of N719 dye ($\times 10^7$ mol/cm^2)
Pure TiO_2	1.92 ± 0.009
0.1%wt. MnO_2/ TiO_2	1.95 ± 0.006
0.5%wt. MnO_2/ TiO_2	3.16 ± 0.005
1.0%wt. MnO_2/ TiO_2	2.72 ± 0.011
3.0%wt. MnO_2/ TiO_2	1.98 ± 0.006

The addition of MnO_2, which possessed a different band gap incorporated an extra energy level between the oxidized dye and the TiO_2 surface, thereby reducing interfacial recombination losses in dye molecules. Consequently, the photovoltaic efficiency of DSSCs was enhanced. One approach was the coating of nanocrystalline metal oxide film. This approach enhanced the physical separation of injected electrons for the oxidized dye redox couple, thereby retarding the recombination reactions [69].

MnO$_2$/TiO$_2$ nanocomposite modified the electronic energy band structure of TiO$_2$. So MnO$_2$/TiO$_2$ absorbed visible light due to its narrowing band gap. The schematic diagram for the excitation of MnO$_2$/TiO$_2$ was shown in Figure 5.3. The electron with high energy transferred from the excited dye molecule to the conduction band of anatase TiO$_2$ and then to the conduction band of MnO$_2$. This electron transfer effectively retarded recombination of the electron [70]. Therefore, the photocatalytic efficiency was improved.
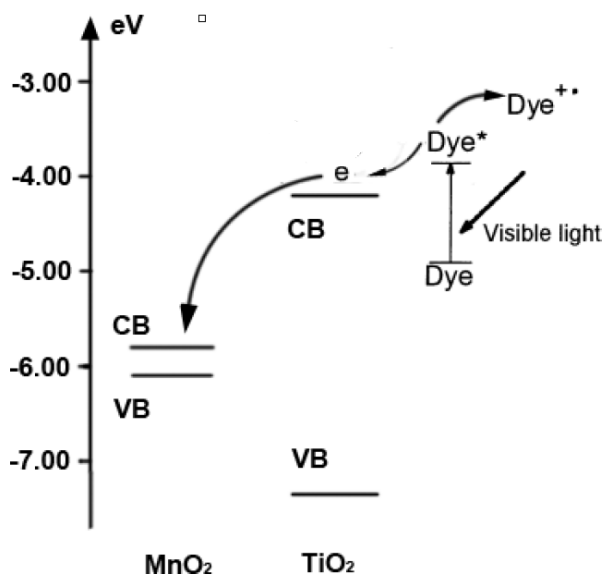
Figure 5.3 The schematic diagram for the excitation of MnO$_2$/TiO$_2$ under visible light irradiation [70]

The I-V characteristics and efficiencies of DSSCs with TiO$_2$ and MnO$_2$/TiO$_2$ electrodes were measured in five replicates of DSSC. Each DSSC was individually prepared and tested. The efficiencies displayed in Table 5.4 was the average value of five DSSCs and the corresponding standard deviation. The valve of each individual cell was shown in Appendix F.

In this research, N719 was employed as the dye for DSSC. TiO_2 and MnO_2 were prepared by sol-gel methods and were coated on fluorine doped tin oxide (FTO) conductive glass. The glass was calcined at 400ºC for two hours. A DSSC was assembled with platinum counter electrode, separated by a sealing film. The electrolyte solution composed of lithium iodide (LiI), iodine (I_2), and 4-tert-butylpyridine (4-TBP) in acetonitrile (molar ratio LiI:I_2:4-TBP = 0.1:0.01:0.1) was added to the space between the two FTO glasses. Then we measured a DSSC for open circuit voltage (V_{OC}) and short-circuited current density (J_{SC}). After that, the fill factor and the photovoltaic conversion efficiency of solar cells under a 50W daylight LED illumination with a light irradiance of 15 mW/cm^2 were determined.

The Electrochemical properties and IV-Curve of DSSCs with MnO_2/TiO_2 electrode were listed in Table 5.4 and displayed in Appendix F. The DSSCs with 0.5 %wt. MnO_2/TiO_2 electrode exhibited the highest J_{SC} and V_{OC}. As a result, it had the highest cell efficiency at 4.83 ± 0.36%. This result was attributed to the highest concentration of dye adsorbed on the electrode. In addition, when MnO_2 content exceeded 0.5 %wt., the J_{SC} and V_{OC} values became lower because the presence of MnO_2 shifted the position of the valence band. The electron transfer was harder to achieve [68]. Therefore, MnO_2 turned into a recombination center.

Table 5.4 Electrochemical properties of DSSCs with MnO_2/TiO_2 electrode coated with N719 dye was calcined at 400ºC for 2 hours

MnO_2/TiO_2 (%wt.)	V_{OC} (V)	J_{SC} (mA/cm^2)	Fill factor	η(%)
0	0.59	1.50	0.55	3.12 ± 0.32
0.1	0.60	1.53	0.48	2.92 ± 0.40
0.5	0.66	1.74	0.64	4.83 ± 0.36
1.0	0.57	1.63	0.42	2.57 ± 0.46
3.0	0.48	0.57	0.38	0.70 ± 0.22

5.1.2 Modification of TiO_2 electrode layer by adding CoO

CoO/TiO_2 sol was prepared via a sol-gel method. The amount of cobalt oxide added to TiO_2 sol was 0.1, 0.5, 1.0, and 3.0%wt. The CoO/TiO_2 electrode was prepared using an ultrasonic spray coater. First, the CoO/TiO_2 sol was sprayed on the FTO glass substrates 500 times. Next, the electrode was calcined at 400ºC for two hours. The CoO/TiO_2 possessed a narrower band gap, thereby enhancing the absorption of solar light. As a result, the photovoltaic efficiency of DSSCs was enhanced [57].

The XRD patterns of CoO/TiO_2 were shown in Figure 5.4. Similar diffraction peaks were observed across all samples. This suggested that the sample consisted of anatase TiO_2 as the main phase with some rutile and brookite. The phase composition of TiO_2 was calculated and was shown in Appendix B. From Table 5.5, no noticeable difference was observed in all sample. The intensity of anatase peaks were changed when increasing CoO contents probably due to large amount of CoO can block the growth of the anatase crystalline before it was calcined.
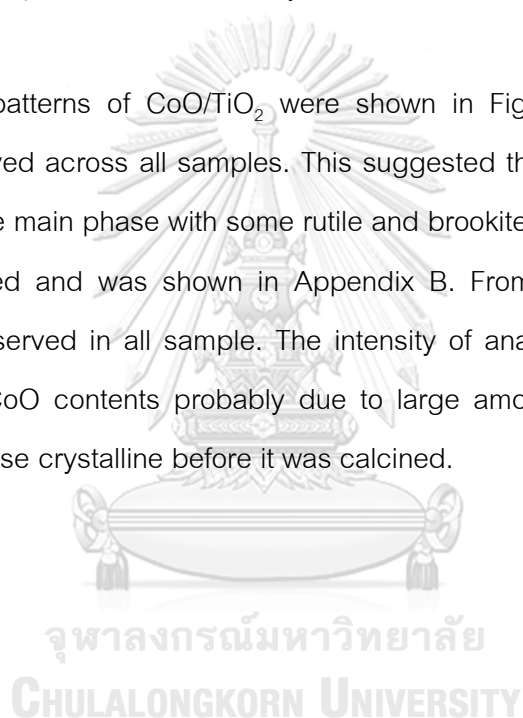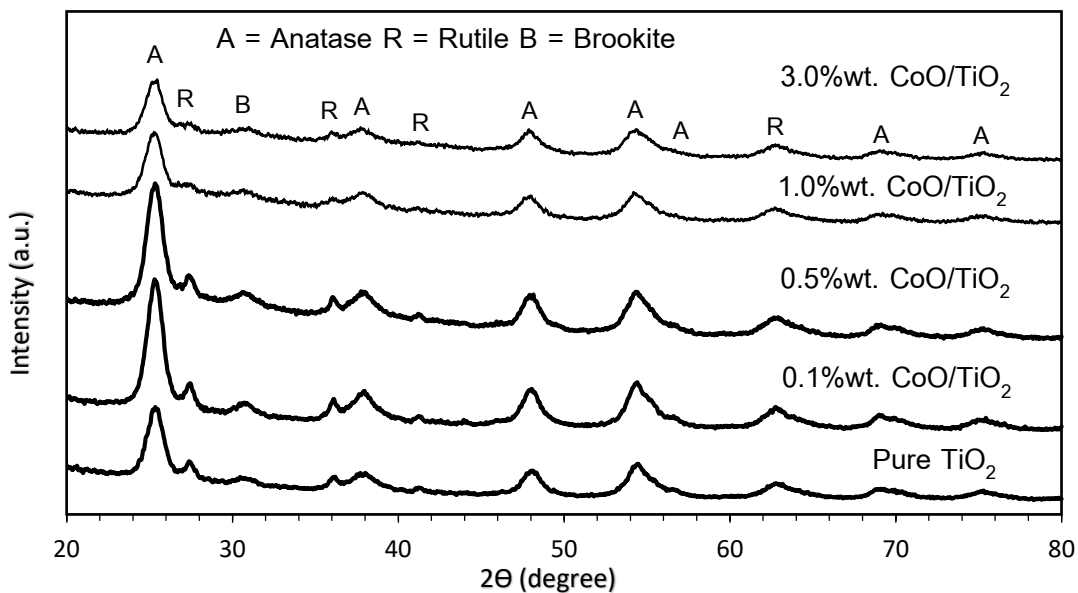
Figure 5.4 XRD patterns of CoO/TiO$_2$ powders at various percentages of CoO

The crystallite size of CoO/TiO$_2$ was shown in table 5.5. The CoO/TiO$_2$ contents showed crystallite size to little change than pure TiO$_2$ when the amount of CoO was 0.1%wt. The crystallite size was as 7.6 nm. However, the crystallite size was slightly increased when the amount of CoO into 0.5-3.0%wt. CoO. That result shows that a little CoO can block the growth of the crystallize size before it was calcined. However, the irregular with more amount of CoO than 0.5%wt had changed of the crystal edge of faceted TiO$_2$ crystal resulting implying higher crystallinity. [71].

The amount of CoO on CoO/TiO$_2$ was measured using ICP-AES analysis. The calculation for the amount of cobalt oxide from ICP was demonstrated in Appendix E. From Table 5.5, the content of CoO/TiO$_2$ was slightly lower than the intended value probably because a variation in the amount of TiO$_2$ present in the sol.

The specific surface area of CoO/TiO_2 powder was determined as shown in Table 5.5. Modification of CoO/TiO_2 was no obvious changed. 0.1%wt CoO/TiO_2 was little change. However, TiO_2 with 0.5-3.0%wt. CoO was little reduced due to the change of the crystal edge of TiO_2 was reduced surface area [71]. It corresponded to the size of the crystal that grows in measurement.

Table 5.5 Crystallite size, specific surface area, amount of CoO and weight fraction of anatase, rutile, and brookite of pure TiO_2 and CoO/TiO_2 powders calcined at 400ºC for two hours

Sample	Crystallite size (nm)	Specific surface area (m^2/g)	Amount of MnO_2 from ICP (%wt.)	Weight fraction		
				W_A	W_R	W_B
Pure TiO_2	8.1	104.3	-	0.66	0.14	0.20
0.1%wt. CoO/ TiO_2	7.6	104.9	0.09	0.70	0.12	0.18
0.5%wt. CoO/ TiO_2	7.7	103.1	0.50	0.71	0.12	0.17
1.0%wt. CoO/ TiO_2	7.8	102.9	0.94	0.72	0.07	0.21
3.0%wt. CoO/ TiO_2	8.0	101.8	2.62	0.71	0.09	0.20

W_A: Weight fraction of anatase phase

W_R: Weight fraction of rutile phase

W_B: Weight fraction of brookite phase

The band gap energy of pure TiO_2 and various CoO/TiO_2 were shown in Figure 5.5 and Table 5.6. The band gap energy of various CoO/TiO_2 was greatly reduced with an increase of CoO concentration. When 3.0%wt. CoO was added to TiO_2 sols, the band gap energy was reduced from 3.15 to 2.50 eV. This result can be explained of the band gap was reduced due to the band gap energy of CoO was shown at 2.2 eV [72] when increasing the content of CoO in TiO_2 will result valence band of CoO/TiO_2 was decreased from insert of valence band of CoO increasing [57].
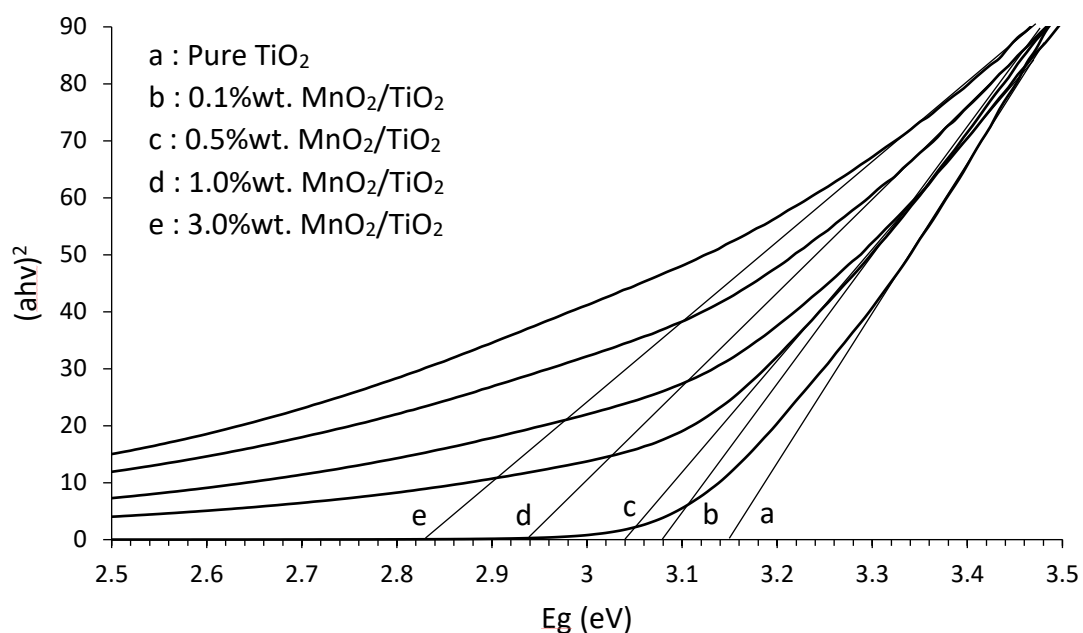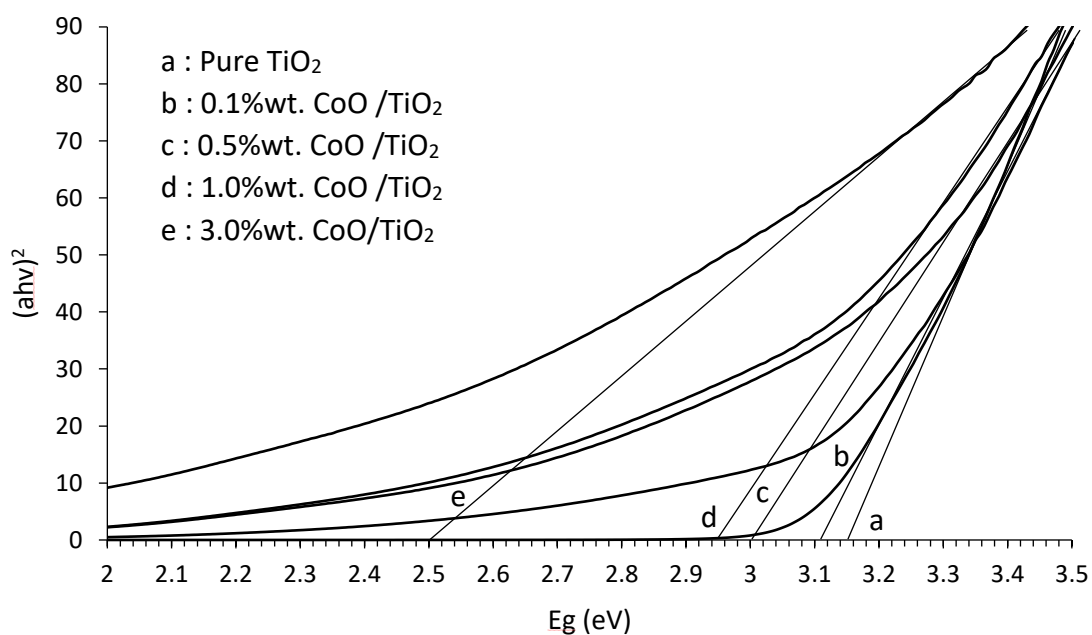
Figure 5.5 UV-visible absorption characteristic between $(\alpha h\nu)^{(1/n)}$ versus photon energy (hν) of pure TiO_2 and CoO/TiO_2

Table 5.6 Band gap energy of TiO_2 and various CoO/TiO_2 that were calcined at 400ºC for 2 hours

Sample	Wavelength (nm)	Band gap energy (eV)
Pure TiO_2	394	3.15
0.1%wt. CoO/ TiO_2	399	3.11
0.5%wt. CoO/ TiO_2	413	3.00
1.0%wt. CoO/ TiO_2	420	2.95
3.0%wt. CoO/ TiO_2	496	2.50

The concentration of N719 dye adsorbed on the CoO/TiO$_2$ photoanode electrode was shown in Table 5.11. The calculation of the amount of dye adsorbed was shown in Appendix C. The concentration of N719 results in the amount of dye adsorption of CoO/TiO$_2$ at 0.5, 1.0, and 3.0%wt. CoO was lower than dye adsorption of pure TiO$_2$ same too. The decreasing amount of adsorbed dye at 3.0%wt. was obtained because the more amount of CoO in TiO$_2$ was caused complexes of cobalt and dye molecule on surface area that was affect to adhesion of dyes. The highest amount of adsorbed dye contained 0.1%wt. CoO/TiO$_2$ at 1.95 ± 0.011 × 10^7 mol/cm^2.

Table 5.7 Concentration of N719 dye contained in the pure TiO$_2$ and CoO/TiO$_2$ electrodes were calcined at 400ºC for 2 hours

Sample	Concentration of N719 dye ($\times 10^7$ mol/cm^2)
Pure TiO$_2$	1.92 ± 0.009
0.1%wt. CoO/ TiO$_2$	1.95 ± 0.011
0.5%wt. CoO/ TiO$_2$	1.53 ± 0.014
1.0%wt. CoO/ TiO$_2$	1.31 ± 0.008
3.0%wt. CoO/ TiO$_2$	0.88 ± 0.007

The current-voltage (I-V) characteristics of DSSCs were displayed in Appendix F and Table 5.8. When the amount of CoO was increased, the short-circuited current density (J_{SC}) was increased slightly but the open circuit voltage (V_{OC}) was noticeably reduced. The highest cell efficiency of 3.23 ± 0.40% was obtained with 0.1%wt. CoO/TiO$_2$ as a result of the highest concentration of N719 dye on the electrode. However, when the CoO content exceeded 0.1%wt., the efficiency of DSSCs become lower may be attributed to this unable to retard recombination to the electrons from excitation of dyes sufficiently [56]. In addition, the position of the CoO conduction band was found above that the conduction band position of TiO$_2$ (see Figure 5.6). This may be

the main reason that the electrons from dyes cannot pass easily and cause more recombination.
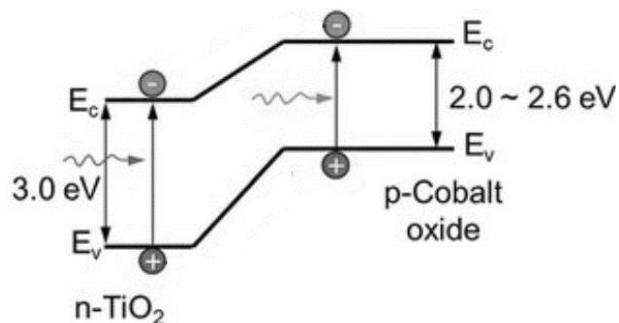
Figure 5.6 The mechanism of photocatalytic of CoO/TiO_2 under visible light irradiation [73]

Table 5.8 Electrochemical properties of DSSCs with CoO/TiO_2 electrode coated with N719 dye was calcined at 400ºC for 2 hours

CoO/TiO_2 (%wt.)	V_{OC} (V)	J_{SC} (mA/cm^2)	Fill factor	η(%)
0	0.59	1.50	0.55	3.12 ± 0.32
0.1	0.55	1.70	0.52	3.23 ± 0.40
0.5	0.51	1.64	0.45	2.49 ± 0.17
1.0	0.49	1.54	0.44	2.20 ± 0.31
3.0	0.28	0.90	0.31	0.61 ± 0.50

5.1.3 Modification of TiO_2 electrode layer by adding SnO_2

SnO_2/TiO_2 sol was prepared via a sol-gel method and added by using the varying amount of SnO_2 into TiO_2 at 0.1, 0.5, 1.0, and 3.0%wt. The SnO_2/TiO_2 electrode was prepared by ultrasonic spray coater. First, the SnO_2/TiO_2 sol was sprayed on the FTO glass substrates 500 times and was calcined at 400ºC for two hours. SnO_2 was used as photoanode in dye-sensitized solar cells because SnO_2facilitated photoelectron transfer and charge separation that suppressed the recombination in the solar cells [58]. Moreover, SnO_2 exhibited high electron mobility of 100-200 cm^2/Vs, which is hundreds of times higher compared with TiO_2. The higher electron mobility promoted the electron transfer in semiconductor oxides [74].

Figure 5.7 shows the XRD patterns of TiO_2 and various SnO_2/TiO_2. The phase composition of TiO_2 was calculated in Appendix B. All diffraction peaks MnO_2/TiO_2 sample confirmed the presence of anatase, rutile and brookite phases of TiO_2 in all SnO_2/TiO_2 samples. No SnO_2 peak was detected in any in all sample because of the small amount of SnO_2 that was added to the TiO_2 sol.
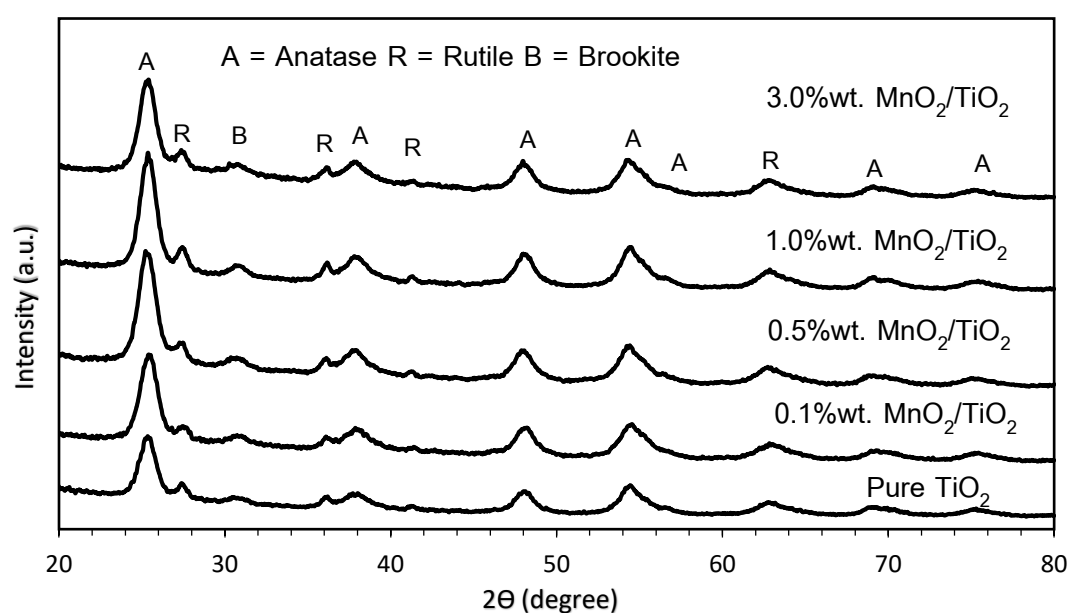
Figure 5.7 XRD patterns of SnO_2/TiO_2 powders at various percentages of SnO_2

All samples were composed of anatase as the major phase and small amount of rutile and brookite phase. The phase composition of TiO_2 in SnO_2/TiO_2 were listed in Table 5.1. The sample calculation of TiO_2 phase composition was shown in Appendix B.

The calculation of the crystallite size was presented in Appendix A. The calculated crystallite size of TiO_2 in SnO_2/TiO_2 was listed in Table 5.13. The size of pure TiO_2 was 8.1 nm when SnO_2 was added to TiO_2, the crystallize size of TiO_2 became smaller because SnO_2 doping tended to hinder the TiO_2 growth.

The ICP-AES results of tin revealed that was presented in the SnO_2/TiO_2 (see in Table 5.9). The actual amount of SnO_2 were slightly lower than the desired valve. The discrepancy of SnO_2 content was a result of a variation in the content of TiO_2 present in the sol.

In Table 5.9 shown, the specific surface area of 0.1 to 1.0%wt. SnO_2/TiO_2 were increased. The highest specific surface area is 0.5%wt. SnO_2/TiO_2 that is 111.0 m2/g. However, the specific surface area of 3.0 %wt. SnO_2/TiO_2 was decreased because of adding SnO_2 in large amount was blocked on TiO_2 surface area.

Table 5.9 Crystallite size, specific surface area, amount of SnO_2 and weight fraction of anatase, rutile, and brookite of pure TiO_2 and SnO_2/TiO_2 powders calcined at 400ºC for two hours

Sample	The crystallite size (nm)	Specific surface area (m^2/g)	Amount of MnO_2 from ICP (%wt.)	Weight fraction		
				W_A	W_R	W_B
Pure TiO_2	8.1	104.3	-	0.66	0.14	0.20
0.1%wt. SnO_2/TiO_2	7.2	106.6	0.10	0.77	0.07	0.16
0.5%wt. SnO_2/TiO_2	7.2	111.0	0.48	0.73	0.09	0.18
1.0%wt. SnO_2/TiO_2	7.6	105.6	0.93	0.71	0.12	0.17
3.0%wt. SnO_2/TiO_2	7.9	102.8	2.71	0.72	0.12	0.17

W_A: Weight fraction of anatase phase

W_R: Weight fraction of rutile phase

W_B: Weight fraction of brookite phase

The band gap energy of SnO_2/TiO_2 was determined in Figure 5.8 and Table 5.10. The band gap was slightly changed at 3.10-3.15 eV for adding 0.1-3.0%wt. SnO_2 in TiO_2. This result can be explained from the SnO_2 content has changed with adding in TiO_2. The band gap of SnO_2/TiO_2 was slightly changed.
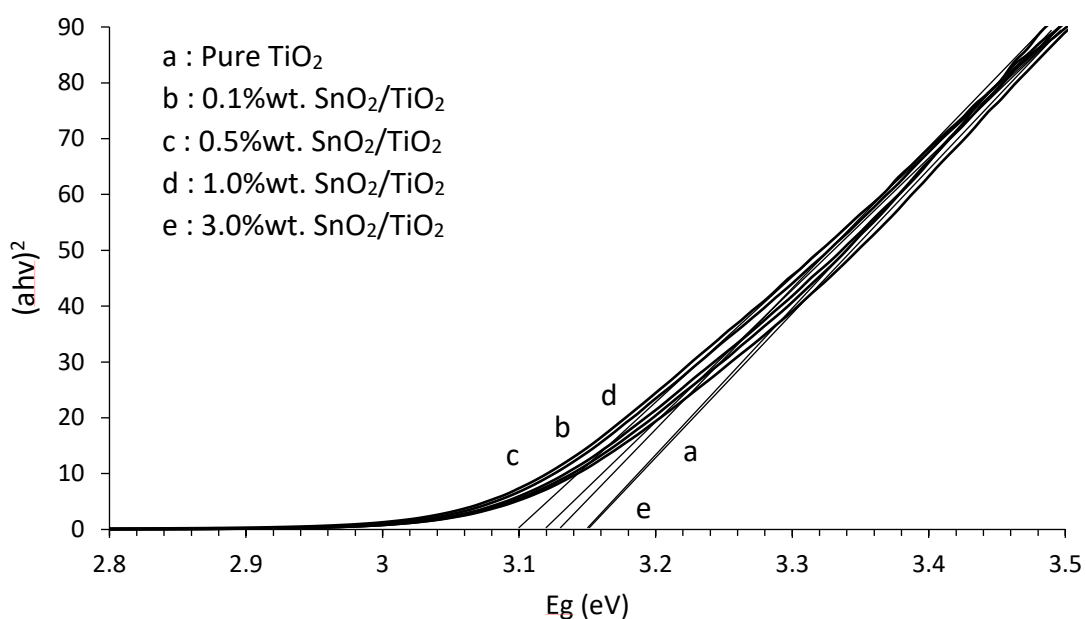
Figure 5.8 UV-visible absorption characteristic between $(\alpha h\nu)^{(1/n)}$ versus photon energy $(h\nu)$ of pure TiO_2 and SnO_2/TiO_2

Table 5.10 Band gap energy of TiO_2 and various SnO_2/TiO_2 that were calcined at 400ºC for 2 hours

Sample	Wavelength (nm)	Band gap energy (eV)
Pure TiO_2	394	3.15
0.1%wt. SnO_2/TiO_2	397	3.12
0.5%wt. SnO_2/TiO_2	400	3.10
1.0%wt. SnO_2/TiO_2	396	3.13
3.0%wt. SnO_2/TiO_2	394	3.15

The amount of 719 dye adsorbed on SnO_2/TiO_2 electrode was displayed in Table 5.11. The calculation of the concentration of adsorbed N719 dye adsorbed was demonstrated in Appendix C. The concentration of adsorbed N719 increased in line with the specific surface area of SnO_2/TiO_2 with the content of SnO_2 was increased. The addition of SnO_2 into TiO_2 brought about in an increase in the isoelectric point (IEP),

leading to better dye adsorption on the surface [75]. The largest amount of adsorbed dye was observed for 0.1%wt. SnO_2/TiO_2 was shown highest at $3.65 \pm 0.019 \times 10^7$ mol/cm^2.

Table 5.11 Concentration of N719 dye contained in the pure TiO_2 and SnO_2/TiO_2 electrodes were calcined at 400ºC for 2 hours

Sample	Concentration of N719 dye ($\times 10^7$ mol/cm^2)
Pure TiO_2	1.92 ± 0.009
0.1%wt. SnO_2/TiO_2	2.14 ± 0.010
0.5%wt. SnO_2/TiO_2	3.65 ± 0.019
1.0%wt. SnO_2/TiO_2	3.39 ± 0.006
3.0%wt. SnO_2/TiO_2	2.34 ± 0.018

The schematic diagram for electron transfer of SnO_2/TiO_2 was shown in Figure 5.9. The electrons that were generated from excitation of dye transferred to the conduction band of TiO_2 and then transferred easily to the conduction band of SnO_2. This phenomenon provided an advantage in repressing the charge recombination. The lifetime of charge carriers significantly improved by the SnO_2 doping compared to pure TiO_2 [76].
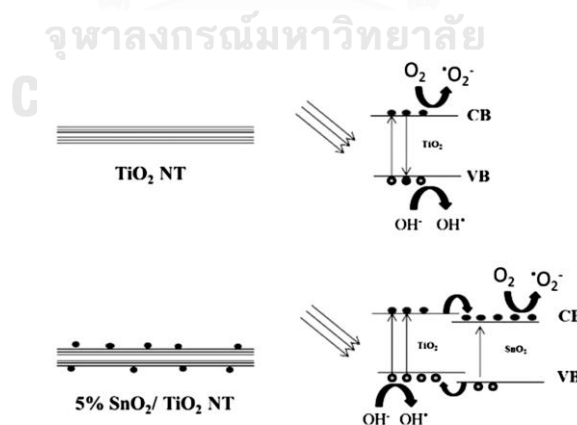
Figure 5.9 The schematic diagram for electron transfer of SnO_2/TiO_2 under visible light irradiation [76]

The electrochemical properties and IV-Curve of DSSCs with SnO_2/TiO_2 electrode were listed in Table 5.15 and displayed in Appendix F. An increase in the content of SnO_2 in TiO_2 resulted in grater DSSC efficiency and the short-current density (J_{SC}) due the amount of dye adsorbed on the electrode and to more electrons that were produced from a light harvest process transfer with a great energy gap between conductive band and lowest vacant molecular orbital of dye [76]. However, they differed only slightly open-circuit voltage (V_{OC}). The 0.5%wt. SnO_2/TiO_2 electrode was shown the best photovoltaic performance, with the short-circuit photocurrent density (J_{SC}), open-circuit voltage (V_{OC}) and fill factor (FF) of 2.80 mA/cm^2, 0.60 V and 0.60, respectively, yielding an overall conversion efficiency of 6.68 ± 0.43%. The 0.5% wt. SnO_2 / TiO_2 electrode has the highest efficiency, indicating that the addition of SnO_2 amount approximately at 0.5% wt. was helped easily to transfer the electron of dye to conduction band, thus being able to reduce the charge recombination [76]. However, adding too much SnO_2 was made itself become recombination center. Therefore resulting in reduced efficiency of DSSC.

Table 5.12 Electrochemical properties of DSSCs with SnO_2/TiO_2 electrode coated with N719 dye was calcined at 400°C for 2 hours

SnO_2/TiO_2 (%wt.)	V_{OC} (V)	J_{SC} (mA/cm^2)	Fill factor	η(%)
0	0.59	1.50	0.55	3.12 ± 0.32
0.1	0.54	1.87	0.51	3.40 ± 0.07
0.5	0.60	2.80	0.60	6.68 ± 0.43
1.0	0.56	2.37	0.63	5.50 ± 0.20
3.0	0.57	1.44	0.71	3.89 ± 0.40

5.2 Modification of dye-sensitized solar cells using double-layered structure

Another interesting way to enhance the efficiency of a DSSC was to employ multilayer structure of film electrode. Electrode with a double-layered structure with different particles in the two layers. The different particle sizes enhanced light-scattering effect inside the dye-sensitized solar cell [61, 62]. From Section 5.1, the 0.5%wt. SnO_2/TiO_2 electrode gave rise to the best overall conversion efficiency of DSSCs at 6.68 ± 0.43% for single-layered structure. The 0.5%wt. SnO_2/TiO_2 was selected as one of the payers in a double-layered structure with TiO_2. We prepared a double-layered for DSSC device, that consisted of one layer of TiO_2 and one then layer of 0.5%wt SnO_2/TiO_2. The specific surface area of a composite of TiO_2 and 0.5%wt. SnO_2/TiO_2 was estimated as an average of the area of the two layers. TiO_2 and 0.5%wt. SnO_2/TiO_2 sol were coated 250 times each on FTO glass using an ultrasonic spray coater and the coated glass was calcined at 400ºC. Three different electrode structures were investigated as followed;

Structure (I): Single-layered structure of 0.5%wt. SnO_2/TiO_2 from Section 5.1.3

A single-layered structure was made entirely with 0.5%wt. SnO_2/TiO_2 that was coated on FTO glass 500 times using an ultrasonic spray coater and was calcined at 400ºC for two hours.

Structure (II): Double-layered structure Type A

A double-layered structure Type A was fabricated with pure TiO_2 for the under-layer and 0.5%wt. SnO_2/TiO_2 for the over-layer film. First, TiO_2 sol was coated on FTO glass 500 times using an ultrasonic spray coater and was calcined at 400ºC for two hours. Next, the FTO glass was coated by 0.5%wt. SnO_2/TiO_2 sol 250 times and was calcined at 400ºC for 30 minutes.

Structure (III): Double-layered structure Type B

A double-layered structure Type B was fabricated with 0.5%wt. SnO_2/TiO_2 for the under-layer and TiO_2 for the over-layer film. First, at 0.5%wt. SnO_2/TiO_2 sol was coated on FTO glass 500 times by using an ultrasonic spray coater and was calcined at 400ºC for two hours. Next, the FTO glass was coated by TiO_2 sol 250 times and was calcined at 400ºC for 30 minutes.

1 = Pure TiO_2

2 = 0.5%wt. SnO_2/TiO_2
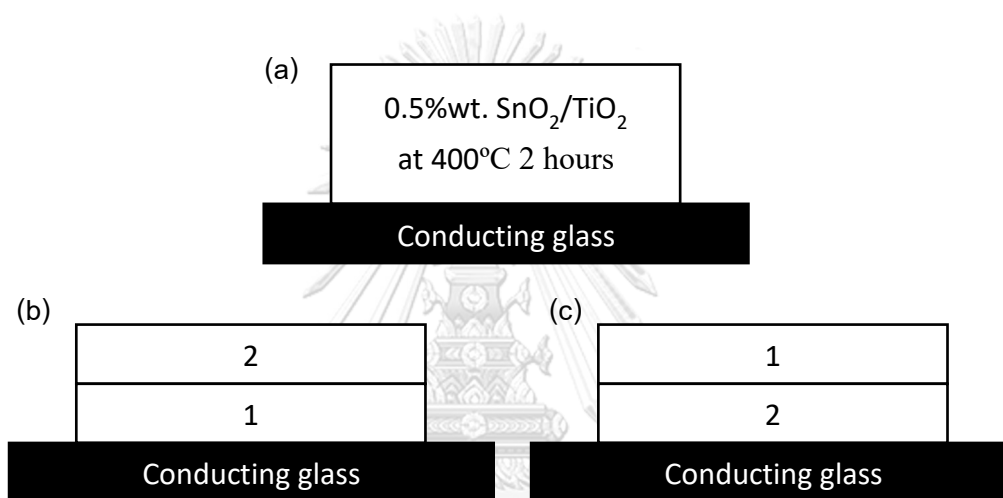
Figure 5.10 Structures of DSSC, (a) Single-layered structure (b) Double-layered structure Type A and (c) Double-layered structure Type B

The schematic diagram three structures of DSSCs was shown in Figure 5.10. Before dye coating, the electrode was gradually heated to 110˚C and held for 10 minutes to remove excess water. Then the electrode was immersed in N719 dye solution immersion for 20-24 hours in the dark. Finally, the electrode was washed with ethanol to remove excess dye and was dried with a blow dryer.

Table 5.13 shows the crystallite size and specific surface area on electrodes with structure I, II, and III. For the single-layered electrode (structure I), the crystallize size of 0.5%wt. SnO_2/TiO_2 was 7.3 nm. The double-layered Type A (structure II) electrode had the TiO_2 crystallize sizes of 8.4 nm for the under-layer film and 6.8 nm for the 0.5%wt. SnO_2/TiO_2 over-layer film while the double-layered Type B (structure III) electrode had the TiO_2 crystallite size of 8.1 nm for the 0.5%wt. SnO_2/TiO_2 under-layer film and 7.1 nm for the TiO_2 over-layer film. The specific surface area of the single structure electrode was 111.0 m^2/g. The specific surface area of double-layered structure electrode for Type A was (105.2+134.6)/2 = 119.9 m^2/g and Type B was (102.8+132.9)/2 = 117.8 m^2/g.

Table 5.13 The properties of single-layered and double-layered structure calcined at various temperature

Structure	Condition (Temperature, times)	Crystalline size (nm)	Surface area (m^2/g)	
(I) Single-layered structure:				
0.5%wt. SnO_2/TiO_2	400ºC, 2 hours	7.3	111.0	
(II) Double-layered structure Type A:				
TiO_2 (Under-layer)	400ºC, 2.5 hours	8.4	105.2	119.9
0.5%wt. SnO_2/TiO_2 (Over-layer)	400ºC, 0.5 hour	6.8	134.6	
(III) Double-layered structure Type B:				
0.5%wt. SnO_2/TiO_2 (Under-layer)	400ºC, 2.5 hours	8.2	102.8	117.8
TiO_2 (Over-layer)	400ºC, 0.5 hour	7.1	132.9	

Table 5.14 listed the concentration of dye adsorbed on the electrode of single-layered and double-layered structure. The adsorbed N719 dye on the electrode was

dissolved with a solution of 0.1M NaOH in deionized and ethanol at volume of ratio 1:1. The highest amount of adsorbed dye was observed for the double-layered Type A electrode at $3.81 \pm 0.011 \times 10^7$ mol/cm^3 because of its larger specific surface area.

Table 5.14 The N719 concentration of single-layered and double-layered structure of DSSC

Structure	Condition (Temperature, times)	Concentration of N719 dye (x10^7 mol/cm^3)
(I) Single-layered structure:		
0.5%wt. SnO$_2$/TiO$_2$	400ºC 2 hours	3.65 ± 0.019
(II) Double-layered structure Type A:		
TiO$_2$ (Under-layer)	400ºC, 2.5 hours	3.81 ± 0.011
0.5%wt. SnO$_2$/TiO$_2$ (Over-layer)	400ºC, 0.5 hour	
(III) Double-layered structure Type B:		
0.5%wt. SnO$_2$/TiO$_2$ (Under-layer)	400ºC, 2.5 hours	3.78 ± 0.005
TiO$_2$ (Over-layer)	400ºC, 0.5 hour	

The band gap energy of TiO$_2$ and 0.5%wt. SnO$_2$/TiO$_2$ was presented in Table 5.15. The band gap was slightly widened to 3.09-3.16 eV.

Table 5.15 Band gap energy of TiO$_2$ and 0.5%wt. SnO$_2$/TiO$_2$ that were calcined at various temperature

Structure	Condition (Temperature, times)	Band gap energy (eV)
(I) Single-layered structure:		
0.5%wt. SnO$_2$/TiO$_2$	400ºC 2 hours	3.10
(II) Double-layered structure Type A:		
TiO$_2$ (Under-layer)	400ºC, 2.5 hours	3.11
0.5%wt. SnO$_2$/TiO$_2$ (Over-layer)	400ºC, 0.5 hour	3.15
(III) Double-layered structure Type B:		
0.5%wt. SnO$_2$/TiO$_2$ (Under-layer)	400ºC, 2.5 hours	3.09
TiO$_2$ (Over-layer)	400ºC, 0.5 hour	3.16

This double-layered structure photoanode can be made to preparing a composite structure of small and large particles in an optimal proportion for light scattering [60]. The light-scattering layer increased the light amount absorbed by dyes because light can distributed on a surface area of particles more than the single-layered structure photoanode. [62]. In present, the light-scattering layer has been adopted to fabricate photoanodes because it can be to more increase efficiency

The comparison of reflection spectra of three structures was displayed in Figure 5.11. The light scattering with the double-layered structure enhances light harvesting of

the DSSCs [77]. The double-layered structure electrode exhibited improvied diffused reflection from 400 to 800 nm, compared to the single-layered electrode. Double-layered Type A electrode possessed higher reflectance in the wavelength range of 300 to 800 nm due to greater difference in crystallite size between the over-layer and under-layer than these in double-layered as Type B and single-layered electrode [60].
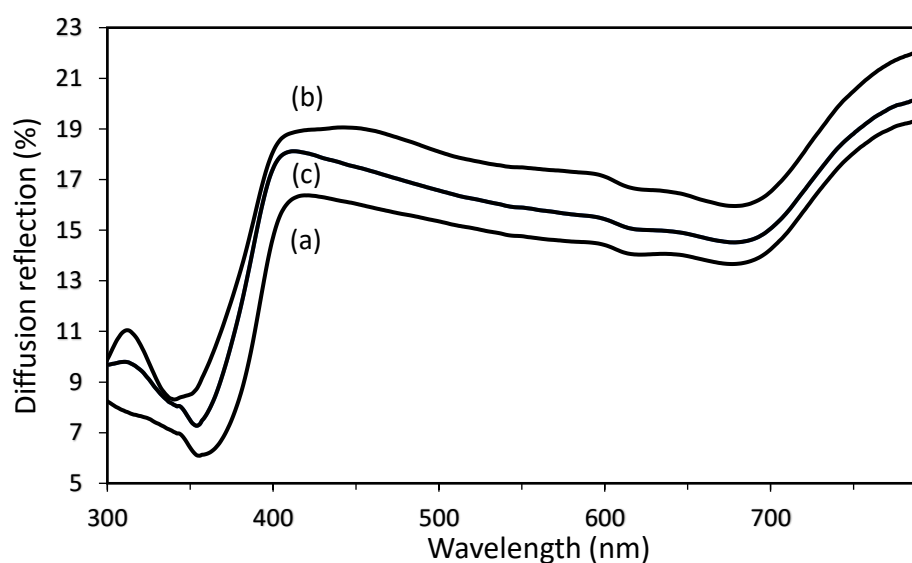
Figure 5.11 Different reflection of DSSC, (a) Single-layered structure (b) Double-layered structure Type A, and (c) Double-layered structure Type B

The electrochemical properties of DSSCs with single-layered and double-layered electrodes was displayed in Table 5.16. The photovoltaic properties were measured in the same manner as described for the single-layered electrode. The open-circuit voltage (V_{OC}) did not chang when switching from the single-layered to double-layered electrode. The double-layered Type A possessed the largest electrochemical properties of the three stuctures. The short circuit current density (J_{SC}) was noticeably increased from 2.80 to 3.38 mA/cm^2 because of the highest can centration of adsorbed dye. When we combined the advantage of enhanced light harvesting efficiency and facilitated electron transport process, the photovoltaic efficiency grew from 6.68 ± 0.43% for the single-layered structure to 8.72 ± 0.31% for double-layered Type B structure.

Table 5.16 Electrochemical properties of single-layered and double-layered structure of DSSC

Structure	V_{OC} (V)	J_{SC} (mA/cm^2)	Fill factor	η(%)
(I) Single-layered structure:				
0.5%wt. SnO$_2$/TiO$_2$	0.60	2.80	0.60	6.68 ± 0.43
(II) Double-layered structure Type A:				
TiO$_2$ (Under-layer) 0.5%wt. SnO$_2$/TiO$_2$ (Over-layer)	0.62	3.38	0.63	8.72 ± 0.31
(III) Double-layered structure Type B:				
0.5%wt. SnO$_2$/TiO$_2$ (Under-layer) TiO$_2$ (Over-layer)	0.60	3.04	0.63	7.59 ± 0.29

CHAPTER 6
CONCLUSION AND RECOMMENDATIONS

6.1 Conclusion

6.1.1 Modification of TiO_2 electrode single-layered by adding MnO_2

MnO_2/TiO_2 was successfully synthesized using a sol-gel method. Introduction of MnO_2 caused the band gap to become narrower. The highest photovoltaic efficiency was obtained with the DSSCs assembled with 0.5 %wt. MnO_2/TiO_2 electrode at 4.83 ± 0.36% because of the increased amount of N719 dye adsorbed on the electrode from the large specific surface area.

6.1.2 Modification of TiO_2 electrode single-layered by adding CoO

The CoO/TiO_2 composite electrode was successfully synthesized by a sol-gel method. The band gap energy of CoO/TiO_2 was reduced so the absorption in the visible region was enhanced. When the CoO content was increased beyond 0.1%wt, the amount of N719 dye adsorbed on the electrode decreased even though the specific surface area remained unchanged. The highest photovoltaic efficiency was 3.23 ± 0.40% obtained for a DSSC with 0.1%wt. CoO/TiO_2 electrode.

6.1.3 Modification of TiO_2 electrode layer by adding SnO_2

Tin dioxide (SnO_2) on TiO_2 thin film was prepared by a sol-gel method via spray coating technique for dye-sensitized solar cells (DSSCs). The crystallite size of the nanoparticles decreased as the amount of SnO_2 was added in the TiO_2 nanocomposite. The DSSC with a 0.5%wt. SnO_2/TiO_2 electrode exhibited highest photovoltaic efficiency at 6.68 ± 0.43%. because the incorporation of SnO_2 into TiO_2 increased the specific surface area and increased dye absorption on photoanode electrode as a consequence.

6.1.4 Modification of dye-sensitized solar cells using double-layered electrode

Double-layered electrodes was employed as a photoanode in DSSC. The double-layered electrodes possessed to high specific surface area and enhanced light-scattering ability. As a result, the photovoltaic efficiency of them was greater than DSSCs with single-layered electrode. DSSCs with double-layered composite films of 0.5%wt. SnO_2/TiO_2 layer and pure TiO_2 layer exhibited the highest efficiency due to the combined effect of two factors, the good light scattering inside the cell and high surface area to increase the amount of dye adsorbed. The efficiency was raised from 6.68 ± 0.43% to 8.72 ± 0.31% for DSSCs with double-layered Type A electrode when compared with single-layered of 1.0%wt. SnO_2/TiO_2 electrode.

6.2 Recommendation for the future work

The following suggestions for future studies will be presented.

1. Improve the double-layered electrode by using a different condition of temperatures and times.

2. Improve the photovoltaic efficiency of DSSC by modifying TiO_2 electrode with other metal oxide.

3. Use a different preparation method of titanium dioxide solution and compare with a sol-gel method.

4. Use other material for counter electrode and compare with platinum counter electrode.

5. Use other ruthenium-based or natural dyes and compare with ruthenium-based N719 dye.

REFERENCES

[1]   Richhariya, G.; Kumar, A.; Tekasakul, P. and Gupta, B., Natural dyes for dye sensitized solar cell: a review. *Renewable and Sustainable Energy Reviews* **2017**, *69*, 705-718.

[2]   Mozaffari, S.; Nateghi, M. R. and Zarandi, M. B., An overview of the challenges in the commercialization of dye sensitized solar cells. *Renewable & Sustainable Energy Reviews* **2017**, *71*, 675-686.

[3]   Iqbal, M. Z. and Khan, S., Progress in the performance of dye sensitized solar cells by incorporating cost effective counter electrodes. *Solar Energy* **2018**, *160*, 130-152.

[4]   Becquerel, A. E., Recherches sur les effets de la radiation chimique de la lumiere solaire au moyen des courants electriques. *Comptes Rendus de L'Academie des Sciences* **1839**, *9* (22), 145-149.

[5]   Ohl, R. S. Light-sensitive device including silicon. United States Patent No. 2402662A, **1941**.

[6]   Chapin, D., New silicon p-n junction photocell for converting solar radiation into electrical power. *Journal of Applied Physics* **1954**, *25* (5), 676-677.

[7]   O'Regan, B. and Grätzel, M., A low-cost, high-efficiency solar cell based on dye-sensitized colloidal TiO_2 films. *Nature* **1991**, *353* (6346), 737-740.

[8]   Green, M. A., Forty years of photovoltaic research at UNSW. *Journal and Proceedings of the Royal Society of New South Wales* **2015**, *148* (455), 2-14.

[9]   Lau, W. S., *ULSI Front-End Technology*. World Scientific: **2017**; p 248.

[10]   Khan, M. Z. H.; Al-Mamun, M. R.; Halder, P. K. and Aziz, M. A., Performance improvement of modified dye-sensitized solar cells. *Renewable and Sustainable Energy Reviews* **2017**, *71*, 602-617.

[11]   Urbani, M.; Ragoussi, M.-E.; Nazeeruddin, M. K. and Torres, T., Phthalocyanines for dye-sensitized solar cells. *Coordination Chemistry Reviews* **2019**, *381*, 1-64.

[12]   Solanki, C. S., *Solar Photovoltaics: Fundamentals, Technologies and Applications*.

Prentice-Hall of India Pvt.Ltd: 2012; p 102-103.

[13] Pervez, A.; Javed, K.; Iqbal, Z.; Shahzad, M.; Khan, U.; Latif, H.; Abbas Shah, S. and Ahmad, N., Fabrication and comparison of dye-sensitized solar cells by using TiO_2 and ZnO as photo electrode. *Optik* 2019, *182*, 175-180.

[14] Sadikin, S. N.; Rahman, M. Y. A.; Umar, A. A. and Aziz, T. H. T., Improvement of dye-sensitized solar cell performance by utilizing graphene-coated TiO_2 films photoanode. *Superlattices and Microstructures* 2019, *128*, 92-98.

[15] Umale, S.; Sudhakar, V.; Sontakke, S. M.; Krishnamoorthy, K. and Pandit, A. B., Improved efficiency of DSSC using combustion synthesized TiO_2. *Materials Research Bulletin* 2019, *109*, 222-226.

[16] Adachi, M.; Murata, Y.; Takao, J.; Jiu, J.; Sakamoto, M. and Wang, F., Highly efficient dye-sensitized solar cells with a titania thin-film electrode composed of a network structure of single-crystal-like TiO_2 nanowires made by the "Oriented attachment" mechanism. *Journal of the American Chemical Society* 2004, *126* (45), 14943-14949.

[17] Liang, Y.; Sun, S.; Deng, T.; Ding, H.; Chen, W. and Chen, Y., The preparation of TiO_2 film by the sol-gel method and evaluation of its self-cleaning property. *Materials* 2018, *11* (3), 1-12.

[18] Sousa, C.; Tosoni, S. and Illas, F., Theoretical approaches to excited-state-related phenomena in oxide surfaces. *Chemical Reviews* 2013, *113* (6), 4456-4495.

[19] Pelaez, M.; Nolan, N. T.; Pillai, S. C.; Seery, M. K.; Falaras, P.; Kontos, A. G.; Dunlop, P. S. M.; Hamilton, J. W. J.; Byrne, J. A.; O'Shea, K.; Entezari, M. H. and Dionysiou, D. D., A review on the visible light active titanium dioxide photocatalysts for environmental applications. *Applied Catalysis B: Environmental* 2012, *125*, 331-349.

[20] Phattalung, S.; F. Smith, M.; Kim, K.; Du, M.-H.; Wei, S.-H.; B. Zhang, S. and Limpijumnong, S., First-principles study of native defects in anatase TiO_2. *Physical Review B* 2006, *73*, 125205.

[21] Bai, F.-Q.; Li, W. and Zhang, H.-X., Theoretical Studies of Titanium Dioxide for Dye-

Sensitized Solar Cell and Photocatalytic Reaction. In *Chapter 10 from the book Titanium Dioxide*, InTech: **2018**; pp 229-248.

[22] W., G. and E., B. Verfahren zur anderung des reflexionsvermögens optischer gläser. German Patent No. 736411C, **1939**.

[23] Li, B.; Wang, X.; Yan, M. and Li, L., Preparation and characterization of nano-TiO2 powder. *Materials Chemistry and Physics* **2003**, *78* (1), 184-188.

[24] Venkatachalam, N.; Palanichamy, M. and Murugesan, V., Sol-gel preparation and characterization of nanosize TiO_2: Its photocatalytic performance. *Materials Chemistry and Physics* **2007**, *104* (2), 454-459.

[25] Harizanov, O. and Harizanova, A., Development and investigation of sol-gel solutions for the formation of TiO_2 coatings. *Solar Energy Materials and Solar Cells* **2000**, *63* (2), 185-195.

[26] Gupta, S. and Tripathi, M., A review on the synthesis of TiO2 nanoparticles by solution route. *Open Chemistry* **2012**, *10* (2), 279-294.

[27] Thomas, S.; Thrithamarassery Gangadharan, D.; Anjusree, G.; T.A, D.; V Nair, S. and Nair, S., A review on counter electrode materials in dye-sensitized solar cells. *Journal of Materials Chemistry A* **2014**, *2* (13), 4474-4490.

[28] Calogero, G.; Calandra, P.; Irrera, A.; Sinopoli, A.; Citro, I. and Di Marco, G., A new type of transparent and low cost counter-electrode based on platinum nanoparticles for dye-sensitized solar cells. *Energy & Environmental Science* **2011**, *4* (5).

[29] Wu, J.; Lan, Z.; Lin, J.; Huang, M.; Huang, Y.; Fan, L.; Luo, G.; Lin, Y.; Xie, Y. and Wei, Y., Counter electrodes in dye-sensitized solar cells. *Chemical Society Reviews* **2017**, *46* (19), 5975-6023.

[30] Kalyanasundaram, K. and Grätzel, M., Efficient Dye-sensitized solar cells for direct conversion of sunlight to electricity. *Mater. Matters* **2009**, *4* (4), 88-93.

[31] Ito, S., Investigation of Dyes for Dye - Sensitized Solar Cells: Ruthenium-Complex Dyes, Metal-Free Dyes, Metal-Complex Porphyrin Dyes and Natural Dyes. In *Chapter 2 from the Solar Cells - Dye-Sensitized Devices*, InTech: **2011**.

[32]   Nazeeruddin, M. K.; Kay, A.; Rodicio, I.; Humphry-Baker, R.; Mueller, E.; Liska, P.; Vlachopoulos, N. and Graetzel, M., Conversion of light to electricity by cis-X2bis(2,2'-bipyridyl-4,4'-dicarboxylate)ruthenium (II) charge-transfer sensitizers (X = Cl⁻, Br⁻, I⁻, CN⁻, and SCN⁻) on nanocrystalline titanium dioxide electrodes. *Journal of the American Chemical Society* **1993**, *115* (14), 6382-6390.

[33]   Nazeeruddin, M. K.; De Angelis, F.; Fantacci, S.; Selloni, A.; Viscardi, G.; Liska, P.; Ito, S.; Takeru, B. and Grätzel, M., Combined experimental and DFT-TDDFT computational study of photoelectrochemical cell ruthenium sensitizers. *Journal of the American Chemical Society* **2005**, *127* (48), 16835-16847.

[34]   Grätzel, M., Dye-sensitized solar cells. *Journal of Photochemistry and Photobiology C: Photochemistry Reviews* **2003**, *4* (2), 145-153.

[35]   Giribabu, L.; Kanaparthi, R. K. and Velkannan, V., Molecular engineering of sensitizers for dye-sensitized solar cell applications. *Chemical Record* **2012**, *12* (3), 306-328.

[36]   Nazeeruddin, M. K.; Péchy, P.; Renouard, T.; Zakeeruddin, S. M.; Humphry-Baker, R.; Comte, P.; Liska, P.; Cevey, L.; Costa, E.; Shklover, V.; Spiccia, L.; Deacon, G. B.; Bignozzi, C. A. and Grätzel, M., Engineering of efficient panchromatic sensitizers for nanocrystalline TiO_2-based solar Cells. *Journal of the American Chemical Society* **2001**, *123* (8), 1613-1624.

[37]   Wang, Z.; M Zakeeruddin, S.; Exnar, I. and Graetzel, M., High efficiency dye-sensitized nanocrystalline solar cells based on ionic liquid polymer gel electrolyte. *Chemical communications (Cambridge, England)* **2002**, *24* (13), 2972-2983.

[38]   Shalini, S.; Balasundaraprabhu, R.; Kumar, T. S.; Prabavathy, N.; Senthilarasu, S. and Prasanna, S., Status and outlook of sensitizers/dyes used in dye sensitized solar cells (DSSC): a review. *International Journal of Energy Research* **2016**, *40* (10), 1303-1320.

[39]   Wu, J.; Lan, Z.; Lin, J.; Huang, M.; Huang, Y.; Fan, L. and Luo, G., Electrolytes in dye-sensitized solar cells. *Chemical Reviews* **2015**, *115* (5), 2136-2173.

[40]   Gonçalves, L. M.; de Zea Bermudez, V.; Ribeiro, H. A. and Mendes, A. M., Dye-

sensitized solar cells: a safe bet for the future. *Energy & Environmental Science* **2008**, *1* (6), 655-667.

[41] Gu, P.; Yang, D.; Zhu, X.; Sun, H.; Wangyang, P.; Li, J. and Tian, H., Influence of electrolyte proportion on the performance of dye-sensitized solar cells. *AIP Advances* **2017**, *7* (10), 105219-105227.

[42] Grätzel, M., Recent advances in sensitized mesoscopic solar cells. *Accounts of Chemical Research* **2009**, *42* (11), 1788-1798.

[43] Li, B.; Wang, L.; Kang, B.; Wang, P. and Qiu, Y., Review of recent progress in solid-state dye-sensitized solar cells. *Solar Energy Materials and Solar Cells* **2006**, *90* (5), 549-573.

[44] Ebrahim, K., Dye Sensitized Solar Cells - Working Principles, Challenges and Opportunities. In *Chapter 8 from the Solar Cells - Dye-Sensitized Devices*, InTech: **2011**; pp 171-204.

[45] Highfield, J., *Advances and Recent Trends in Heterogeneous Photo(Electro)-Catalysis for Solar Fuels and Chemicals*. Routledge: **2015**; Vol. 20, p 6739-6793.

[46] Hankins, M., *Stand-Alone Solar Electric Systems: The Earthscan Expert Handbook on Planning, Design and Installation*. Earthscan Publications, Limited: **2010**; p 132.

[47] Lindholm, F. A.; Fossum, J. G. and Burgess, E. L., Application of the superposition principle to solar-cell analysis. *IEEE Transactions on Electron Devices* **1979**, *26* (3), 165-171.

[48] Diantoro, M.; Suprayogi, T.; Hidayat, A.; Taufiq, A.; Fuad, A. and Suryana, R., Shockley's equation fit analyses for solar cell parameters from I-V Curves. *International Journal of Photoenergy* **2018**, *2018*, 1-7.

[49] Schlabbach, J., *Short-circuit Currents (Energy Engineering)*. Institution of Engineering and Technology: **2005**; p 336.

[50] Baruch, P.; De Vos, A.; Landsberg, P. T. and Parrott, J. E., On some thermodynamic aspects of photovoltaic solar energy conversion. *Solar Energy Materials and Solar Cells* **1995**, *36* (2), 201-222.

[51] Ronald, A. S. and Andrés, C., Contactless determination of current–voltage

characteristics and minority-carrier lifetimes in semiconductors from quasi-steady-state photoconductance data. *Applied Physics Letters* **1996**, *69* (17), 2510-2512.

[52] Martin, A. G., Solar cell fill factors: General graph and empirical expressions. *Solid-State Electronics* **1981**, *24* (8), 90062-90069.

[53] Prasetio, A.; Habieb, A. M.; Alkian, I.; Arifin, Z. and Widiyandari, H., Dye-sensitized solar cell based on TiO_2/MnO_2 composite film as working electrode. *Journal of Physics: Conference Series* **2017**, *877* (1), 1-7.

[54] Shalan, A. E. and Rashad, M. M., Incorporation of Mn^{2+} and Co^{2+} to TiO_2 nanoparticles and the performance of dye-sensitized solar cells. *Applied Surface Science* **2013**, *283*, 975-981.

[55] Yacoubi, B.; Samet, L.; Bennaceur, J.; Lamouchi, A. and Chtourou, R., Properties of transition metal doped-titania electrodes: Impact on efficiency of amorphous and nanocrystalline dye-sensitized solar cells. *Materials Science in Semiconductor Processing* **2015**, *30*, 361-367.

[56] Ünlü, B.; Çakar, S. and Özacar, M., The effects of metal doped TiO_2 and dithizone-metal complexes on DSSCs performance. *Solar Energy* **2018**, *166*, 441-449.

[57] Khan, M. I., Synthesis, characterization and application of Co doped TiO_2 multilayer thin films. *Results in Physics* **2018**, *9*, 359-363.

[58] Musyaro, A.; Huda, I.; Indayani, W.; Gunawan, B.; Yudhoyono, G. and Endarko, E., Fabrication and characterization dye sensitized solar cell (DSSC) based on TiO2/SnO2 composite. *AIP Conference Proceedings* **2017**, *1788* (1), 30062.

[59] Javed, H. M. A.; Que, W.; Yin, X.; Kong, L. B.; Iqbal, J. and Salman Mustafa, M., Investigation on the surface modification of TiO_2 nanohexagon arrays based photoanode with SnO_2 nanoparticles for highly-efficient dye-sensitized solar cells. *Materials Research Bulletin* **2019**, *109*, 21-28.

[60] Wang, G.; Zhu, X. and Yu, J., Bilayer hollow/spindle-like anatase TiO_2 photoanode for high efficiency dye-sensitized solar cells. *Journal of Power Sources* **2015**, *278*, 344-351.

[61] Zhao, L.; Li, J.; Shi, Y.; Wang, S.; Hu, J.; Dong, B.; Lu, H. and Wang, P., Double

light-scattering layer film based on TiO$_2$ hollow spheres and TiO$_2$ nanosheets: Improved efficiency in dye-sensitized solar cells. *Journal of Alloys and Compounds* **2013**, *575*, 168-173.

[62]   Wu, W. Q.; Xu, Y. F.; Rao, H. S.; Su, C. Y. and Kuang, D. B., A double layered TiO$_2$ photoanode consisting of hierarchical flowers and nanoparticles for high-efficiency dye-sensitized solar cells. *Nanoscale* **2013**, *5* (10), 4362-4369.

[63]   Paul, S., Bestimmung der Grösse und der inneren Struktur von Kolloidteilchen mittels Röntgenstrahlen. *Nachrichten von der Gesellschaft der Wissenschaften zu Göttingen* **1918**, *26*, 98-100.

[64]   Cuce, E.; Cuce, P. M. and Bali, T., An experimental analysis of illumination intensity and temperature dependency of photovoltaic cell parameters. *Applied Energy* **2013**, *111*, 374-382.

[65]   Davoud, M. T.; Madatov, R. and Farhadi, P., Investigation of light intensity and temperature dependency of solar cells electric parameters. *Electric power engineering & control systems* **2013**, 90-93.

[66]   Ahmad, K.; Mohammad, A. and Mobin, S. M., Hydrothermally grown α-MnO$_2$ nanorods as highly efficient low cost counter-electrode material for dye-sensitized solar cells and electrochemical sensing applications. *Electrochimica Acta* **2017**, *252*, 549-557.

[67]   Reyes-Coronado, D.; Rodriguez-Gattorno, G.; Espinosa-Pesqueira, M. E.; Cab, C.; de Coss, R. and Oskam, G., Phase-pure TiO$_2$ nanoparticles: anatase, brookite and rutile. *Nanotechnology* **2008**, *19* (14), 145605.

[68]   Roose, B.; Pathak, S. and Steiner, U., Doping of TiO$_2$ for sensitized solar cells. *Chemical Society Reviews* **2015**, *44* (22), 8326-49.

[69]   Palomares, E.; Clifford, J. N.; Haque, S. A.; Lutz, T. and Durrant, J. R., Slow charge recombination in dye-sensitised solar cells (DSSC) using Al$_2$O$_3$ coated nanoporous TiO$_2$ films. *Chemical communications (Cambridge, England)* **2002**, (14), 1464-1465.

[70]   Xue, M.; Huang, L.; Wang, J. Q.; Wang, Y.; Gao, L.; Zhu, J. H. and Zou, Z. G., The

direct synthesis of mesoporous structured MnO_2/TiO_2 nanocomposite: a novel visible-light active photocatalyst with large pore size. *Nanotechnology* **2008**, *19* (18), 185604.

[71]   Savio, A. K. P. D.; Fletcher, J.; Smith, K.; Iyer, R.; Bao, J. M. and Robles Hernández, F. C., Environmentally effective photocatalyst CoO/TiO_2 synthesized by thermal precipitation of Co in amorphous TiO_2. *Applied Catalysis B: Environmental* **2016**, *182*, 449-455.

[72]   Drasovean, R. and Condurache-Bota, S., Structural characterization and optical properties of Co_3O_4 and CoO films. *Journal of Optoelectronics and Advanced Materials* **2009**, *11*, 2141-2144.

[73]   Ramakrishnan, V.; Hyun, K.; Park, J. and Lyong Yang, B., Cobalt Oxide Nanoparticles on TiO_2 Nanorod/FTO as a Photoanode with Enhanced Visible Light Sensitization. *RSC Advances* **2016**, *6* (12), 9789–9795.

[74]   Xie, F.; Wang, J.; Li, Y.; Dou, J. and Wei, M., One-step synthesis of hierarchical SnO2/TiO2 composite hollow microspheres as an efficient scattering layer for dye-sensitized solar cells. *Electrochimica Acta* **2019**, *296*, 142-148.

[75]   Wali, Q.; Bakr, Z. H.; Manshor, N. A.; Fakharuddin, A. and Jose, R., SnO_2/TiO_2 hybrid nanofibers for efficient dye-sensitized solar cells. *Solar Energy* **2016**, *132*, 395-404.

[76]   Rajkumar, K.; Vairaselvi, P.; Saravanan, P.; Vinod, V. T. P.; Cerník, M. and Rajendra Kumar, R. T., Visible-light-driven SnO_2/TiO_2 nanotube nanocomposite for textile effluent degradation. *RSC Advances* **2015**, *5* (26), 20424-20431.

[77]   Luo, J.; Gao, L.; Sun, J. and Liu, Y., A bilayer structure of a titania nanoparticle/highly-ordered nanotube array for low-temperature dye-sensitized solar cells. *RSC Advances* **2012**, *2* (5).

APPENDICES

APPENDIX A CALCULATION OF THE CRYSTALLITE SIZE

Calculation of the crystallite size by Debye-Scherrer equation

The crystallite size can be calculated from 2θ profile analysis, FWHM, by Debye-Scherrer equation (A.1) that was suitable for partical size below 100 nm.

Debye-Scherrer equation:

$$D = \frac{K\lambda}{\beta cos\theta} \tag{A.1}$$

Where

D = Average size of the crystal (Å)

K = Dimensionless shape factor (0.9)

λ = The x-ray wavelength (1.54439 Å for CuK$_\alpha$)

β = The x-ray diffraction broadening (radian)

θ = Observed peak angle (degree)

The broadening of a single diffraction peak is the product of the crystallite dimensions in the direction perpendicular to the planes that produced the diffraction peak. The X-ray diffraction broadening can be obtained by using Warren's equation (A.2).

Warren's equation:

$$\beta^2 = \beta_M^2 - \beta_S^2$$

$$\beta = \sqrt{\beta_M^2 - \beta_S^2} \tag{A.2}$$

Where

β_M = Measured peak width in radians at half peak height

β_S = Corresponding width of a standard material

Example : Calculation of the crystallite site of pure TiO_2 calcined at 400ºC for two hours

The half-weight width (101) diffraction peak

$$\beta_M \quad = \quad 1.1295 \quad\quad degree$$

$$\beta_M \quad = \quad 0.019713 \quad\quad radian$$

The corresponding half-height width of peak of TiO_2

$$\beta_S \quad = \quad 0.003836 \quad\quad radian$$

The pure width

$$\beta = \sqrt{\beta_M^2 - \beta_S^2}$$

$$\beta = \sqrt{0.019713^2 - 0.003836^2}$$

$$\beta = 0.019336 \ radian$$

Where

λ	=	1.01117	Å
β	=	0.019336	radian
2θ	=	25.3465	degree
θ	=	12.6732	degree

The crystallite size (D) $\quad = \quad \dfrac{0.9 \times 1.01117}{0.0193 \cos 12.6732}$

$$= \quad 80.97 \quad Å$$

$$= \quad 8.1 \quad nm$$

APPENDIX B CALCULATION OF WEIGHT FRACTION OF ANATASE, RUTILE AND BROOKITE PHASE OF TiO$_2$

Calculation of the weight fraction

The phase of TiO$_2$ can be calculated from the integrated intensities of peaks at 2θ of 25.3° was assigned to anatase TiO$_2$, whereas the peak at 27.4° corresponded to be rutile phase and the peak at 30.6° was associated to brookite.

The weight fraction of TiO2 sample can be calculated as follows equation (B.1)-(B.3).

$$W_A = \frac{K_A A_A}{K_A A_A + K_B A_B + K_R} \quad (B.1)$$

$$W_B = \frac{K_B A_B}{K_A A_A + K_B A_B + K_R} \quad (B.2)$$

$$W_R = \frac{K_R}{K_A A_A + K_B A_B + K_R} \quad (B.3)$$

Where

W_A	=	Weight fraction of anatase phase TiO$_2$
W_B	=	Weight fraction of brookite phase TiO$_2$
W_R	=	Weight fraction of rutile phase TiO$_2$
A_A	=	The intensity of anatase peak
A_B	=	The intensity of brookite peak
A_R	=	The intensity of rutile peak
K_A	=	The coefficient factor of anatase (0.886)
K_B	=	The coefficient factor of brookite (2.721)

Example : Calculation of the phase contents TiO_2 calcined at 400ºC for two hours

Where

The integrated intensities of anatase (A_A)   =   742

The integrated intensities of brookite (A_B)   =   73

The integrated intensities of rutile (A_R)   =   141

The weight fraction of the phase content can be calculated by as follows:

$$W_A = \frac{742(0.866)}{742(0.866)+73(2.721)+141} = 0.66$$

$$W_B = \frac{73(2.721)}{742(0.866)+73(2.721)+141} = 0.20$$

$$W_R = \frac{141}{742(0.866)+73(2.721)+141} = 0.14$$

APPENDIX C DETERMINATION OF THE AMOUNT OF RUTHENIUM-BASED DYE ADSORBED ON SURFACE

Mensuration of the amount of ruthenium-based dye adsorbed

The amount of N719 dye adsorbed was measured by UV-Visible Absorption Spectroscopy on the absorption peak at 310 nm. In this study, three electrodes were used and the dye was dissolved out to surface electrode by using a mixed solution of 0.1 M NaOH in deionized water and ethanol with molar ratio 1:1 volume fraction.

The calibration curve of concentration of N719 dye with absorbance was illustrated in the following Figure C.1 and the concentration of N719 dye contained in pure TiO2 and second metal oxide/TiO_2 was shown in Table C.1 -C.2.

Figure C.1 The calibration curve of concentration of N719 adsorbed dye

Table C.1 The concentration of N719 dye contained in pure TiO_2 and second metal oxide/TiO_2 electrodes of calcined at 400ºC for 2 hours 500 coats at various content

Electrode	Concentration of N719 dye (×107 mol/cm2)			
	1	2	3	Average
Pure TiO_2	2.01	1.83	1.93	1.92 ± 0.009
0.1%wt. MnO_2/TiO_2	1.93	2.02	1.91	1.95 ± 0.006
0.5%wt. MnO_2/TiO_2	3.14	3.22	3.12	3.16 ± 0.005
1.0%wt. MnO_2/TiO_2	2.67	2.64	2.85	2.72 ± 0.011
3.0%wt. MnO_2/TiO_2	1.93	1.96	2.04	1.98 ± 0.006
0.1%wt. CoO/TiO_2	1.92	2.07	1.86	1.95 ± 0.011
0.5%wt. CoO/TiO_2	1.38	1.67	1.55	1.53 ± 0.014
1.0%wt. CoO/TiO_2	1.28	1.39	1.24	1.31 ± 0.008
3.0%wt. CoO/TiO_2	0.91	0.92	0.80	0.88 ± 0.007
0.1%wt. SnO_2/TiO_2	2.23	2.15	2.03	2.14 ± 0.0010
0.5%wt. SnO_2/TiO_2	3.68	3.44	3.82	3.65 ± 0.019
1.0%wt. SnO_2/TiO_2	3.35	3.36	3.45	3.39 ± 0.006
3.0%wt. SnO_2/TiO_2	2.32	2.53	2.17	2.34 ± 0.018

Table C.2 The concentration of N719 dye contained in double-layered electrode of under-layer calcined at 400ºC for 2 hours 30 minutes 250 coats and over-layer calcined at 400ºC for 30 minutes 250 coats at various content

Electrode	Concentration of N719 dye (×10^7 mol/cm^2)			
	1	2	3	Average
0.5%wt. SnO_2/TiO_2 as over layer TiO_2 as under layer	3.78	3.93	3.72	3.81 ± 0.011
TiO_2 as over layer 0.5%wt. SnO_2/TiO_2 as under layer	3.80	3.72	3.81	3.78 ± 0.005

APPENDIX D THE CALCULATION OF THE BAND GAP ENERGY FROM UV-VIS SPECTRA

Determination of the bandgap

The band gap energy of TiO_2 or modified TiO_2 can be determined by UV-Visible Absorption Spectroscopy with plotting the graph between $(\alpha h\nu)^{(1/n)}$ versus photon energy ($h\nu$).

where

α = The optical absorption coefficient can be calculated by Equation (D.1).

$$\alpha = \frac{2.303A}{t} \tag{D.1}$$

where

A = Absorbance

t = The thickness of the sample

$h\nu$ = The photon energy can be calculated from its wavelength by Equation (D.2).

$$h\nu = Eg = \frac{hC}{\lambda} \tag{D.2}$$

Where

Eg = The band gap energy of the catalyst (eV)

h = The plank constant (6.62×10^{-34} Joules·sec)

λ = The wavelength (meters)

C = The speed of light (3.0×10^8 meter/sec)

Note: 1 eV is $1.6 \times 10-19$ Joules and 1 m is 10^9 nm (conversion factor)

Finally, this was given equation for the photon energy at its wavelength (D.3).

$$h\nu = \frac{1240}{\lambda} \tag{D.3}$$

n = the power factor n for allowed direct (0.5)

Example : Calculation of the band gap in pure TiO_2

To determine the band gap of TiO_2. The extrapolation for the straight-line portion of the curves to zero absorption coefficient value produced the valve of the energy band gap energy.

The plot between $(\alpha h\nu)^{(1/n)}$ versus photon energy $(h\nu)$ was shown in Figure D.1

Figure D.1 An example for a plot between $(\alpha h\nu)^{(1/0.5)}$ versus photon energy $(h\nu)$ of TiO_2

From this Figure presented the band gap of pure TiO_2 is 3.15 eV

APPENDIX E THE CALCULATION OF AMOUNT OF METAL OXIDE FROM ICP-AES

Calculation of ICP-AES results

The results from ICP-AES characterization were calculation the contents of metal oxide doped in TiO_2.

Example : Calculation of the SnO_2 contents in 0.5%wt. SnO_2/TiO_2

(1) For 0.5%wt. SnO_2/TiO_2, the initial weight of catalyst powder was 0.050 g. Hence, the calculation of Tin (Sn) contents as follows:

The amount of ... in catalyst were;

In 1.0 g of catalyst, had a SnO_2 content was 0.005 g

In 0.050 g of catalyst, had a SnO_2 content was $\dfrac{0.005 \times 0.050}{1.0}$ g

$$= 0.250 \times 10^{-3} \text{ g}$$

$$= 0.250 \quad\quad \text{mg}$$

For digestion, sample were diluted to 100 cm^3

Therefore, the sample had a concentration were $\dfrac{0.25 \times 1000}{100}$

$$= 2.500 \text{ ppm (mg/L of } SnO_2)$$

(2) From the result of ICP-AES, shown the concentration of sample 1.896 ppm

Converting to concentration of SnO_2 was $\dfrac{1.896 \times 150.71}{118.71}$

$$= \quad 2.407 \text{ ppm}$$

When

The molecular weight of Tin dioxide (SnO^2) is 150.71 g/mol

The molecular weight of Tin (Sn) is 118.71 g/mol

(3) Therefore, the SnO_2/TiO_2 contents in catalyst were calculated by

SnO_2 concentration of 2.500 ppm refer to 0.5%wt. SnO_2/TiO_2 in catalyst

SnO_2 concentration of 2.407 ppm refer to $\dfrac{2.407 \times 0.5}{2.500}$

$$= 0.48\%wt.\ SnO_2/TiO_2$$

APPENDIX F THE ELECTROCHEMICAL PROPERTIES OF DSSCS

The electrochemical properties of dye-sensitized solar cell

The electrochemical properties of DSSCs as pure TiO_2 and modified TiO_2 with second metal oxide MnO_2, CoO, and SnO_2 electrode was measured by I-V characterization under a light irradiance (Pin) of 15 mW/cm^2. In this study, five sample were used and the photovoltaic efficiency (η) of cell given is the average valve follow by the standard derivation.

The electrochemical properties were Shown in Table F.1 - F.15

The IV-Curves were Shown in Figure F.1 – F.15

Figure F.1 IV-Curve of DSSC of pure TiO_2 electrode calcined at 400ºC for two hours 500 coats with N719 dye

Table F.1 Electrochemical properties of DSSC of pure TiO_2 electrode calcined at 400ºC for two hours 500 coats with N719 dye

No.	V_{OC} (Volt)	J_{SC} (mA/cm²)	Vmax (Volt)	Jmax (mA/cm²)	Pmax (mW/cm²)	FF	η (%)
1	0.61	1.50	0.47	1.09	0.51	0.56	3.42
2	0.59	1.68	0.39	1.05	0.41	0.41	2.73
3	0.57	1.41	0.45	1.11	0.50	0.61	3.31
4	0.56	1.78	0.42	1.21	0.50	0.50	3.34
5	0.60	1.11	0.49	0.87	0.42	0.64	2.83
Average	0.59	1.50	0.44	1.07	0.47	0.55	3.12 ± 0.32

Figure F.2 IV-Curve of DSSC of 0.1%wt. MnO_2/TiO_2 electrode calcined at 400ºC for two

hours 500 coats with N719 dye

Table F.2 Electrochemical properties of DSSC of 0.1%wt. MnO_2/TiO_2 electrode calcined

at 400ºC for two hours 500 coats with N719 dye

No.	V_{OC} (Volt)	J_{SC} (mA/cm^2)	Vmax (Volt)	Jmax (mA/cm^2)	Pmax (mW/cm^2)	FF	η (%)
1	0.63	1.57	0.46	0.97	0.44	0.45	2.96
2	0.61	1.69	0.40	0.98	0.39	0.38	2.61
3	0.63	1.43	0.46	1.06	0.48	0.54	3.21
4	0.58	1.52	0.39	0.94	0.36	0.41	2.43
5	0.57	1.44	0.45	1.12	0.51	0.62	3.38
Average	0.60	1.53	0.43	1.01	0.44	0.48	2.92 ± 0.40

Figure F.3 IV-Curve of DSSC of 0.5%wt. MnO_2/TiO_2 electrode calcined at 400ºC for two

hours 500 coats with N719 dye

Table F.3 Electrochemical properties of DSSC of 0.5%wt. MnO_2/TiO_2 electrode calcined

at 400ºC for two hours 500 coats with N719 dye

No.	V_{OC} (Volt)	J_{SC} (mA/cm^2)	Vmax (Volt)	Jmax (mA/cm^2)	Pmax (mW/cm^2)	FF	η (%)
1	0.62	1.86	0.48	1.56	0.75	0.65	5.00
2	0.62	1.98	0.49	1.65	0.80	0.66	5.33
3	0.69	1.63	0.54	1.22	0.66	0.59	4.39
4	0.68	1.58	0.53	1.31	0.70	0.65	4.66
5	0.68	1.64	0.54	1.32	0.71	0.64	4.76
Average	0.66	1.74	0.52	1.41	0.72	0.64	4.83 ± 0.36

Figure F.4 IV-Curve of DSSC of 1.0%wt. MnO_2/TiO_2 electrode calcined at 400ºC for two

hours 500 coats with N719 dye

Table F.4 Electrochemical properties of DSSC of 1.0%wt. MnO_2/TiO_2 electrode calcined

at 400ºC for two hours 500 coats with N719 dye

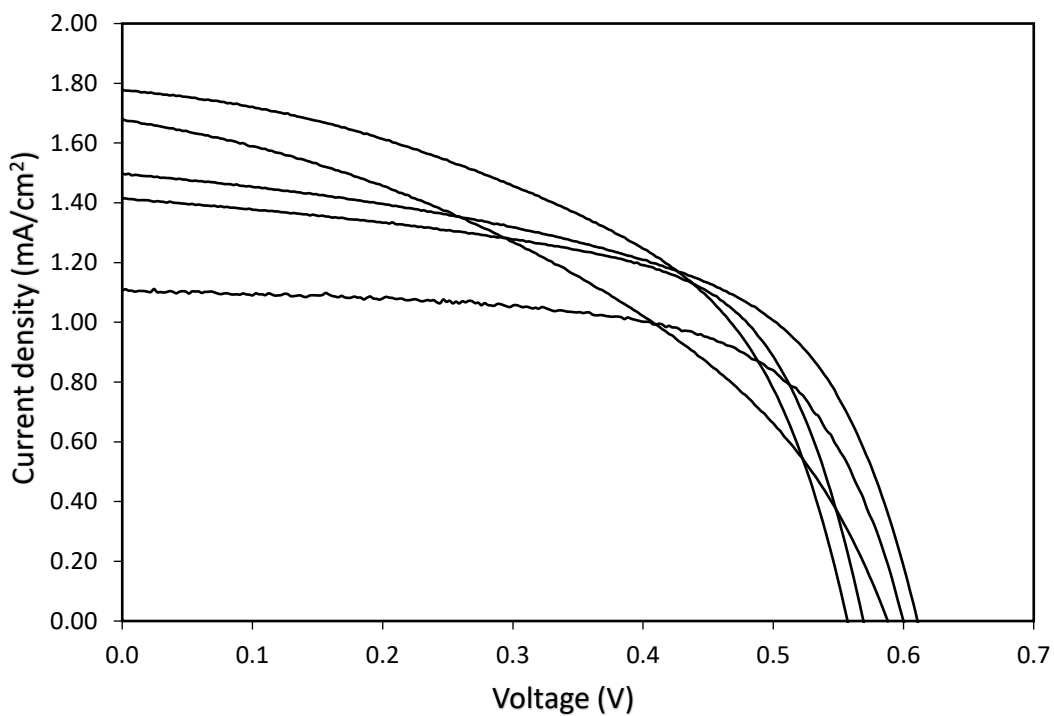| No.	V_{OC} (Volt)	J_{sc} (mA/cm^2)	Vmax (Volt)	Jmax (mA/cm^2)	Pmax (mW/cm^2)	FF	η (%)
1	0.50	1.50	0.37	1.09	0.40	0.54	2.70
2	0.51	1.49	0.31	0.91	0.28	0.36	1.84
3	0.62	1.68	0.41	1.01	0.41	0.40	2.75
4	0.60	1.79	0.41	1.12	0.46	0.43	3.08
5	0.60	1.70	0.41	0.90	0.37	0.36	2.45
Average	0.57	1.63	0.38	1.01	0.38	0.42	2.57 ± 0.46

Figure F.5 IV-Curve of DSSC of 3.0%wt. MnO_2/TiO_2 electrode calcined at 400°C for two

hours 500 coats with N719 dye

Table F.5 Electrochemical properties of DSSC of 3.0%wt. MnO_2/TiO_2 electrode calcined

at 400°C for two hours 500 coats with N719 dye

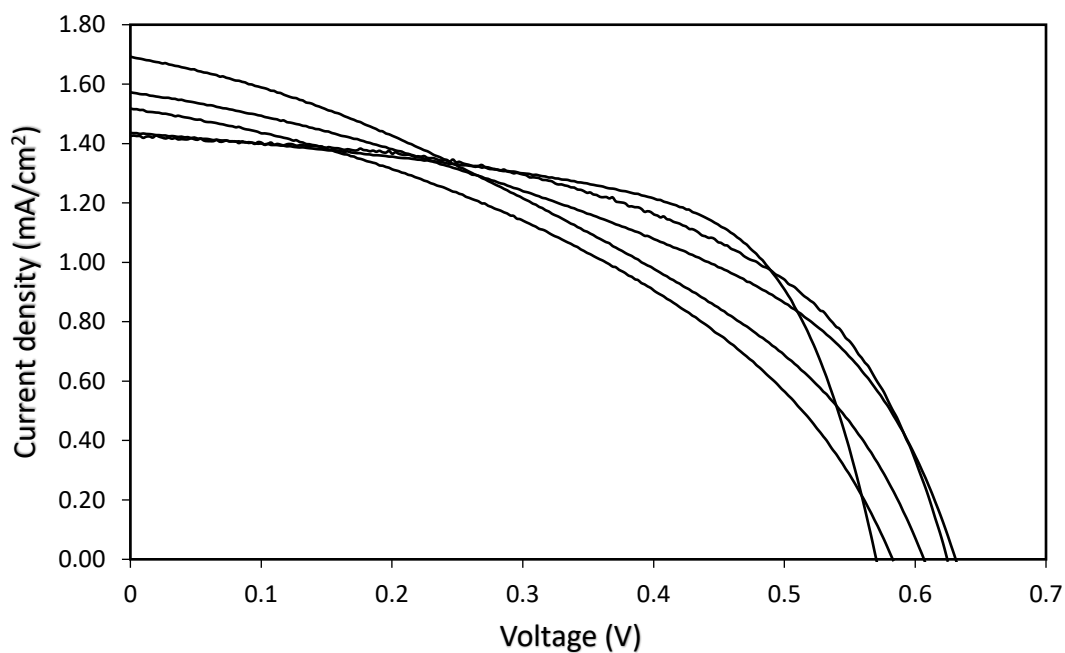| No.	V_{oc} (Volt)	J_{sc} (mA/cm^2)	Vmax (Volt)	Jmax (mA/cm^2)	Pmax (mW/cm^2)	FF	η (%)
1	0.54	0.58	0.34	0.42	0.14	0.46	0.97
2	0.38	0.54	0.23	0.31	0.07	0.36	0.48
3	0.50	0.43	0.27	0.26	0.07	0.33	0.48
4	0.55	0.60	0.33	0.36	0.12	0.36	0.79
5	0.45	0.72	0.26	0.46	0.12	0.37	0.80
Average	0.48	0.57	0.29	0.36	0.11	0.38	0.70 ± 0.22

Figure F.6 IV-Curve of DSSC of 0.1%wt. CoO/TiO$_2$ electrode calcined at 400ºC for two

hours 500 coats with N719 dye

Table F.6 Electrochemical properties of DSSC of 0.1%wt. CoO/TiO$_2$ electrode calcined

at 400ºC for two hours 500 coats with N719 dye

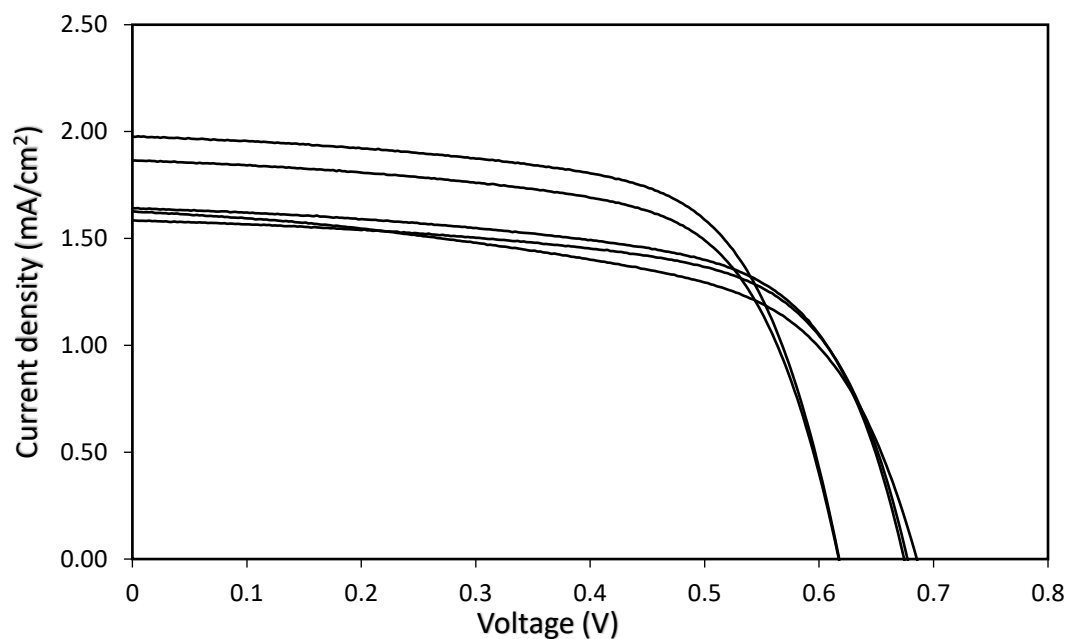| No.	V$_{OC}$ (Volt)	J$_{SC}$ (mA/cm^2)	Vmax (Volt)	Jmax (mA/cm^2)	Pmax (mW/cm^2)	FF	η (%)
1	0.57	1.65	0.42	1.21	0.51	0.54	3.39
2	0.57	1.75	0.43	1.26	0.54	0.55	3.61
3	0.57	1.83	0.43	1.25	0.53	0.51	3.55
4	0.53	1.35	0.41	1.03	0.42	0.58	2.78
5	0.52	1.92	0.35	1.23	0.42	0.43	2.83
Average	0.55	1.70	0.41	1.20	0.49	0.52	3.23 ± 0.40

Figure F.7 IV-Curve of DSSC of 0.5%wt. CoO/TiO_2 electrode calcined at 400ºC for two

hours 500 coats with N719 dye

Table F.7 Electrochemical properties of DSSC of 0.5%wt. CoO/TiO_2 electrode calcined

at 400ºC for two hours 500 coats with N719 dye

No.	V_{OC} (Volt)	J_{SC} (mA/cm²)	Vmax (Volt)	Jmax (mA/cm²)	Pmax (mW/cm²)	FF	η (%)
1	0.50	1.76	0.32	1.18	0.38	0.44	2.54
2	0.49	1.83	0.31	1.14	0.35	0.39	2.33
3	0.51	1.83	0.35	1.16	0.41	0.44	2.75
4	0.53	1.60	0.37	1.03	0.38	0.44	2.50
5	0.53	1.19	0.40	0.88	0.35	0.56	2.35
Average	0.51	1.64	0.35	1.08	0.37	0.45	2.49 ± 0.17

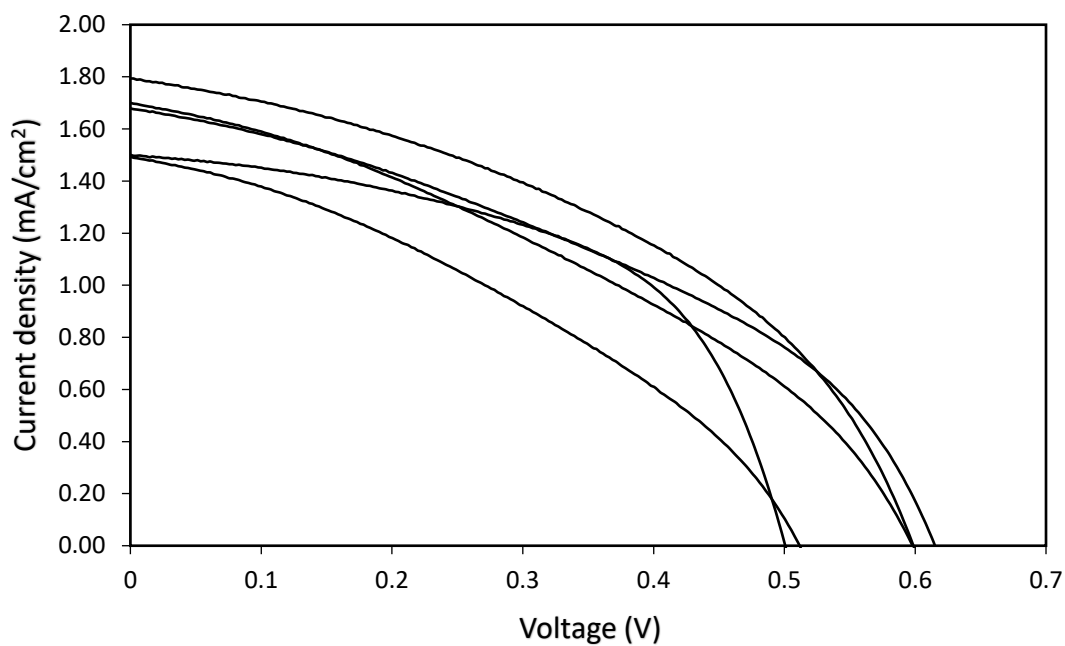**Figure F.8** IV-Curve of DSSC of 1.0%wt. CoO/TiO$_2$ electrode calcined at 400°C for two

hours 500 coats with N719 dye

Table F.8 Electrochemical properties of DSSC of 1.0%wt. CoO/TiO$_2$ electrode calcined

at 400°C for two hours 500 coats with N719 dye

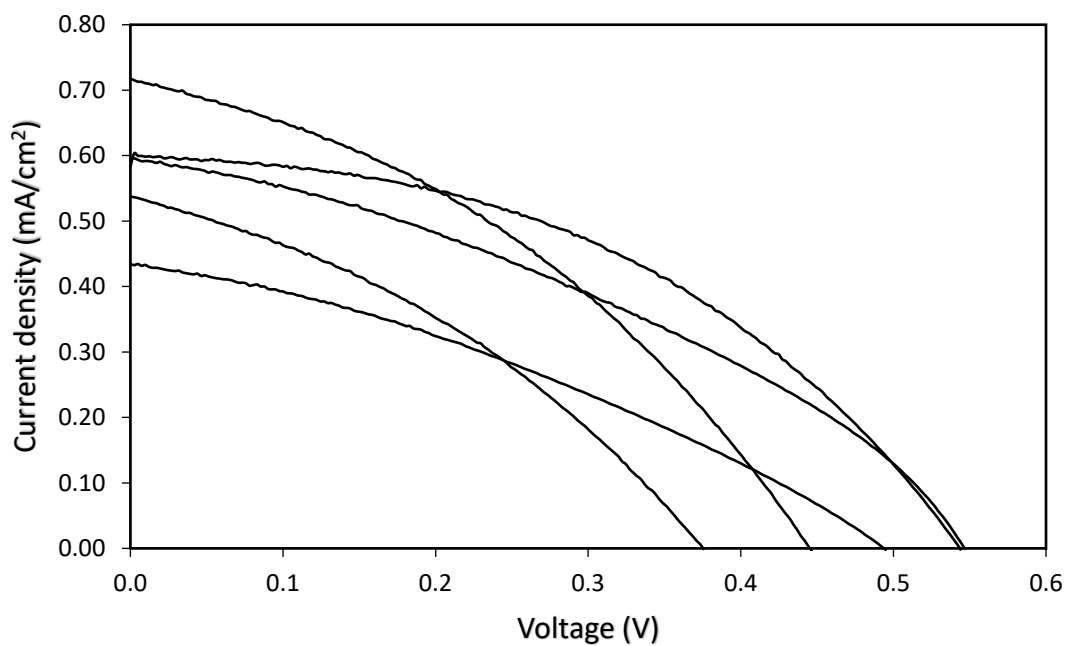| No.	V$_{OC}$ (Volt)	J$_{sc}$ (mA/cm^2)	Vmax (Volt)	Jmax (mA/cm^2)	Pmax (mW/cm^2)	FF	η (%)
1	0.48	1.42	0.31	0.98	0.31	0.46	2.07
2	0.53	1.59	0.38	0.98	0.37	0.44	2.46
3	0.54	1.62	0.38	1.04	0.39	0.45	2.60
4	0.46	1.47	0.29	0.96	0.28	0.42	1.88
5	0.46	1.57	0.29	1.03	0.30	0.42	2.01
Average	0.49	1.54	0.33	1.00	0.33	0.44	2.20 ± 0.31

Figure F.9 IV-Curve of DSSC of 3.0%wt. CoO/TiO$_2$ electrode calcined at 400ºC for two

hours 500 coats with N719 dye

Table F.9 Electrochemical properties of DSSC of 3.0%wt. CoO/TiO$_2$ electrode calcined

at 400ºC for two hours 500 coats with N719 dye

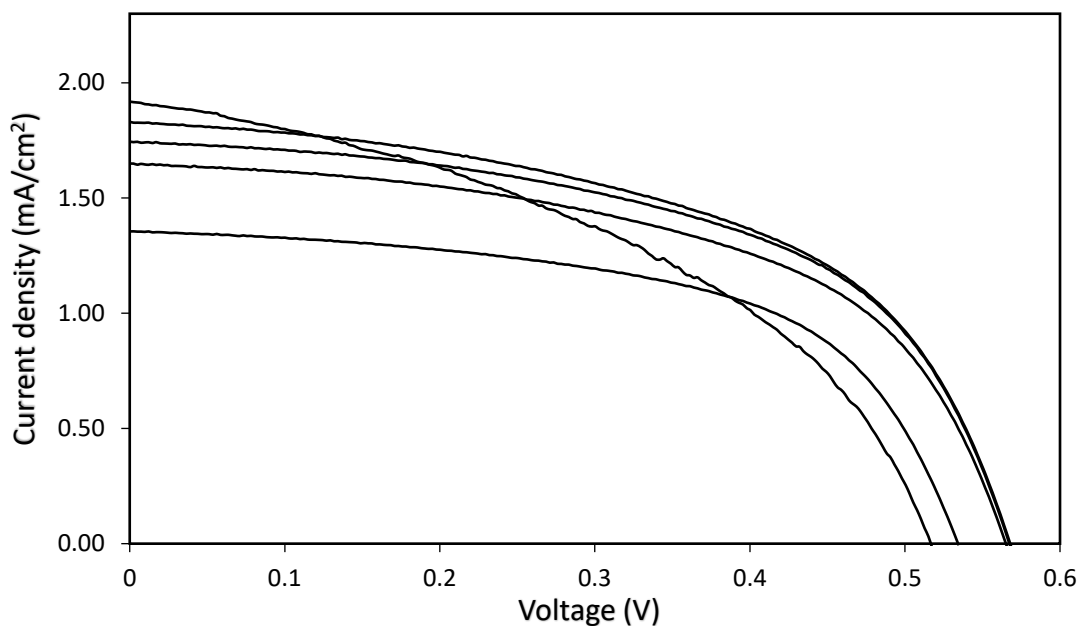| No.	V_{OC} (Volt)	J_{SC} (mA/cm^2)	Vmax (Volt)	Jmax (mA/cm^2)	Pmax (mW/cm^2)	FF	η (%)
1	0.36	1.36	0.20	0.77	0.15	0.31	1.01
2	0.19	0.37	0.11	0.21	0.02	0.31	0.15
3	0.19	0.33	0.10	0.18	0.02	0.31	0.13
4	0.39	1.49	0.22	0.84	0.18	0.32	1.23
5	0.28	0.96	0.16	0.54	0.08	0.31	0.56
Average	0.28	0.90	0.16	0.51	0.09	0.31	0.61 ± 0.50

Figure F.10 IV-Curve of DSSC of 0.1%wt. SnO_2/TiO_2 electrode calcined at 400ºC for two hours 500 coats with N719 dye

Table F.10 Electrochemical properties of DSSC of 0.1%wt. SnO_2/TiO_2 electrode calcined at 400ºC for two hours 500 coats with N719 dye

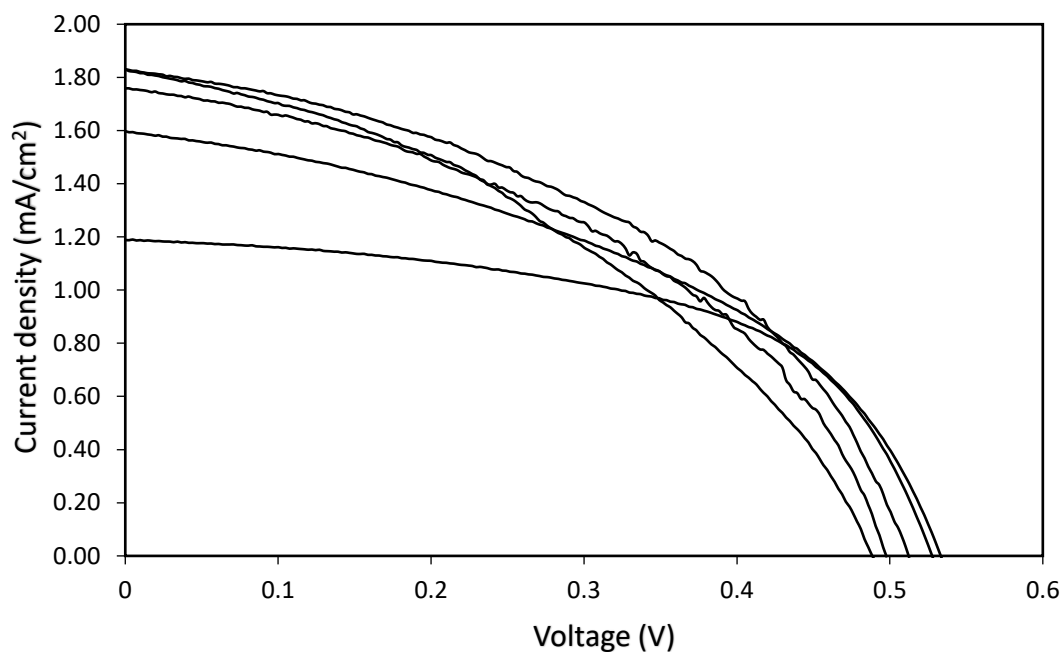| No.	V_{oc} (Volt)	J_{sc} (mA/cm^2)	Vmax (Volt)	Jmax (mA/cm^2)	Pmax (mW/cm^2)	FF	η (%)
1	0.54	1.85	0.40	1.29	0.51	0.51	3.42
2	0.54	1.84	0.40	1.26	0.50	0.50	3.33
3	0.55	1.80	0.41	1.24	0.50	0.51	3.35
4	0.53	1.91	0.39	1.35	0.53	0.52	3.51
5	0.53	1.94	0.39	1.33	0.51	0.50	3.42
Average	0.54	1.87	0.40	1.29	0.51	0.51	3.40 ± 0.07

Figure F.11 IV-Curve of DSSC of 0.5%wt. SnO_2/TiO_2 electrode calcined at 400ºC for two

hours 500 coats with N719 dye

Table F.11 Electrochemical properties of DSSC of 0.5%wt. SnO_2/TiO_2 electrode calcined

at 400ºC for two hours 500 coats with N719 dye

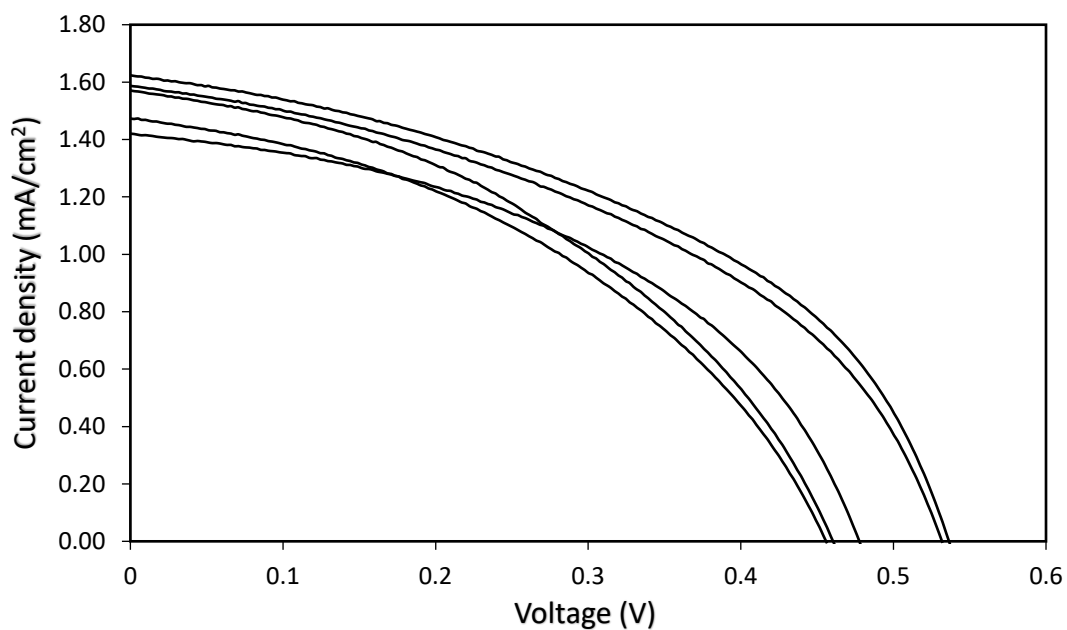| No.	V_{OC} (Volt)	J_{SC} (mA/cm²)	Vmax (Volt)	Jmax (mA/cm²)	Pmax (mW/cm²)	FF	η (%)
1	0.61	2.94	0.45	2.38	1.08	0.60	7.22
2	0.61	2.79	0.41	2.23	0.91	0.54	6.07
3	0.61	2.83	0.45	2.25	1.01	0.59	6.71
4	0.59	2.69	0.46	2.24	1.03	0.65	6.88
5	0.57	2.73	0.43	2.25	0.97	0.63	6.49
Average	0.60	2.80	0.44	2.27	1.00	0.60	6.68 ± 0.43

Figure F.12 IV-Curve of DSSC of 1.0%wt. SnO_2/TiO_2 electrode calcined at 400ºC for two

hours 500 coats with N719 dye

Table F.12 Electrochemical properties of DSSC of 1.0%wt. SnO_2/TiO_2 electrode calcined
at 400ºC for two hours 500 coats with N719 dye

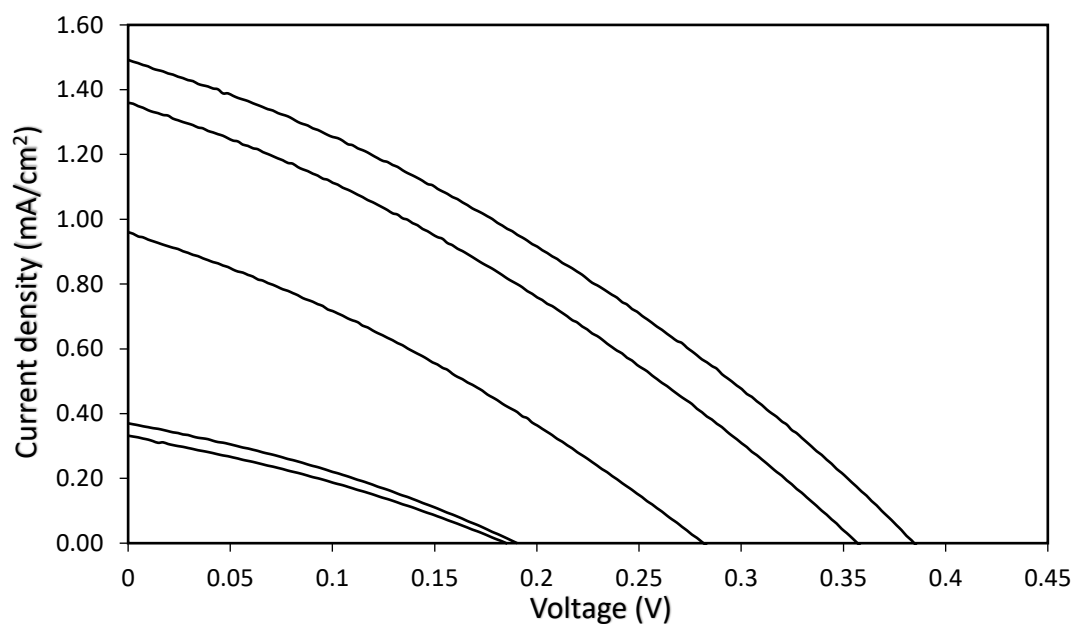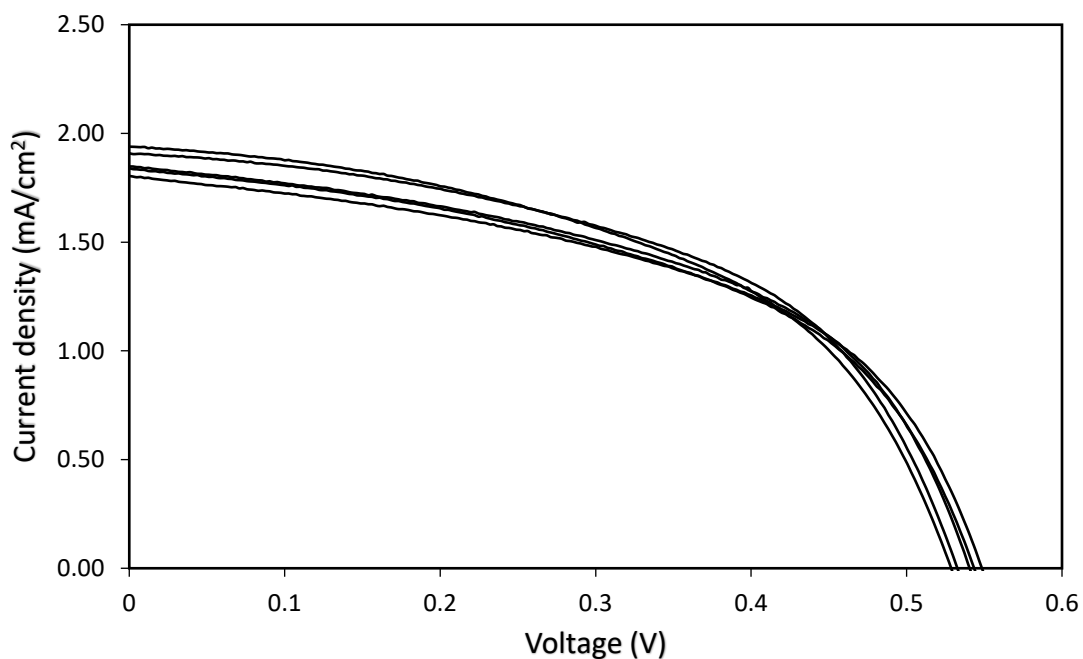| No.	V_{OC} (Volt)	J_{SC} (mA/cm²)	Vmax (Volt)	Jmax (mA/cm²)	Pmax (mW/cm²)	FF	η (%)
1	0.56	2.34	0.43	1.88	0.80	0.61	5.34
2	0.56	2.37	0.44	1.85	0.82	0.62	5.46
3	0.55	2.15	0.44	1.82	0.80	0.67	5.31
4	0.56	2.50	0.42	2.05	0.86	0.62	5.75
5	0.56	2.47	0.42	2.02	0.85	0.62	5.67
Average	0.56	2.37	0.43	1.93	0.83	0.63	5.50 ± 0.20

Figure F.13 IV-Curve of DSSC of 3.0%wt. SnO_2/TiO_2 electrode calcined at 400ºC for two

hours 500 coats with N719 dye

Table F.13 Electrochemical properties of DSSC of 3.0%wt. SnO_2/TiO_2 electrode calcined

at 400ºC for two hours 500 coats with N719 dye

No.	V_{OC} (Volt)	J_{sc} (mA/cm^2)	Vmax (Volt)	Jmax (mA/cm^2)	Pmax (mW/cm^2)	FF	η (%)
1	0.57	1.43	0.45	1.31	0.59	0.72	3.92
2	0.57	1.49	0.44	1.29	0.57	0.68	3.81
3	0.57	1.65	0.44	1.54	0.68	0.72	4.55
4	0.58	1.33	0.45	1.22	0.55	0.71	3.64
5	0.57	1.31	0.45	1.17	0.53	0.70	3.51
Average	0.57	1.44	0.45	1.30	0.58	0.71	3.89 ± 0.40

Figure F.14 IV-Curve of DSSC of double-layered electrode of pure TiO_2 as under-layer calcined at 400ºC for 2 hours 30 minutes 250 coats and 0.5%wt. SnO_2/TiO_2 as over-layer calcined at 400ºC for 30 minutes 250 coats

Table F.14 Electrochemical properties of DSSC of double-layered electrode of pure TiO_2 as under-layer calcined at 400ºC for 2 hours 30 minutes 250 coats and 0.5%wt. SnO_2/TiO_2 as over-layer calcined at 400ºC for 30 minutes 250 coats

No.	V_{OC} (Volt)	J_{SC} (mA/cm^2)	Vmax (Volt)	Jmax (mA/cm^2)	Pmax (mW/cm^2)	FF	η (%)
1	0.59	3.17	0.46	2.72	1.25	0.67	8.35
2	0.63	3.39	0.49	2.78	1.37	0.65	9.13
3	0.63	3.13	0.50	2.53	1.27	0.64	8.49
4	0.63	3.34	0.50	2.69	1.33	0.64	8.90
5	0.61	3.85	0.47	2.80	1.31	0.56	8.74
Average	0.62	3.38	0.48	2.70	1.31	0.63	8.72 ± 0.31

Figure F.15 IV-Curve of DSSC of double-layered electrode of 0.5%wt. SnO_2/TiO_2 as under-layer calcined at 400ºC for 2 hours 30 minutes 250 coats and pure TiO_2 as over-layer calcined at 400ºC for 30 minutes 250 coats

Table F.15 Electrochemical properties of DSSC of double-layered electrode of 0.5%wt. SnO_2/TiO_2 as under-layer calcined at 400ºC for 2 hours 30 minutes 250 coats and pure TiO_2 as over-layer calcined at 400ºC for 30 minutes 250 coats

No.	V_{OC} (Volt)	J_{SC} (mA/cm^2)	Vmax (Volt)	Jmax (mA/cm^2)	Pmax (mW/cm^2)	FF	η (%)
1	0.63	2.83	0.49	2.29	1.12	0.64	7.49
2	0.61	3.42	0.47	2.55	1.21	0.58	8.05
3	0.58	2.95	0.46	2.50	1.15	0.67	7.66
4	0.61	2.99	0.47	2.39	1.13	0.62	7.51
5	0.58	3.01	0.45	2.41	1.09	0.62	7.25
Average	0.60	3.04	0.47	2.43	1.14	0.63	7.59 ± 0.29

APPENDICES

APPENDIX A CALCULATION OF THE CRYSTALLITE SIZE

Calculation of the crystallite size by Debye-Scherrer equation

The crystallite size can be calculated from 2θ profile analysis, FWHM, by Debye-Scherrer equation (A.1) that was suitable for partical size below 100 nm.

Debye-Scherrer equation:

$$D = \frac{K\lambda}{\beta cos\theta} \tag{A.1}$$

Where

D = Average size of the crystal (Å)

K = Dimensionless shape factor (0.9)

λ = The x-ray wavelength (1.54439 Å for CuK$_\alpha$)

β = The x-ray diffraction broadening (radian)

θ = Observed peak angle (degree)

The broadening of a single diffraction peak is the product of the crystallite dimensions in the direction perpendicular to the planes that produced the diffraction peak. The X-ray diffraction broadening can be obtained by using Warren's equation (A.2).

Warren's equation:

$$\beta^2 = \beta_M^2 - \beta_S^2$$

$$\beta = \sqrt{\beta_M^2 - \beta_S^2} \tag{A.2}$$

Where

β_M = Measured peak width in radians at half peak height

β_S = Corresponding width of a standard material

Example : Calculation of the crystallite site of pure TiO_2 calcined at 400ºC for two hours

The half-weight width (101) diffraction peak

$$\beta_M \quad = \quad 1.1295 \quad degree$$

$$\beta_M \quad = \quad 0.019713 \quad radian$$

The corresponding half-height width of peak of TiO_2

$$\beta_S \quad = \quad 0.003836 \quad radian$$

The pure width

$$\beta = \sqrt{\beta_M^2 - \beta_S^2}$$

$$\beta = \sqrt{0.019713^2 - 0.003836^2}$$

$$\beta = 0.019336 \; radian$$

Where

λ	=	1.01117	Å
β	=	0.019336	radian
2θ	=	25.3465	degree
θ	=	12.6732	degree

$$\text{The crystallite size (D)} \quad = \quad \frac{0.9 \times 1.01117}{0.0193 \cos 12.6732}$$

$$= \quad 80.97 \quad \text{Å}$$

$$= \quad 8.1 \quad \text{nm}$$

APPENDIX B CALCULATION OF WEIGHT FRACTION OF ANATASE, RUTILE AND BROOKITE PHASE OF TiO$_2$

Calculation of the weight fraction

The phase of TiO$_2$ can be calculated from the integrated intensities of peaks at 2θ of 25.3° was assigned to anatase TiO$_2$, whereas the peak at 27.4° corresponded to be rutile phase and the peak at 30.6° was associated to brookite.

The weight fraction of TiO2 sample can be calculated as follows equation (B.1)-(B.3).

$$W_A = \frac{K_A A_A}{K_A A_A + K_B A_B + K_R} \tag{B.1}$$

$$W_B = \frac{K_B A_B}{K_A A_A + K_B A_B + K_R} \tag{B.2}$$

$$W_R = \frac{K_R}{K_A A_A + K_B A_B + K_R} \tag{B.3}$$

Where

W_A	=	Weight fraction of anatase phase TiO$_2$
W_B	=	Weight fraction of brookite phase TiO$_2$
W_R	=	Weight fraction of rutile phase TiO$_2$
A_A	=	The intensity of anatase peak
A_B	=	The intensity of brookite peak
A_R	=	The intensity of rutile peak
K_A	=	The coefficient factor of anatase (0.886)
K_B	=	The coefficient factor of brookite (2.721)

Example : Calculation of the phase contents TiO_2 calcined at 400ºC for two hours

Where

The integrated intensities of anatase (A_A)　　=　　742

The integrated intensities of brookite (A_B)　　=　　73

The integrated intensities of rutile (A_R)　　=　　141

The weight fraction of the phase content can be calculated by as follows:

$$W_A = \frac{742(0.866)}{742(0.866)+73(2.721)+141} = 0.66$$

$$W_B = \frac{73(2.721)}{742(0.866)+73(2.721)+141} = 0.20$$

$$W_R = \frac{141}{742(0.866)+73(2.721)+141} = 0.14$$

APPENDIX C DETERMINATION OF THE AMOUNT OF RUTHENIUM-BASED DYE ADSORBED ON SURFACE

Mensuration of the amount of ruthenium-based dye adsorbed

The amount of N719 dye adsorbed was measured by UV-Visible Absorption Spectroscopy on the absorption peak at 310 nm. In this study, three electrodes were used and the dye was dissolved out to surface electrode by using a mixed solution of 0.1 M NaOH in deionized water and ethanol with molar ratio 1:1 volume fraction.

The calibration curve of concentration of N719 dye with absorbance was illustrated in the following Figure C.1 and the concentration of N719 dye contained in pure TiO2 and second metal oxide/TiO_2 was shown in Table C.1 -C.2.
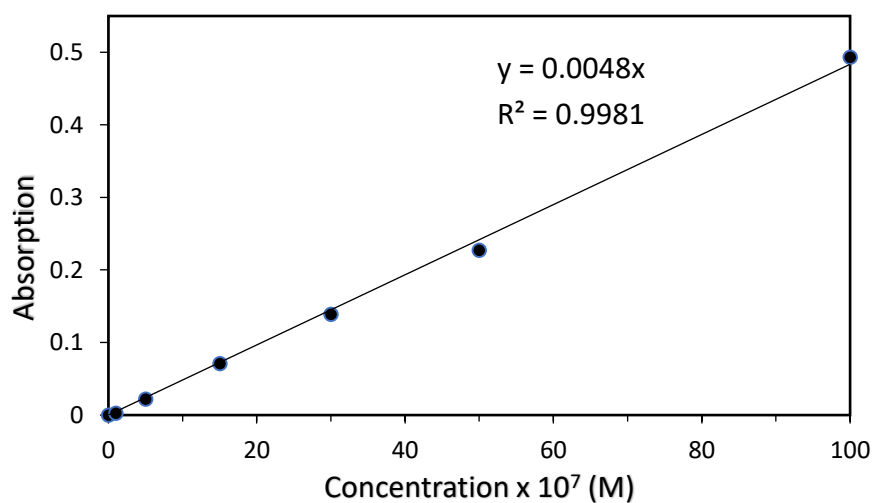

$$y = 0.0048x$$
$$R^2 = 0.9981$$

Figure C.1 The calibration curve of concentration of N719 adsorbed dye

Table C.1 The concentration of N719 dye contained in pure TiO_2 and second metal oxide/TiO_2 electrodes of calcined at 400ºC for 2 hours 500 coats at various content

Electrode	Concentration of N719 dye (×107 mol/cm2)			
	1	2	3	Average
Pure TiO_2	2.01	1.83	1.93	1.92 ± 0.009
0.1%wt. MnO_2/TiO_2	1.93	2.02	1.91	1.95 ± 0.006
0.5%wt. MnO_2/TiO_2	3.14	3.22	3.12	3.16 ± 0.005
1.0%wt. MnO_2/TiO_2	2.67	2.64	2.85	2.72 ± 0.011
3.0%wt. MnO_2/TiO_2	1.93	1.96	2.04	1.98 ± 0.006
0.1%wt. CoO/TiO_2	1.92	2.07	1.86	1.95 ± 0.011
0.5%wt. CoO/TiO_2	1.38	1.67	1.55	1.53 ± 0.014
1.0%wt. CoO/TiO_2	1.28	1.39	1.24	1.31 ± 0.008
3.0%wt. CoO/TiO_2	0.91	0.92	0.80	0.88 ± 0.007
0.1%wt. SnO_2/TiO_2	2.23	2.15	2.03	2.14 ± 0.0010
0.5%wt. SnO_2/TiO_2	3.68	3.44	3.82	3.65 ± 0.019
1.0%wt. SnO_2/TiO_2	3.35	3.36	3.45	3.39 ± 0.006
3.0%wt. SnO_2/TiO_2	2.32	2.53	2.17	2.34 ± 0.018

Table C.2 The concentration of N719 dye contained in double-layered electrode of under-layer calcined at 400ºC for 2 hours 30 minutes 250 coats and over-layer calcined at 400ºC for 30 minutes 250 coats at various content

Electrode	Concentration of N719 dye (×10^7 mol/cm^2)			
	1	2	3	Average
0.5%wt. SnO_2/TiO_2 as over layer TiO_2 as under layer	3.78	3.93	3.72	3.81 ± 0.011
TiO_2 as over layer 0.5%wt. SnO_2/TiO_2 as under layer	3.80	3.72	3.81	3.78 ± 0.005

APPENDIX D THE CALCULATION OF THE BAND GAP ENERGY FROM UV-VIS SPECTRA

Determination of the bandgap

The band gap energy of TiO_2 or modified TiO_2 can be determined by UV-Visible Absorption Spectroscopy with plotting the graph between $(\alpha h\nu)^{(1/n)}$ versus photon energy ($h\nu$).

where

α = The optical absorption coefficient can be calculated by Equation (D.1).

$$\alpha = \frac{2.303A}{t} \qquad (D.1)$$

where

A = Absorbance

t = The thickness of the sample

$h\nu$ = The photon energy can be calculated from its wavelength by Equation (D.2).

$$h\nu = Eg = \frac{hC}{\lambda} \qquad (D.2)$$

Where

Eg = The band gap energy of the catalyst (eV)

h = The plank constant (6.62×10^{-34} Joules·sec)

λ = The wavelength (meters)

C = The speed of light (3.0×10^{8} meter/sec)

Note: 1 eV is 1.6×10-19 Joules and 1 m is 10^{9} nm (conversion factor)

Finally, this was given equation for the photon energy at its wavelength (D.3).

$$h\nu = \frac{1240}{\lambda} \qquad (D.3)$$

n = the power factor n for allowed direct (0.5)

Example : Calculation of the band gap in pure TiO_2

To determine the band gap of TiO_2. The extrapolation for the straight-line portion of the curves to zero absorption coefficient value produced the valve of the energy band gap energy.

The plot between $(\alpha h\nu)^{(1/n)}$ versus photon energy $(h\nu)$ was shown in Figure D.1
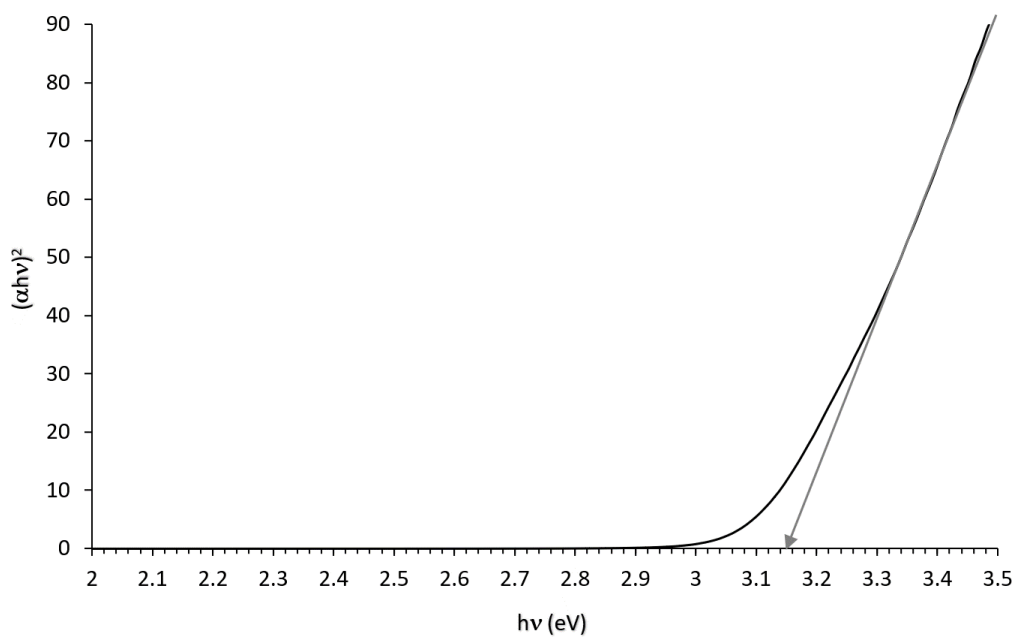

Figure D.1 An example for a plot between $(\alpha h\nu)^{(1/0.5)}$ versus photon energy $(h\nu)$ of TiO_2

From this Figure presented the band gap of pure TiO_2 is 3.15 eV

APPENDIX E THE CALCULATION OF AMOUNT OF METAL OXIDE FROM ICP-AES

Calculation of ICP-AES results

The results from ICP-AES characterization were calculation the contents of metal oxide doped in TiO_2.

Example : Calculation of the SnO_2 contents in 0.5%wt. SnO_2/TiO_2

(1) For 0.5%wt. SnO_2/TiO_2, the initial weight of catalyst powder was 0.050 g. Hence, the calculation of Tin (Sn) contents as follows:

The amount of ... in catalyst were;

In 1.0 g of catalyst, had a SnO_2 content was 0.005 g

In 0.050 g of catalyst, had a SnO_2 content was $\dfrac{0.005 \times 0.050}{1.0}$ g

$$= 0.250 \times 10^{-3} \text{ g}$$

$$= 0.250 \quad \text{mg}$$

For digestion, sample were diluted to 100 cm^3

Therefore, the sample had a concentration were $\dfrac{0.25 \times 1000}{100}$

$$= 2.500 \text{ ppm (mg/L of } SnO_2)$$

(2) From the result of ICP-AES, shown the concentration of sample 1.896 ppm

Converting to concentration of SnO_2 was $\dfrac{1.896 \times 150.71}{118.71}$

$$= 2.407 \text{ ppm}$$

When

The molecular weight of Tin dioxide (SnO^2) is 150.71 g/mol

The molecular weight of Tin (Sn) is 118.71 g/mol

(3) Therefore, the SnO_2/TiO_2 contents in catalyst were calculated by

SnO_2 concentration of 2.500 ppm refer to 0.5%wt. SnO_2/TiO_2 in catalyst

SnO_2 concentration of 2.407 ppm refer to $\dfrac{2.407 \times 0.5}{2.500}$

$= 0.48$%wt. SnO_2/TiO_2

APPENDIX F THE ELECTROCHEMICAL PROPERTIES OF DSSCS

The electrochemical properties of dye-sensitized solar cell

The electrochemical properties of DSSCs as pure TiO_2 and modified TiO_2 with second metal oxide MnO_2, CoO, and SnO_2 electrode was measured by I-V characterization under a light irradiance (Pin) of 15 mW/cm^2. In this study, five sample were used and the photovoltaic efficiency (η) of cell given is the average valve follow by the standard derivation.

The electrochemical properties were Shown in Table F.1 - F.15

The IV-Curves were Shown in Figure F.1 – F.15

Figure F.1 IV-Curve of DSSC of pure TiO$_2$ electrode calcined at 400ºC for two hours 500 coats with N719 dye

Table F.1 Electrochemical properties of DSSC of pure TiO$_2$ electrode calcined at 400ºC for two hours 500 coats with N719 dye

No.	V$_{OC}$ (Volt)	J$_{SC}$ (mA/cm^2)	Vmax (Volt)	Jmax (mA/cm^2)	Pmax (mW/cm^2)	FF	η (%)
1	0.61	1.50	0.47	1.09	0.51	0.56	3.42
2	0.59	1.68	0.39	1.05	0.41	0.41	2.73
3	0.57	1.41	0.45	1.11	0.50	0.61	3.31
4	0.56	1.78	0.42	1.21	0.50	0.50	3.34
5	0.60	1.11	0.49	0.87	0.42	0.64	2.83
Average	0.59	1.50	0.44	1.07	0.47	0.55	3.12 ± 0.32

Figure F.2 IV-Curve of DSSC of 0.1%wt. MnO_2/TiO_2 electrode calcined at 400ºC for two

hours 500 coats with N719 dye

Table F.2 Electrochemical properties of DSSC of 0.1%wt. MnO_2/TiO_2 electrode calcined

at 400ºC for two hours 500 coats with N719 dye

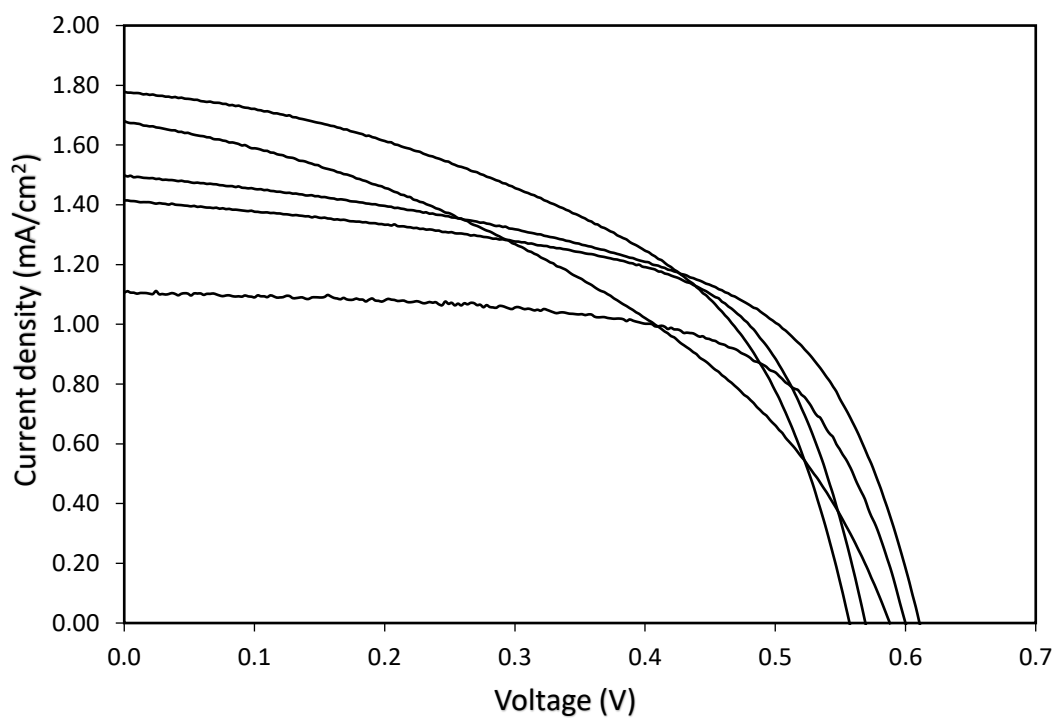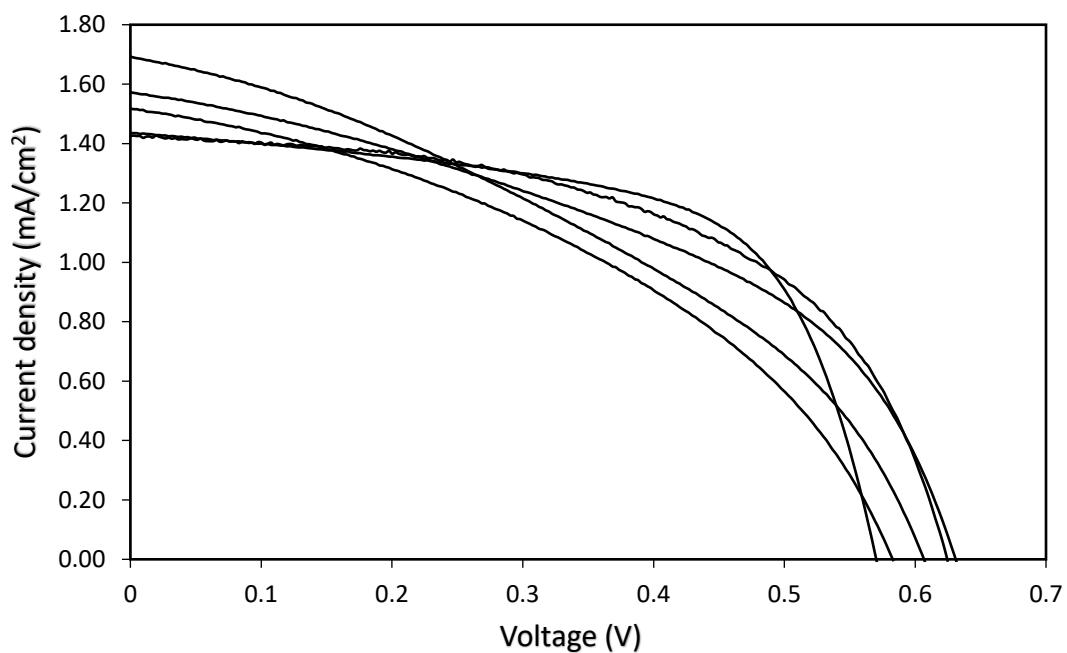| No.	V_{oc} (Volt)	J_{sc} (mA/cm^2)	Vmax (Volt)	Jmax (mA/cm^2)	Pmax (mW/cm^2)	FF	η (%)
1	0.63	1.57	0.46	0.97	0.44	0.45	2.96
2	0.61	1.69	0.40	0.98	0.39	0.38	2.61
3	0.63	1.43	0.46	1.06	0.48	0.54	3.21
4	0.58	1.52	0.39	0.94	0.36	0.41	2.43
5	0.57	1.44	0.45	1.12	0.51	0.62	3.38
Average	0.60	1.53	0.43	1.01	0.44	0.48	2.92 ± 0.40

Figure F.3 IV-Curve of DSSC of 0.5%wt. MnO_2/TiO_2 electrode calcined at 400ºC for two

hours 500 coats with N719 dye

Table F.3 Electrochemical properties of DSSC of 0.5%wt. MnO_2/TiO_2 electrode calcined

at 400ºC for two hours 500 coats with N719 dye

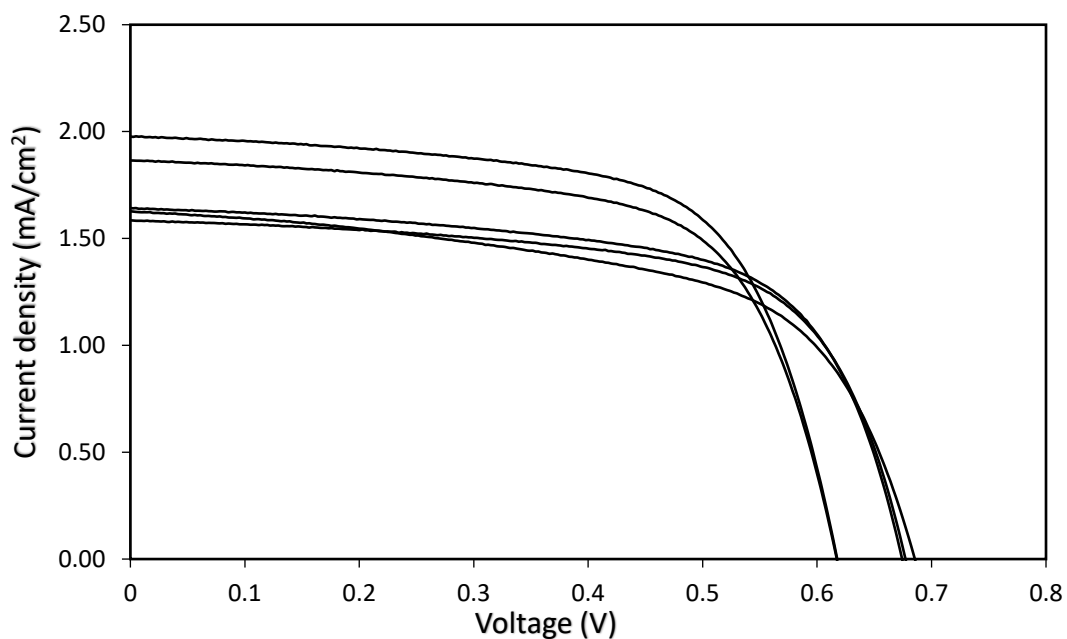| No.	V_{OC} (Volt)	J_{SC} (mA/cm^2)	Vmax (Volt)	Jmax (mA/cm^2)	Pmax (mW/cm^2)	FF	η (%)
1	0.62	1.86	0.48	1.56	0.75	0.65	5.00
2	0.62	1.98	0.49	1.65	0.80	0.66	5.33
3	0.69	1.63	0.54	1.22	0.66	0.59	4.39
4	0.68	1.58	0.53	1.31	0.70	0.65	4.66
5	0.68	1.64	0.54	1.32	0.71	0.64	4.76
Average	0.66	1.74	0.52	1.41	0.72	0.64	4.83 ± 0.36

Figure F.4 IV-Curve of DSSC of 1.0%wt. MnO_2/TiO_2 electrode calcined at 400ºC for two hours 500 coats with N719 dye

Table F.4 Electrochemical properties of DSSC of 1.0%wt. MnO_2/TiO_2 electrode calcined at 400ºC for two hours 500 coats with N719 dye

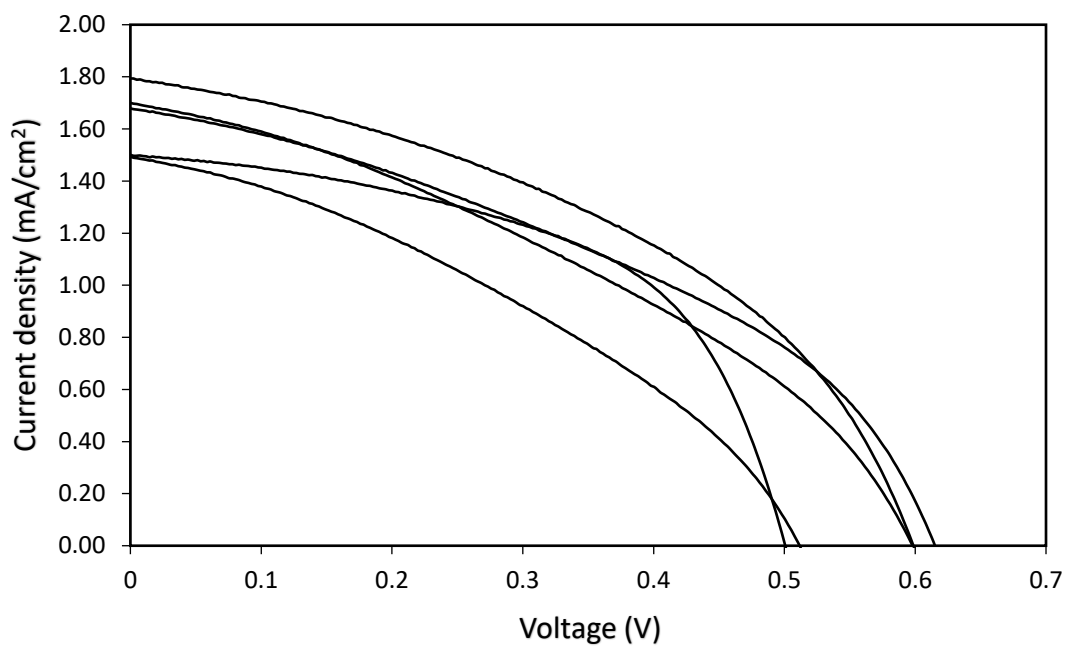| No.	V_{OC} (Volt)	J_{SC} (mA/cm^2)	Vmax (Volt)	Jmax (mA/cm^2)	Pmax (mW/cm^2)	FF	η (%)
1	0.50	1.50	0.37	1.09	0.40	0.54	2.70
2	0.51	1.49	0.31	0.91	0.28	0.36	1.84
3	0.62	1.68	0.41	1.01	0.41	0.40	2.75
4	0.60	1.79	0.41	1.12	0.46	0.43	3.08
5	0.60	1.70	0.41	0.90	0.37	0.36	2.45
Average	0.57	1.63	0.38	1.01	0.38	0.42	2.57 ± 0.46

Figure F.5 IV-Curve of DSSC of 3.0%wt. MnO$_2$/TiO$_2$ electrode calcined at 400ºC for two

hours 500 coats with N719 dye

Table F.5 Electrochemical properties of DSSC of 3.0%wt. MnO$_2$/TiO$_2$ electrode calcined

at 400ºC for two hours 500 coats with N719 dye

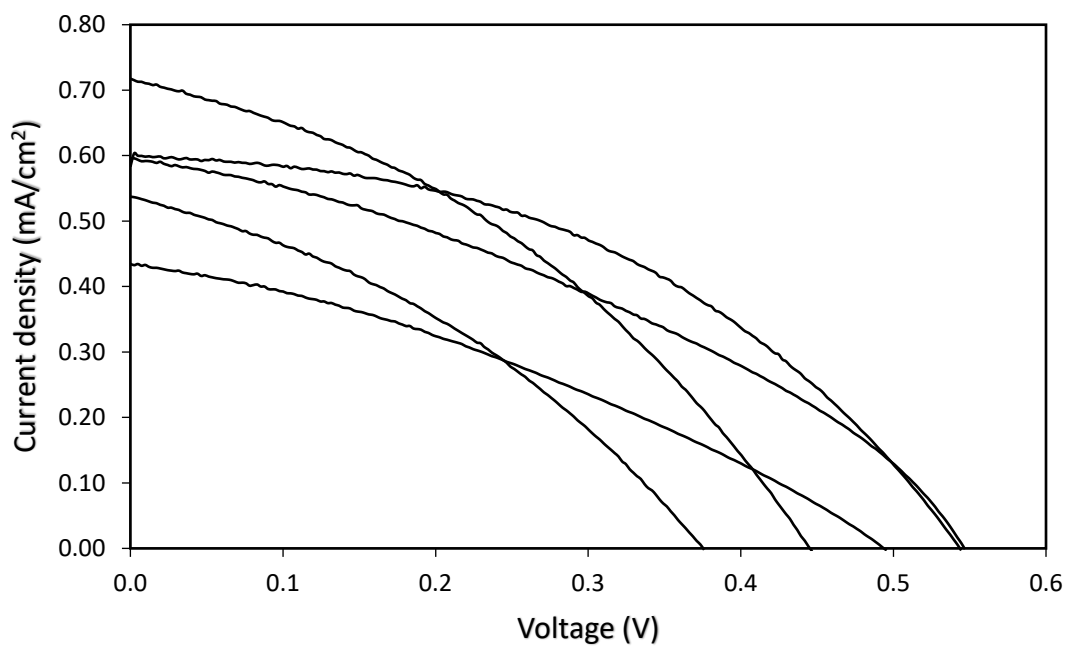| No.	V$_{oc}$ (Volt)	J$_{sc}$ (mA/cm^2)	Vmax (Volt)	Jmax (mA/cm^2)	Pmax (mW/cm^2)	FF	η (%)
1	0.54	0.58	0.34	0.42	0.14	0.46	0.97
2	0.38	0.54	0.23	0.31	0.07	0.36	0.48
3	0.50	0.43	0.27	0.26	0.07	0.33	0.48
4	0.55	0.60	0.33	0.36	0.12	0.36	0.79
5	0.45	0.72	0.26	0.46	0.12	0.37	0.80
Average	0.48	0.57	0.29	0.36	0.11	0.38	0.70 ± 0.22

Figure F.6 IV-Curve of DSSC of 0.1%wt. CoO/TiO$_2$ electrode calcined at 400ºC for two hours 500 coats with N719 dye

Table F.6 Electrochemical properties of DSSC of 0.1%wt. CoO/TiO$_2$ electrode calcined at 400ºC for two hours 500 coats with N719 dye

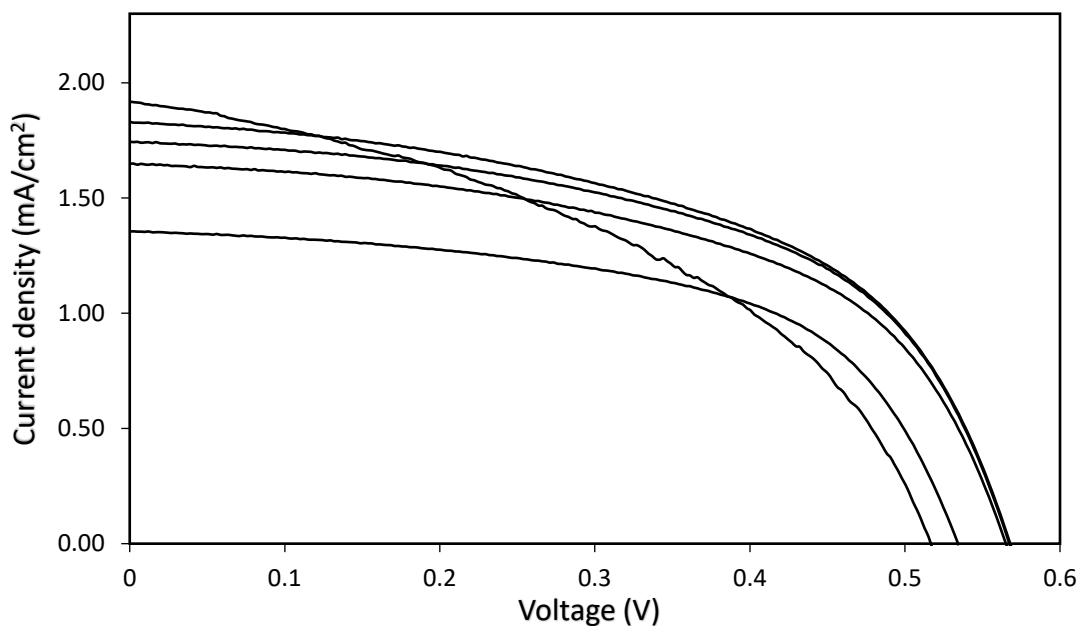| No.	V_{OC} (Volt)	J_{SC} (mA/cm^2)	Vmax (Volt)	Jmax (mA/cm^2)	Pmax (mW/cm^2)	FF	η (%)
1	0.57	1.65	0.42	1.21	0.51	0.54	3.39
2	0.57	1.75	0.43	1.26	0.54	0.55	3.61
3	0.57	1.83	0.43	1.25	0.53	0.51	3.55
4	0.53	1.35	0.41	1.03	0.42	0.58	2.78
5	0.52	1.92	0.35	1.23	0.42	0.43	2.83
Average	0.55	1.70	0.41	1.20	0.49	0.52	3.23 ± 0.40

Figure F.7 IV-Curve of DSSC of 0.5%wt. CoO/TiO$_2$ electrode calcined at 400ºC for two

hours 500 coats with N719 dye

Table F.7 Electrochemical properties of DSSC of 0.5%wt. CoO/TiO$_2$ electrode calcined

at 400ºC for two hours 500 coats with N719 dye

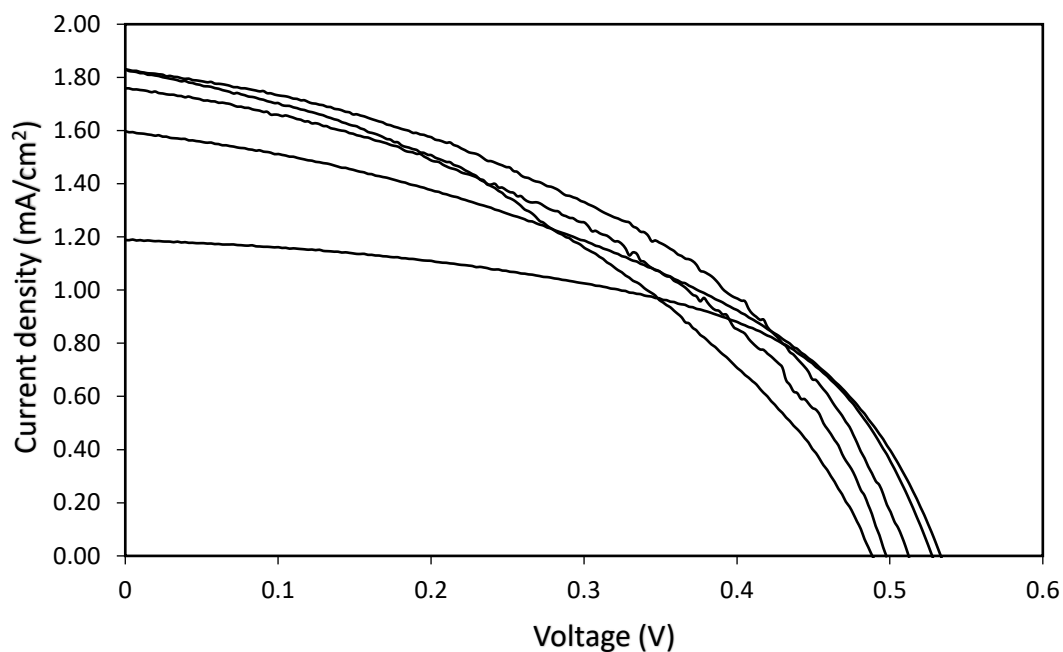| No.	V$_{OC}$ (Volt)	J$_{SC}$ (mA/cm^2)	Vmax (Volt)	Jmax (mA/cm^2)	Pmax (mW/cm^2)	FF	η (%)
1	0.50	1.76	0.32	1.18	0.38	0.44	2.54
2	0.49	1.83	0.31	1.14	0.35	0.39	2.33
3	0.51	1.83	0.35	1.16	0.41	0.44	2.75
4	0.53	1.60	0.37	1.03	0.38	0.44	2.50
5	0.53	1.19	0.40	0.88	0.35	0.56	2.35
Average	0.51	1.64	0.35	1.08	0.37	0.45	2.49 ± 0.17

Figure F.8 IV-Curve of DSSC of 1.0%wt. CoO/TiO$_2$ electrode calcined at 400ºC for two

hours 500 coats with N719 dye

Table F.8 Electrochemical properties of DSSC of 1.0%wt. CoO/TiO$_2$ electrode calcined

at 400ºC for two hours 500 coats with N719 dye

No.	V_{oc} (Volt)	J_{sc} (mA/cm^2)	Vmax (Volt)	Jmax (mA/cm^2)	Pmax (mW/cm^2)	FF	η (%)
1	0.48	1.42	0.31	0.98	0.31	0.46	2.07
2	0.53	1.59	0.38	0.98	0.37	0.44	2.46
3	0.54	1.62	0.38	1.04	0.39	0.45	2.60
4	0.46	1.47	0.29	0.96	0.28	0.42	1.88
5	0.46	1.57	0.29	1.03	0.30	0.42	2.01
Average	0.49	1.54	0.33	1.00	0.33	0.44	2.20 ± 0.31

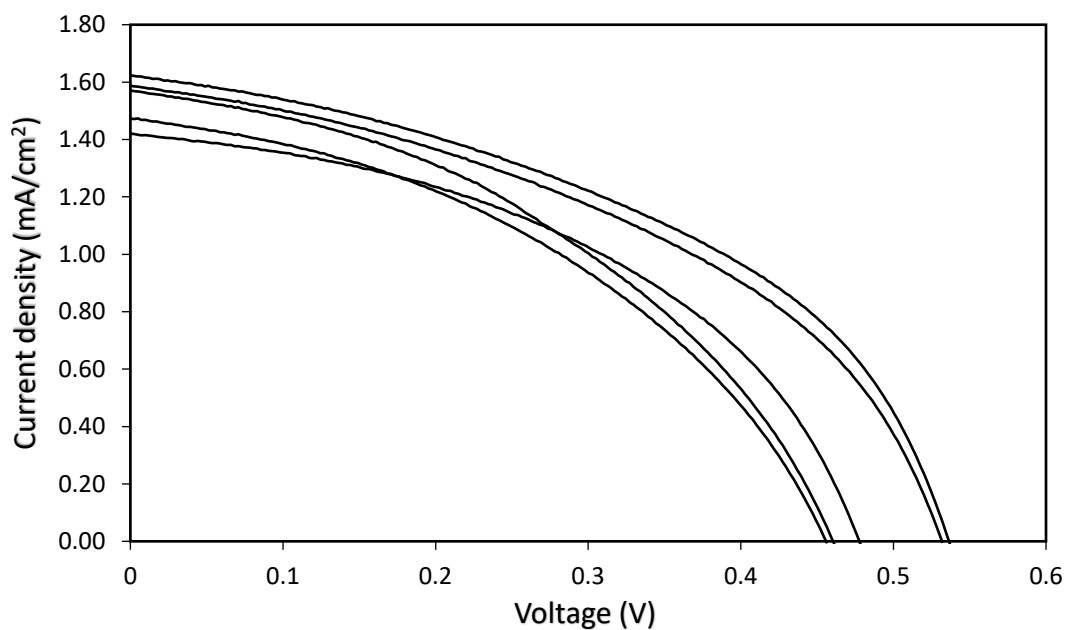**Figure F.9** IV-Curve of DSSC of 3.0%wt. CoO/TiO$_2$ electrode calcined at 400ºC for two hours 500 coats with N719 dye

Table F.9 Electrochemical properties of DSSC of 3.0%wt. CoO/TiO$_2$ electrode calcined at 400ºC for two hours 500 coats with N719 dye

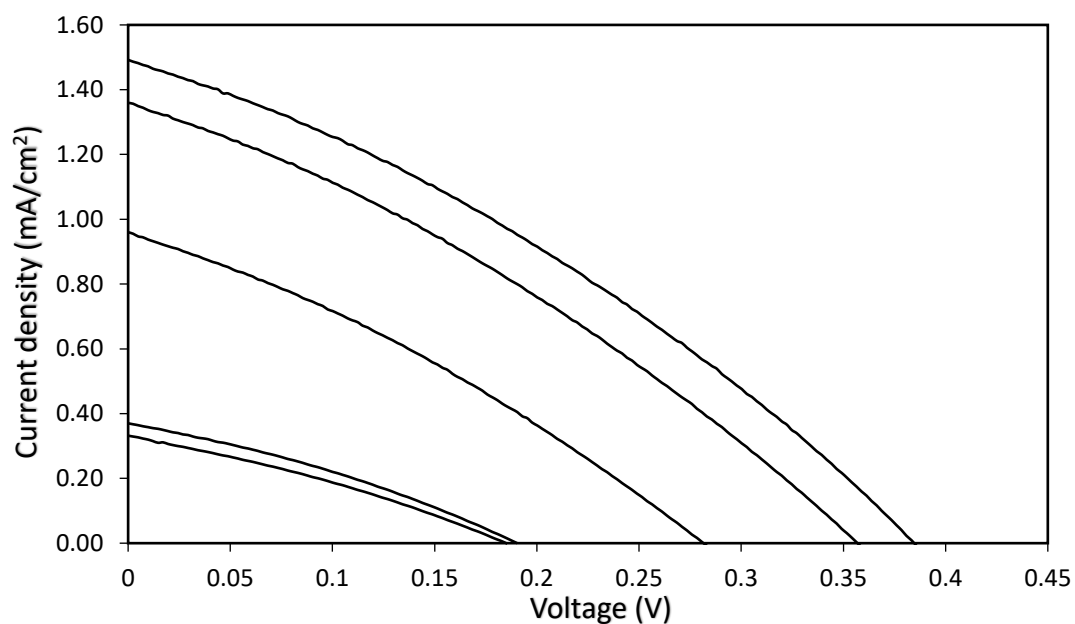| No.	V$_{OC}$ (Volt)	J$_{SC}$ (mA/cm^2)	Vmax (Volt)	Jmax (mA/cm^2)	Pmax (mW/cm^2)	FF	η (%)
1	0.36	1.36	0.20	0.77	0.15	0.31	1.01
2	0.19	0.37	0.11	0.21	0.02	0.31	0.15
3	0.19	0.33	0.10	0.18	0.02	0.31	0.13
4	0.39	1.49	0.22	0.84	0.18	0.32	1.23
5	0.28	0.96	0.16	0.54	0.08	0.31	0.56
Average	0.28	0.90	0.16	0.51	0.09	0.31	0.61 ± 0.50

Figure F.10 IV-Curve of DSSC of 0.1%wt. SnO_2/TiO_2 electrode calcined at 400ºC for two

hours 500 coats with N719 dye

Table F.10 Electrochemical properties of DSSC of 0.1%wt. SnO_2/TiO_2 electrode calcined

at 400ºC for two hours 500 coats with N719 dye

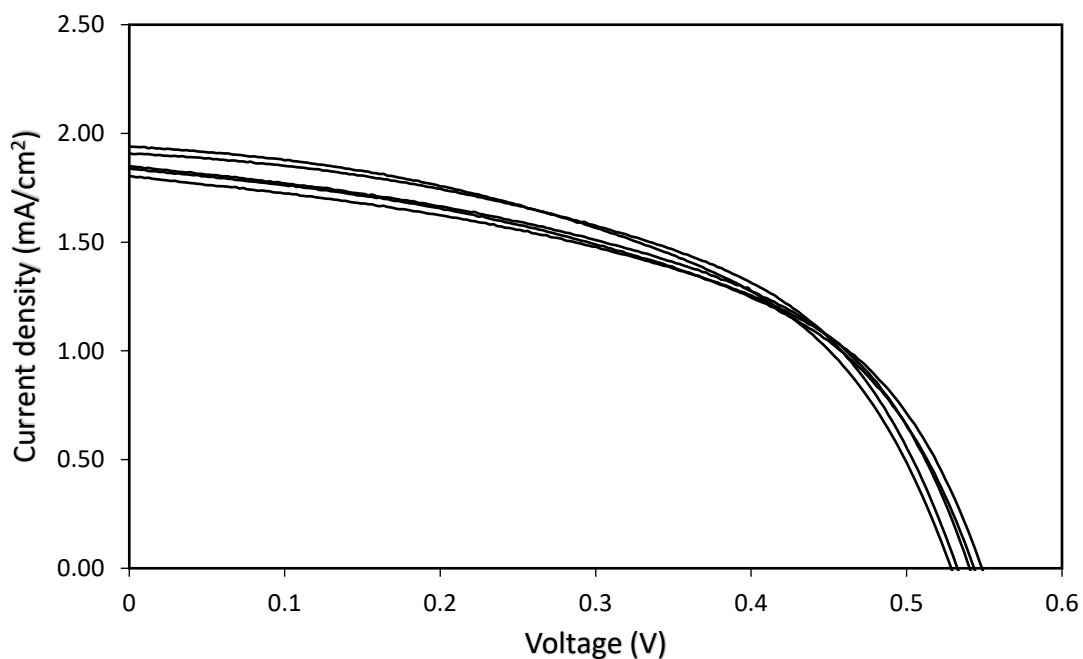| No.	V_{OC} (Volt)	J_{SC} (mA/cm^2)	Vmax (Volt)	Jmax (mA/cm^2)	Pmax (mW/cm^2)	FF	η (%)
1	0.54	1.85	0.40	1.29	0.51	0.51	3.42
2	0.54	1.84	0.40	1.26	0.50	0.50	3.33
3	0.55	1.80	0.41	1.24	0.50	0.51	3.35
4	0.53	1.91	0.39	1.35	0.53	0.52	3.51
5	0.53	1.94	0.39	1.33	0.51	0.50	3.42
Average	0.54	1.87	0.40	1.29	0.51	0.51	3.40 ± 0.07

Figure F.11 IV-Curve of DSSC of 0.5%wt. SnO_2/TiO_2 electrode calcined at 400ºC for two

hours 500 coats with N719 dye

Table F.11 Electrochemical properties of DSSC of 0.5%wt. SnO_2/TiO_2 electrode calcined

at 400ºC for two hours 500 coats with N719 dye

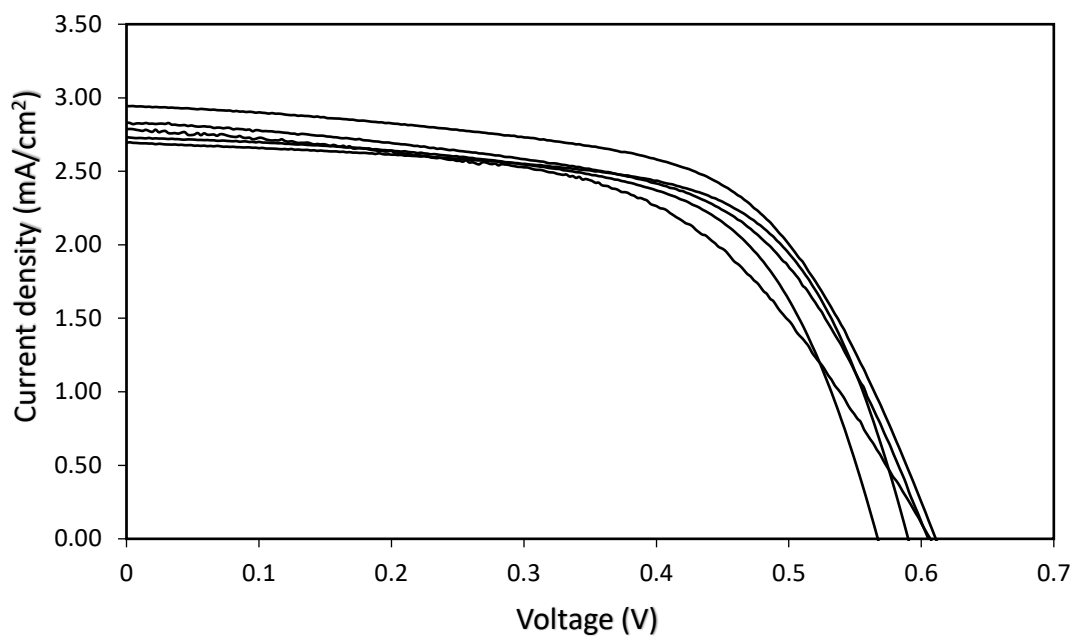| No.	V_{OC} (Volt)	J_{SC} (mA/cm^2)	Vmax (Volt)	Jmax (mA/cm^2)	Pmax (mW/cm^2)	FF	η (%)
1	0.61	2.94	0.45	2.38	1.08	0.60	7.22
2	0.61	2.79	0.41	2.23	0.91	0.54	6.07
3	0.61	2.83	0.45	2.25	1.01	0.59	6.71
4	0.59	2.69	0.46	2.24	1.03	0.65	6.88
5	0.57	2.73	0.43	2.25	0.97	0.63	6.49
Average	0.60	2.80	0.44	2.27	1.00	0.60	6.68 ± 0.43

Figure F.12 IV-Curve of DSSC of 1.0%wt. SnO_2/TiO_2 electrode calcined at 400ºC for two

hours 500 coats with N719 dye

Table F.12 Electrochemical properties of DSSC of 1.0%wt. SnO_2/TiO_2 electrode calcined

at 400ºC for two hours 500 coats with N719 dye

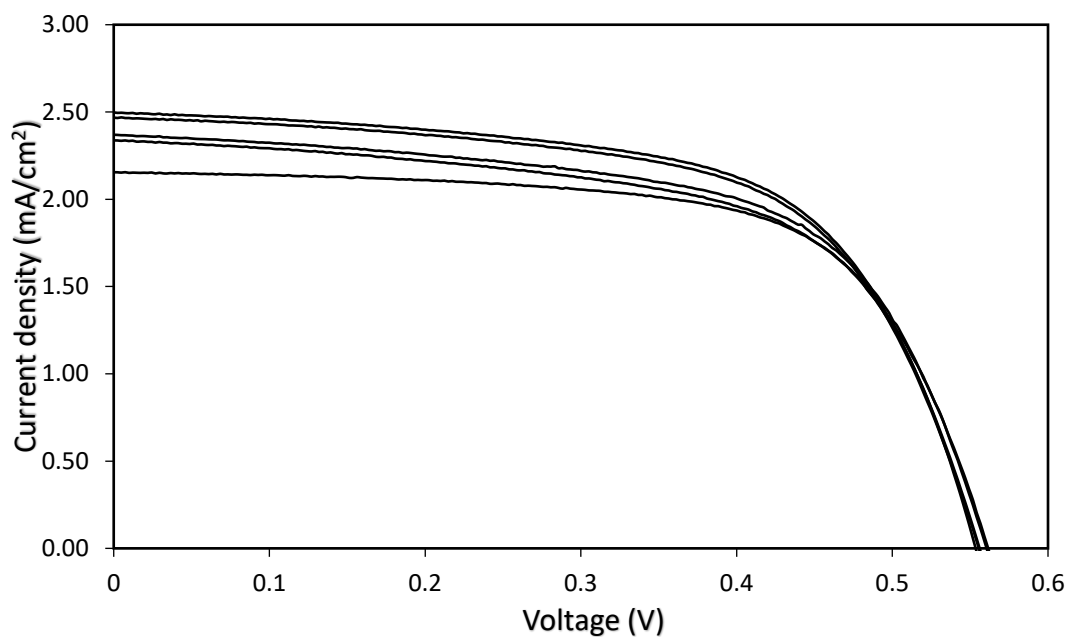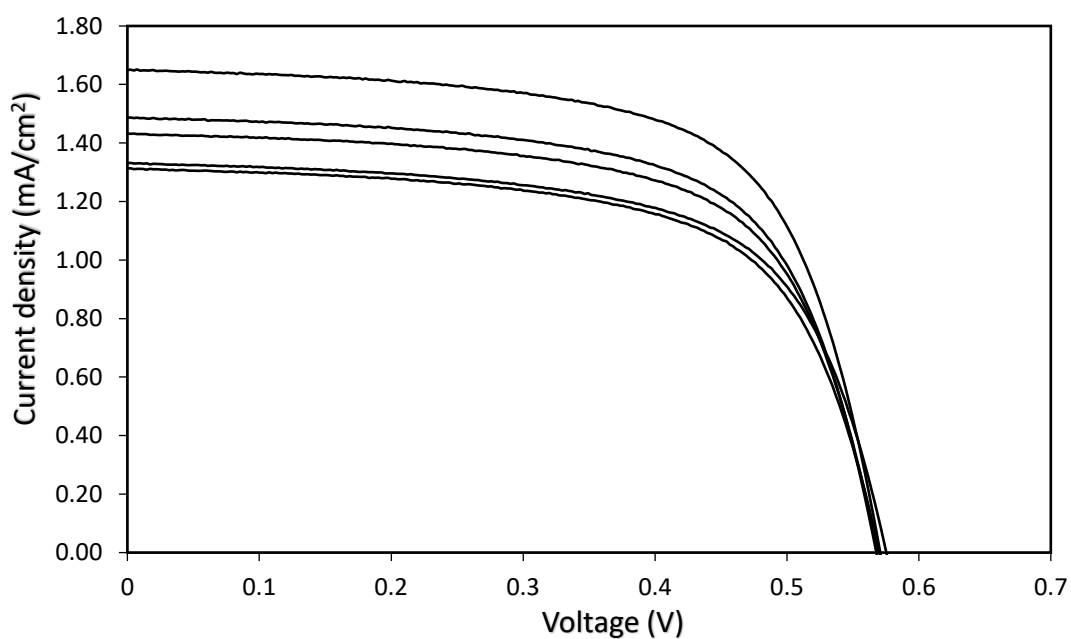| No.	V_{OC} (Volt)	J_{sc} (mA/cm^2)	Vmax (Volt)	Jmax (mA/cm^2)	Pmax (mW/cm^2)	FF	η (%)
1	0.56	2.34	0.43	1.88	0.80	0.61	5.34
2	0.56	2.37	0.44	1.85	0.82	0.62	5.46
3	0.55	2.15	0.44	1.82	0.80	0.67	5.31
4	0.56	2.50	0.42	2.05	0.86	0.62	5.75
5	0.56	2.47	0.42	2.02	0.85	0.62	5.67
Average	0.56	2.37	0.43	1.93	0.83	0.63	5.50 ± 0.20

Figure F.13 IV-Curve of DSSC of 3.0%wt. SnO_2/TiO_2 electrode calcined at 400ºC for two

hours 500 coats with N719 dye

Table F.13 Electrochemical properties of DSSC of 3.0%wt. SnO_2/TiO_2 electrode calcined

at 400ºC for two hours 500 coats with N719 dye

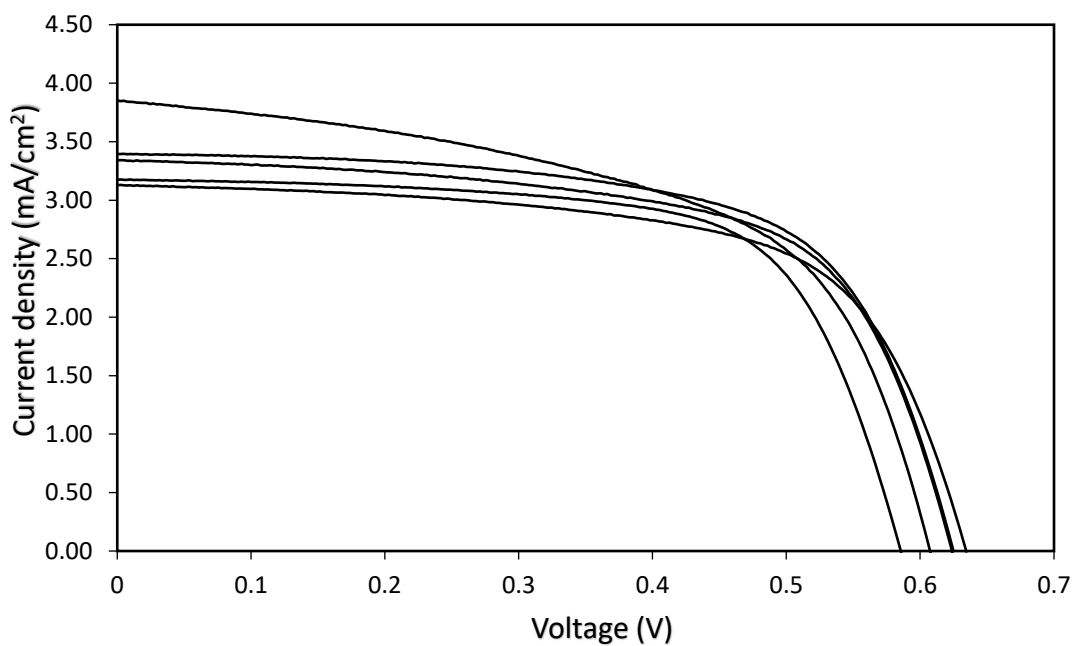| No.	V_{oc} (Volt)	J_{sc} (mA/cm^2)	Vmax (Volt)	Jmax (mA/cm^2)	Pmax (mW/cm^2)	FF	η (%)
1	0.57	1.43	0.45	1.31	0.59	0.72	3.92
2	0.57	1.49	0.44	1.29	0.57	0.68	3.81
3	0.57	1.65	0.44	1.54	0.68	0.72	4.55
4	0.58	1.33	0.45	1.22	0.55	0.71	3.64
5	0.57	1.31	0.45	1.17	0.53	0.70	3.51
Average	0.57	1.44	0.45	1.30	0.58	0.71	3.89 ± 0.40

Figure F.14 IV-Curve of DSSC of double-layered electrode of pure TiO_2 as under-layer calcined at 400ºC for 2 hours 30 minutes 250 coats and 0.5%wt. SnO_2/TiO_2 as over-layer calcined at 400ºC for 30 minutes 250 coats

Table F.14 Electrochemical properties of DSSC of double-layered electrode of pure TiO_2 as under-layer calcined at 400ºC for 2 hours 30 minutes 250 coats and 0.5%wt. SnO_2/TiO_2 as over-layer calcined at 400ºC for 30 minutes 250 coats

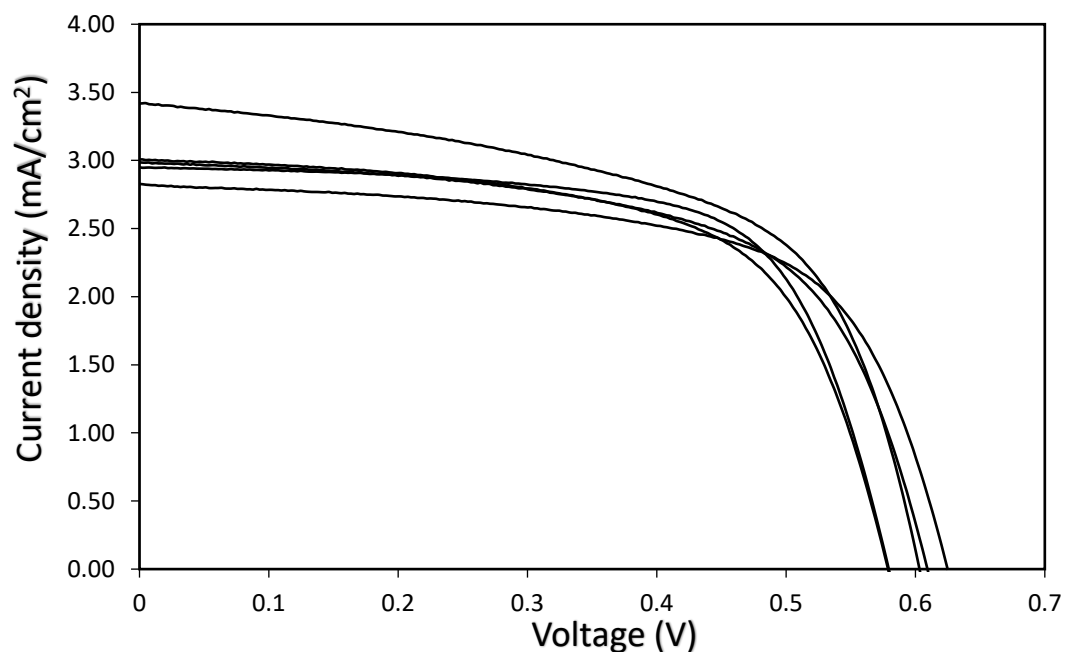| No.	V_{OC} (Volt)	J_{SC} (mA/cm^2)	Vmax (Volt)	Jmax (mA/cm^2)	Pmax (mW/cm^2)	FF	η (%)
1	0.59	3.17	0.46	2.72	1.25	0.67	8.35
2	0.63	3.39	0.49	2.78	1.37	0.65	9.13
3	0.63	3.13	0.50	2.53	1.27	0.64	8.49
4	0.63	3.34	0.50	2.69	1.33	0.64	8.90
5	0.61	3.85	0.47	2.80	1.31	0.56	8.74
Average	0.62	3.38	0.48	2.70	1.31	0.63	8.72 ± 0.31

Figure F.15 IV-Curve of DSSC of double-layered electrode of 0.5%wt. SnO_2/TiO_2 as under-layer calcined at 400ºC for 2 hours 30 minutes 250 coats and pure TiO_2 as over-layer calcined at 400ºC for 30 minutes 250 coats

Table F.15 Electrochemical properties of DSSC of double-layered electrode of 0.5%wt. SnO_2/TiO_2 as under-layer calcined at 400ºC for 2 hours 30 minutes 250 coats and pure TiO_2 as over-layer calcined at 400ºC for 30 minutes 250 coats

No.	V_{oc} (Volt)	J_{sc} (mA/cm^2)	Vmax (Volt)	Jmax (mA/cm^2)	Pmax (mW/cm^2)	FF	η (%)
1	0.63	2.83	0.49	2.29	1.12	0.64	7.49
2	0.61	3.42	0.47	2.55	1.21	0.58	8.05
3	0.58	2.95	0.46	2.50	1.15	0.67	7.66
4	0.61	2.99	0.47	2.39	1.13	0.62	7.51
5	0.58	3.01	0.45	2.41	1.09	0.62	7.25
Average	0.60	3.04	0.47	2.43	1.14	0.63	7.59 ± 0.29

VITA

NAME   Supasun Thanadvanichkul

DATE OF BIRTH   16 December 1994

PLACE OF BIRTH   Bangkok

INSTITUTIONS ATTENDED   Graduated high school from Sriboonyanon school in 2013.

                        Graduated Bachelor's Degrees faculty of Applied Science in

                        Industrial Chemistry, King Mongkut's University of

                        Technology North Bangkok, Thailand in 2016

HOME ADDRESS   101/247 Moo 4 Soi 4 M.Suetrong T.Saima A.Maung,

                        Nonthaburi 11000